ANALES DE LA DIVISION DE ESTUDIOS DE POSGRADO 1985

PREFACIO

Dentro de los fines de la Universidad Nacional Autónoma de México se encuentran los de docencia, investigación y difusión de la cultura.

Uno de los medios importantes para el logro de estos fines es la vía impresa, ya que la expresión escrita es una de las principales formas de registro y preservación por tiempo indefinido del conocimiento.

El avance de la humanidad ha dependido, en gran parte, de la utilización de los desarrollos científicos y humanísticos como fuerzas orientadoras y de soporte para la innovación y el cambio. Por tanto, la información científica y técnica es un recurso acumulativo, ya que el conocimiento se construye sobre conocimiento; y la posesión y aplicación oportuna y adecuada de éste es esencial para el progreso. Con ésto se resalta la gran importancia que tiene el difundirlo rápida y fielmente, so pena de perderse o distorsionarse.

La Facultad de Ingeniería, motivada por reflexiones como las anteriores, se enorgullece de presentar los *Anales de la División de Posgrado*, que en su primer número corresponde a 1985, en donde se encuentran algunos de los trabajos representativos de la labor científica que realizan sus profesores-investigadores.

Con ellos se pretende el doble objetivo de difundir artículos y tesis presentadas cada año, así como el de contar con un medio de presentación de la labor de la División en los ambientes académicos y profesionales, tanto nacionales como internacionales.

DR. OCTAVIO A. RASCON CHAVEZ
Director de la
Facultad de Ingeniería
UNAM

PREFACE

Education, research and dissemination of culture are among the objectives of the National University of Mexico (UNAM).

Printed work is one of the most important means to achieve these goals, because knowledge is effectively recorded and preserved by man's written expression.

Scientific and humanistic developments, as the essense of change and innovation, have been the driving force for the advancement of mankind. Therefore, information of all kinds is a cumulative resource: knowledge is built upon knowledge. Its possession and adequate application is fundamental for progress. This points out the importance of a fast and reliable spread of knowledge, in order to prevent its distortion or destruction.

The School of Engineering, motivated by these reflections, is proud to present the first volume of the *Graduate School Annals*, which corresponds to 1985. It includes some of the most relevant work done by the Faculty of the Graduate School as well as by some of the graduate students.

With the Annals a twofold objective is intended: to present research papers and theses elaborated during each year, and to promote the Graduate School at a national as well as an international level.

DR. OCTAVIO A. RASCON CHAVEZ
Head of the School of Engineering
UNAM

INDICE

LA DIVISION DE ESTUDIOS DE POSGRADO

En la DEPFI se preparan profesionistas para la docencia y para la investigación creativa, a través de la transmisión eficiente y motivadora de conocimientos a las nuevas generaciones, lo cual origina la investigación para el desarrollo de la tecnología adecuada a nuestras necesidades.

GRADUATE SCHOOL OF ENGINEERING

The Graduate School of Engineering prepares professionals for creative research and teaching, through the efficient and motivating transmission of knowledge to the new generations, which originates the research for the development of the proper technology for our needs.

LA DIVISION DE ESTUDIOS DE POSGRADO

La División de Estudios de Posgrado, DEPFI, es una de las siete Divisiones que conforman la Facultad de Ingeniería. Fue creada en 1957 y por sus aulas han pasado más de 5,200 alumnos, de los cuales el 79% han sido mexicanos y el 21% extranjeros, principalmente de Centro y Sud-América. La formación de los estudiantes ha estado a cargo de 510 profesores: 129 con grado de doctor, 235 con el de maestro y 146 con el de licenciado; de ellos, 7% extranjeros.
El Posgrado consta de tres niveles: Cursos de Especialización, Maestría y Doctorado. En la Especialización se busca el mejoramiento y actualización de los conocimientos en una rama específica; en la Maestría, además del objetivo anterior, se capacita al alumno en la investigación y en la docencia; y en el Doctorado, la meta es formar investigadores creativos de alto nivel que compartan los nuevos conocimientos con sus alumnos.

GRADUATE SCHOOL OF ENGINEERING

The Graduate School of Engineering, DEPFI, is one of the seven Divisions that constitute the School of Engineering. It was created in 1957 and more than 5,200 students have passed through the institution: 79% mexicans and 21% foreigners, principally from Central and South America. Aproximately 510 professors have been on charge of the students' formation: 129 with a Doctoral degree, 235 with a Masters degree and 146 with a Bachellor's degree; 7% of them foreigners.
The Graduate School has three programs: Specialization Courses, Master's degree and Doctor's degree. The aim of the Specialization Courses is the improvement and actualization of knowledge in a specific field; in the Master's degree, besides this objective, the students are prepared in research and in teaching; in the Doctoral program the aim is to form creative researchers of high level with abilities of sharing their knowledge with the students.

ORGANIZACION ACADEMICA

Académicamente la DEPFI se ha estructurado en seis Subjefaturas: Civil, Recursos del Agua y Suelo, Recursos del Subsuelo, Ambiental, Mecánica Eléctrica y Sistemas.
Actualmente se ofrecen nueve especializaciones, trece maestrías y nueve doctorados, en los siguientes campos:

ACADEMIC ORGANIZATION

Academically the Graduate School of Engineering is structured in six departments: Civil Engineering, Water and Ground Resources, Subground Resources, Environmental Engineering, Systems, and Electrical and Mechanical Engineering.
Nowadays nine Specializations are offered, thirteen Master's degree and nine Doctoral programs, in the following fields:

ESPECIALIZACIONES EN

- Construcción
- Métodos artificiales de producción petrolera
- Perforación de pozos petroleros
- Recuperación secundaria del petróleo
- Proyecto de instalaciones eléctricas
- Proyecto de instalaciones mecánicas
- Obras hidráulicas
- Obras marítimas
- Seguridad de instalaciones industriales de explotación petrolera

SPECIALIZATION IN ENGINEERING

- Construction
- Artificial lift methods for hydrocarbon production
- Petroleum well drilling
- Secondary recovery processes
- Design of electric instalations
- Design of mechanical instalations
- Hydraulic works
- Maritime structures
- Industrial safety engineering for petroleum exploitation facilities

MAESTRIAS EN

- Ambiental
- Aprovechamientos hidráulicos
- Construcción
- Eléctrica
- Energética
- Estructuras
- Exploración de recursos energéticos del subsuelo
- Hidráulica
- Investigación de operaciones
- Mecánica
- Mecánica de suelos
- Petrolera
- Planeación

MASTER DEGREE IN ENGINEERING

- Environmental
- Water resources
- Construction
- Electrical
- Energetics
- Structures
- Exploration for energy resources from the subsurface
- Hydraulics
- Operation research
- Mechanics
- Soil mechanics
- Petroleum
- Planning

DOCTORADOS EN

- Ambiental
- Aprovechamientos hidráulicos
- Eléctrica
- Estructuras
- Hidráulica
- Investigación de operaciones
- Mecánica de suelos
- Mecánica
- Petrolera

DOCTORAL DEGREE IN ENGINEERING

- Environmental
- Water resources
- Electricity
- Structures
- Hydraulics
- Operation research
- Soil mechanics
- Mechanics
- Petroleum

SERVICIOS DE APOYO ACADEMICO

- Dentro de las secciones académicas está la de Matemáticas que no ofrece grado, pero brinda soporte a las demás.
- Los laboratorios permiten el desarrollo de habilidades específicas y la observación directa de prácticas y experimentos.
- La Biblioteca conjunta de la División de Posgrado y del Instituto de Ingeniería, mantiene al día la información para las tareas de docencia e investigación.
- La Unidad de Cómputo presta servicio a la actividad académico-administrativa de alumnos y profesores.
- Difusión se encarga de establecer los canales adecuados para mantener una comunicación eficiente de la DEPFI de manera interna y externa.
- Sección Editorial da apoyo editorial a las publicaciones producto de la investigación y de la elaboración de textos en la DEPFI.
- Servicios Educativos se ocupa de la actualización y superación pedagógica del personal docente y del alumnado.

ACADEMIC SUPPORT SERVICES

- Among the academic sections, Mathematics does not offer an academic degree, but gives support to the other sections.
- Laboratories allow the development of specific abilities and the direct observation of practices and experiments.
- The Library of the Graduate School and The Engineering Institute keeps the information for the research and educational labor.
- Computer Center gives service to the academic and administrative activity of professores and students.
- Diffusion Services are commited to establish the adecuate channels in order to keep an active communication inside and outside the DEPFI.
- Editorial Services give publishing support to the publications of paper which result from the research projects.
- Educative Services are incharge of the actualization and improvement of professors and students.

ALGUNOS ARTICULOS PUBLICADOS POR PERSONAL DE CARRERA EN 1985

SOME PAPERS PUBLISHED BY FACULTY MEMBERS IN 1985

A. Buzo, F. Kuhlmann, C. Rivera.

RATE DISTORTION BOUNDS FOR QUOTIENT BASED

DISTORTION FUNCTIONS WITH APPLICATION TO LPC SYSTEMS

Proceedings Twenty-Third Annual Allerton Conference

on Communication, Control, and Computing.

Allerton House, Monticello, Illinois

University of Illinois at Urbana-Champaign

October 2-4, 1985

RATE DISTORTION BOUNDS FOR QUOTIENT BASED
DISTORTION FUNCTIONS WITH
APPLICATION TO LPC SYSTEMS

ANDRES BUZO, FEDERICO KUHLMANN, CARLOS RIVERA
Universidad Nacional Autónoma de México
División de Estudios de Posgrado
Facultad de Ingeniería
P.O. Box 70-256
04510 México, D.F.
MEXICO

ABSTRACT

In many linear predictive coding (LPC) speech compression systems, the encoding of the LPC parameters is performed using a product codebook scheme. One approach is to organize the set of reproduction LPC models as the Cartesian product of a vector codebook describing the shape of each reproduction LPC model and a scalar codebook describing the gain or energy. In this paper, we obtain theoretical bounds of the rate distortion function for the gain term of LPC systems (which used about 10 to 25 percent of the transmission rate), as well as an asymptotic approximation to the performance of the optimal scalar quantizer of these gain terms, when the overall fidelity criterion is the Itakura-Saito distortion measure. These approximations and bounds are compared with experimental results.

I. INTRODUCTION

In an LPC speech compression system the speech frames are characterized by an all-pole filter described by its z-transform $\sigma/A(z)$ (or simply σ/A), where σ is the filter gain,

$$A(z) = 1 + \sum_{k=1}^{m} a_k z^{-k},$$

and the excitation signal is either a periodic pulse train with period τ, zero time-average mean and unit time-average energy for voiced sounds (where τ is equal to the pitch value), or a zero-mean, unit variance sequence of independent random variables for unvoiced sounds. The set of parameters $a_1, \ldots, a_m, \sigma, \tau$ that define this model have to be extracted from the sampled speech signal, quantized and transmitted to the receiver. The rate of such parameter extraction is usually on the order of 50-100 Hz to follow the time varying overall characteristics of the input speech signal. At the receiver, speech can then be synthesized using the above all-pole model and the voiced-unvoiced information.

From rate distortion theory [1] it is known that, in order to achieve a low rate at a given distortion, it is better to quantize the whole set of parameters $a_1, \ldots, a_m$, σ, τ as a single vector or block. Since there does not exist a meaningful distortion measure for LPC systems that explicitly uses the pitch τ, this last quantity is usually encoded separately, which results in a suboptimal compression system with a product code scheme. Coding of the excitation parameter is therefore not considered here. In [2], Gray et-al proposed a system that quantizes a vector which includes the parameters a and σ of the above model, using the modified Itakura-Saito distortion measure [3] as the fidelity criterion. Even though this distortion measure is not universally accepted, it is used explicitly or implicitly in LPC systems and it has the form

$$d_{IS}(|\sigma/A|^2, |\hat{\sigma}/\hat{A}|^2) = \frac{\alpha}{\hat{\sigma}^2} - \ln \frac{\sigma^2}{\hat{\sigma}^2} - 1 \tag{1}$$

where

$$\alpha = \int_{-\pi}^{\pi} |\hat{A}(e^{j\theta})|^2 \left|\frac{\sigma}{A(e^{j\theta})}\right|^2 \frac{d\theta}{2\pi}, \tag{2}$$

σ/A is the all-pole model to be quantized and $\hat{\sigma}/\hat{A}$ is its quantized version.

A suboptimal system which allows relatively large rates to be simulated with reasonably small memory requirements was proposed in [4], using the same distortion measure as the one in [2] and (1) but with a different expression obtained by adding and subtracting $\ln \alpha$ to the right term of (1), that is,

$$\left(\ln \frac{\alpha}{\sigma^2}\right) + \left(\frac{\alpha}{\hat{\sigma}^2} - \ln \frac{\alpha}{\hat{\sigma}^2} - 1\right). \tag{3}$$

This expression reflects the so-called "gain separation" property of the Itakura-Saito distortion measure. The first summand in (3) does not depend on $\hat{\sigma}$, while the second is nonnegative and equals zero if and only if $\hat{\sigma}^2 = \alpha$. Thus the first term is the gain-optimized distortion (i.e. Itakura distor tion) and is the value of the distortion when σ/A is encoded as $\sqrt{\alpha}/\hat{A}$. The second term is the contribution to the distortion when $\sqrt{\alpha}$ is quantized as $\hat{\sigma}$. Thus, appropiately defining d' and d", both of the distortion measures (1) and (3) have the form

$$d_{IS}\left(|\sigma/A|^2, |\hat{\sigma}/\hat{A}|^2\right)=d'\left(|\sigma/A|^2, |1/\hat{A}|^2\right) + d''\left(\sigma^2_{opt}, \hat{\sigma}^2\right), \qquad (4)$$

where

$$\sigma_{opt} = \sqrt{\alpha}. \qquad (5)$$

Using this "gain separation" property, a scheme to encode the LPC parameters is presented in [4]. It basically consists of encoding the normalized all-pole model 1/A, using d' and computing the value of the optimal gain $\sqrt{\alpha}$. Then the optimal gain $\sqrt{\alpha}$ is encoded with distortion d". We will refer to d" as the *scalar Itakura-Saito distortion.*

Algorithms to design the quantizers of the all pole model and the gain term using d' and d" respectively are given in [4].

A further simplification was proposed later for designing the normalized all-pole model quantizer. It consists of using $\frac{\alpha}{\sigma^2} - 1$ (called the gain-normalized Itakura-Saito distortion) instead of $\ln \frac{\alpha}{\sigma^2}$ (called the gain-optimized distortion). The approach was successful, in the sense that a system based on vector quantization with 10 bits per frame for the normalized filter 1/A, scalar quantization with 5 bits per frame for the optimal gain, 5 bits per frame for the pitch (at 50 models per second this yields 50 (10+5+5)=1000 bps) resulted in quantitative and subjective quality close to that of an LPC system with approximately optimal scalar quantization and optimal bit allocation at a rate of 2150 bps.

Thus, it can be seen that the gain plays an important role in these encoding systems [4] (25 percent of the transmission rate). Furthermore, when the parameters of the normalized all pole-model (or a transformation of them) are scalar-quantized, then the value of the optimal gain, using the Itakura-Saito distortion as fidelity criterion after they are quantized, is given by (5), and the fidelity criterion that should be used to design a quantizer for the optimal gain is the second term of the right hand side of (4). The gain usually requires about 10% of the transmission rate in these systems.

Another possible application of quotient based distortions can be found in the encoding of the excitation signal of LPC systems. Since the excitation signal s_n for voiced sounds is a nondeterministic periodic pulse train, $(s_n = s_{n+\tau})$ for a particular speech frame it can be represented in terms of its Fourier series as

$$s_n = \sum_{k=0}^{t-1} a_k \cos \frac{2\pi k}{t} n + b_k \sin \frac{2\pi k}{t} n \ .$$

Encoding this waveform can be done using a variety of fidelity criteria, and in particular, it can be done with a criterion closely related to the one used for encoding the LPC models, that is, a discrete version of the Itakura-Saito distortion [7]:

$$d_D = \frac{1}{2t} \sum_{k=0}^{t-1} \left\{ \frac{S_k}{\hat{S}_k} - \ln \frac{S_k}{\hat{S}_k} - 1 \right\},$$

where $S_k = E\left\{ a_k^2 + b_k^2 \right\}$. This measure, as well as its continuous version, both are based on cross-entropy concepts [2,7].

In this paper we present bounds for the rate-distortion function for quotient based distortion measures, and in particular for bandwidth compression systems that use the scalar Itakura-Saito distortion as fidelity criterion. In addition, an asymptotic approximation to the performance of the optimal scalar quantizer of these gain terms is derived. Finally, we use these bounds to evaluate the performance of an LPC gain quantizer in a product-codebook environment as described above, when the overal encoder performance is determined by means of the Itakura-Saito distortion function.

II. BOUNDS TO THE RATE-DISTORTION FUNCTION FOR THE SCALAR ITAKURA-SAITO DISTORTION

A. Quotient based distortion measures.

Let the n-dimensional vector $\underset{\sim}{x} = (x_1, \ldots, x_n)$ be the output of a continuos amplitude, discrete time source. Assume that the components of $\underset{\sim}{x}$ are independent, identically distributed (i.i.d) random variables with absolutely continuous probability distribution function and density function $P(x)$. Let $\underset{\sim}{y} = (y_1, \ldots, y_n)$ be an n-dimensional vector which is a member of the reproduction alphabet. The distortion that results from reproducing $\underset{\sim}{x}$ as $\underset{\sim}{y}$ is given by $d_n(\underset{\sim}{x},\underset{\sim}{y})=\frac{1}{n}\sum_{k=1}^{n} d(x_k,y_k)$ where $\{d_n,\ 1\leq n<\infty\}$ is the single letter fidelity criterion generated by the nonnegative function d. We know that the rate-distortion function R(D)[1] is a tool to determine the least rate at which information about the source must be conveyed to the user in order to achieve a prescribed fidelity as measured by the average value of a given distortion function. In particular, for a quotient type distortion measure, $d(x,y)=\rho(x/y)$ and a positive source $(P(x)=0,\ x<0)$, from Berger's results [1] and [10] it follows that:

Proposition 1.

For a positive, discrete memoryless source, using a quotient based single letter fidelity criterion, the rate distortion function R(D) is parametrically lower bounded by

$$R(D_s)\ \geq\ R_L(D_s)=h(P)-\int_0^\infty dx\ P(x)\ell n\,x-h(F_s)+\int_0^\infty dxF_s(x)\ell n\,x\ , \tag{7}$$

$$D_s=\int_0^\infty dxF_s(x)\rho(x)\ , \tag{8}$$

where h(P) is the differential entropy of the probability density $P(\cdot)$, $F_s(x)$ is a probability density function defined by

$$F_s(x)=\frac{1}{x}\,e^{-s\rho(x)}\left(\int_0^\infty\frac{dz}{z}\,e^{-s\rho(z)}\right)^{-1} \tag{9}$$

and s is a positive real parameter. In addition, for any positive value of this parameter, the lower bound $R_L(D)$ (called the Shannon lower bound), coincides with R(D) (i.e., (7) is a equality) if and only if the random variables x associated with the source output can be represented as the product of two independent random variables, one of which is distributed according to the probability density function $F_s(x)$, as given by (9). This in turn is equivalent to the fact that the integral equation

$$P(x)\ =\int_0^\infty\frac{dy}{y}\,F_s\left(\frac{x}{y}\right)\,Q_s(y) \tag{10}$$

has a solution $Q_s(y)$ which is a valid density function.

Proposition 2.

For a nonnegative discrete memoryless source under a quotient single-letter distortion measure, the rate distortion function is upper bounded by

$$R(D_s)\ \leq\ R_u(D_s)=h(Q_s)-\int_0^\infty dxQ_s(x)\ell n\,x-\ h(F_s)+\int_0^\infty dxF_s(x)\ell n\,x\ , \tag{11}$$

where

$$Q_s(y) = \int_0^\infty dx\ q_s(y|x)\ P(x) \tag{12}$$

$$q_s(y|x) = F_s(x/y)x/y^2, \tag{13}$$

and D_s is given in (8).

We now turn to the particular case in which the single-letter fidelity criterion is the scalar version of the Itakura-Saito distortion measure.

B.1 Scalar version of the Itakura-Saito measure.

Let the scalar Itakura-Saito single letter distortion measure between source and reproduction symbols be given as in the right hand component d" in (4), namely by,

$$d_{IS}(x,y) = x/y - \ell n\ x/y - 1, \tag{14}$$

and let

$$\rho(z) = z - \ell n\ z - 1 \tag{15}$$

Substituting (15) into (9), it can be easily concluded that for the scalar Itakura-Saito measure and for any source distribution, the density $F_s(x)$ (of the multiplicative noise see Berger,[1,pp 94]) is the gamma density with unit mean and second moment given by $E(x^2) = (s+1)/s$, that is

$$F_s(x) = \frac{s^s}{\Gamma(s)} x^{s-1} e^{-sx}, \tag{16}$$

where $\Gamma(s)$ is the gamma function

Using this density in the last two terms of the right side of (7) yields

$$h(F_s) = s + \ell n\ \Gamma(s) - \ell n\ s - (s-1)\ \psi(s) \tag{17}$$

$$\int_0^\infty dx F_s(x) \ell n\, x = \psi(s) - \ell n\, s = -D_s \tag{18}$$

where D_s is given by (8) and $\psi(s)$ is the psi function. Therefore, upon substituting (15)-(17) into (7) and (8), the parametric equations for the lower bound of the rate distortion function result in

$$R_L(D_s) = h(P) - E(\ell nx) - (s - s\psi(s) + \ell n\ \Gamma(s)) \tag{19}$$

$$D_s = \ell n\ s - \psi(s). \tag{20}$$

It can be observed from (19) that this lower bound is, as expected, a function of the source output probability density function $P(\cdot)$. We now turn to the analysis of particular cases.

B.2 Gamma source.

As it will be seen later, the gamma distribution plays a similar role in the context of the scalar Itakura-Saito distortion measure, as does a Gaussian distribution in the context of mean-squared-error encoding. Thus, assume that the density function P(x) of the discrete memoryless source is of the gamma family with parameters (α,β), that is

$$P(x) = \frac{\beta^{-\alpha} x^{\alpha-1} e^{-x/\beta}}{\Gamma(\alpha)}, \quad x \geq 0, \tag{21}$$

with positive parameters α and β

Thus, (19) can be reduced to the form

$$R_L(D_s) = (\alpha - s) + \ln\frac{\Gamma(\alpha)}{\Gamma(s)} - \Big(\alpha\,\psi(\alpha) - s\,\psi(s)\Big) \tag{22}$$

Let D_{max} be the minimum average distortion at zero transmission rate. Then $D_{max} = \min_y E\,\{d_{IS}(x,y)\} = E\{d_{IS}(x, E\{x\})\} = -\,E\{\ln x\} + \ln E\{x\}$, and for the gamma source this yields

$$D_{max} = \ln\alpha - \psi(\alpha). \tag{23}$$

An interesting property of gamma sources using d_{IS} as the single letter fidelity criterion, and the lower bound defined parametrically by means of (22) and (20) is given in the following proposition (all the proofs are given in [10]).

Proposition 3.

The Shannon lower bound $R_L(D)$ to the rate distortion function of a discrete memoryless gamma source with parameters α and β (see (21)) under the scalar Itakura-Saito distortion measure, coincides with R(D) on the interval $0 \leq D \leq D_{max}$. This rate distortion function will be denoted by $R_{G,\alpha}(D)$.

B.3 General source distribution.

Consider now the case where the discrete memoryless source has an unknown distribution, and only the mean value and the maximum distortion at zero rate is known. The following propositions give the greatest Shannon lower bound and an upper bound for the rate distortion function.

Proposition 4.

Let Λ be the family of positive discrete memoryless sources with mean value equal to a and minimum average distortion at zero rate equal to D_{max}, i.e., $-E\{\ell n\ x\} + \ell n\ E\{x\} = D_{max}$.

The source that achieves the greatest Shannon lower bound of the rate distortion function has a marginal density function which is a gamma function with parameters (α,β), where α is given by the solution of the equation $\ell n\ \alpha - \psi(\alpha) = D_{max}$, and $\beta = a/\alpha$. That is, $R_{G,\alpha}(D) = \max_{P\in\Lambda} R_L(Ds)$.

Proposition 5.

Let a positive discrete memoryless source be such that the mean value of the output and the minimum average distortion at zero rate are given by $E\{x\}=a$, $-E\{\ell nx\} + \ell n\ E\{x\} = D_{max}$.

Then the rate distortion function is upper bounded as

$$R(D_s) < R_u(D_s) = (r-s) + \ell n \frac{\Gamma(r)}{\Gamma(s)} - (r\psi(r) - s\psi(s)),\ D_s = \ell n\ s - \psi(s) \qquad (24)$$

for all $s > 1$ or equivalently, for distortions $D_s < C = 0.57721$ ... (Euler's constant), and the parameter r is the solution to $\ln r - \psi(r) = D_{max} - D_s + \ell n \frac{s}{s-1}$. Furthermore, when $D_s \to 0$, then $R_u(D_s) \to R_{G,\alpha}(D_s)$. It can be concluded that if $\tilde{R}(D)$ is the rate distortion function with respect to the scalar Itakura-Saito measure, of the worst source with minimum average distortion at zero rate equal to D_{max}, then, $R_{G,\alpha}(D) \leq \tilde{R}(D) \leq \bar{R}_u(D)$, and so, asymptotically, *the gamma source is the worst case to be encoded with the scalar Itakura-Saito measure, when only the minimum average distortion at zero rate is known.*

In the next section the bounds that were derived in the previous paragraphs are used to evaluate the performance of Lloyd's scalar quantization of a memoryless gamma source when the distortion is measured by the scalar Itakura-Saito function. A better evaluation is one based on lower bounds derived as asymptotic performances of optimal scalar quantizers as $N \to \infty$. These results are based on Berger's derivations [2, ch. 5] and [8].

B.4 Asymptotically optimal quantization

Given a fixed N, an optimal quantizer minimizes a distortion function over the N reproduction points and over the boundaries between the levels. Gish and Pierce [9] derived asymptotic approximations for the distortion, as N is large and when the distortion is a function of the difference between source and reproduction symbols. This was later generalized for other distortions and to several dimensions. In particular, we follow [8] to obtain an asymptotic lower bound for the quantizer which minimizes the scalar

Itakura-Saito distortion. Let a discrete-time memoryless source generate positive, i.i.d, random variables with density $P(x)$ whose support is (a,b). Let T_k be the thresholds of an N level scalar quantizer ($a=T_0, b=T_N$). If the single letter distortion from reproducing x by y is of the quotient type, $\rho(\frac{x}{y})$, then the average distortion is

$$D = E\,\{\rho(x/Q(x))\} = \sum_{k=1}^{N} \int_{T_{k-1}}^{T_k} P(x)\,\rho(\hat{x}/x_k)\,dx. \qquad (25)$$

If N is large and $\rho(\frac{x}{y})$ is the scalar Itakura-Saito function, then the average distortion can be bounded as shown in the next proposition.

Proposition 6.

Under the above set of hypotheses, and if $P(x)$ is gamma with parameters (α,β), then [10]:

$$\bar{D} \geq \frac{1}{\Gamma(\alpha)} \sum_{k=1}^{\infty} \frac{1}{(2k+1)!} \frac{1}{(2N)^{2k}} (2k+1)^{\alpha} \left[\Gamma\left(\frac{\alpha}{2k+1}\right)\right]^{2k+1} \qquad (26)$$

III. EXPERIMENTAL EVALUATION

Two sets of eight scalar quantizers were designed with Lloyd's Algorithms [10] : one was based on a training sequence of gain terms, generated from 11000 frames of pre-processed sampled male speech. The training sequence of optimal gains was obtained from 11000 sets of LPC coefficentes, quantizing the normalized all-pole model coefficients using [4] and computing the gain for each frame using (5). D_{max} was estimated with arithmetic means. Since our results are interesting when applied to a gamma source (the LPC gains are not gamma), a second set of scalar quantizers was designed, using a training sequence of 25000 samples from a memoryless gamma source, with D_{max} as computed from the LPC optimal gains of the first training sequence. We also compute the bounds for $R_1(D)$ of a source with a fixed but unknown distribution (we omit the subindex 1). From the experimental D_{max}, using proposition 4 and 5, we compute the worst case Shannon lower bound $R_{G,\alpha}(D)$ and the upper bound $R_u(D)$ of (24). The functions $R_{G,\alpha}(D)$, $R_u(D)$ are presented in Fig.1, from which it can be seen that the worst case rate distortion function for the optimal LPC gains source is practically known in the range $D<0.1$ or $R>2.5$ bits/gain term ($R_u(D)-R_{G,\alpha}(D)<0.06$ for $D<0.1$). The worst case rate distortion function is within 2% of the rate distortion function for the above memoryless gamma source, $R_{G,\alpha}(D)$. The performance of Lloyd's quantizer for the source which generates the optimal LPC gains, inside as well as outside the training sequence is also shown. The quantizer performance is within 3% of the worst-case source with the same D_{max} (from 1 to 8 bits/sample). Fig. 2 shows the rate distortion function for the gamma source with scalar Itakura-Saito function, a lower bound to the asymptotic performance of the optimal scalar quantizer, and the performance of the scalar quantizer designed with [5,6] . Note that for a fixed distortion, the best scalar quantizer is at least one bit/sample above the rate distortion bound for large rates. For lower rates (5 bits/sample) the performance of the designed quantizer and the lower bound to the asymptotic approximation coincide, (but the validity of the asymptotic approximation is questionable in this region). It can be seen that scalar quantizing a gamma source at 5 bits/sample, a reduction of 1.3 bits/sample is in principle possible for the same D.

IV. CONCLUSIONS

Some information theoretic results, previously applied to difference distortions can be extended to measures based on quotients. The Itakura-Saito distortion, used in speech coding [2,3] , has a scalar version which is quotient based, and shares the above properties with the original Itakura-Saito function. The performance of Lloyd's quantizer (scalar) for a source of optimal

LPC gains using the scalar Itakura-Saito distortion, is comparable to the rate distortion function, with the same fidelity criterion, of the worst-case source (gamma) with the zero-rate minimum distortion (for R>2 bits/symbol). The worst-case source for the scalar Itakura-Saito distortion and a given D_{max} is gamma.

REFERENCES

[1] T. Berger, Rate Distortion Theory: A Mathematical Basis for Data Compression, Prentice Hall, Englewood Cliffs, NJ, 1971. [2] R.M. Gray, A.H. Gray, Jr., G. Rebolledo, and J.E. Shore, "Rate distortion speech coding with a minimum discrimination information distortion measure", IEEE Trans. Inform. Theory Vol. IT-12, pp.708-721, Nov. 1981.[3] R.M. Gray, A. Buzo, A.H. Gray and Y. Matsuyama, "Distortion Measures for Speech Processing", IEEE Trans. on Acoust., Speech, and Signal Processing, Vol.ASSP-28, pp.367-376, Aug.1980. [4]M.J. Sabin and R.M. Gray, "Product Code Vector Quantizers for Waveform and Voice Coding", IEEE Trans. Acoust., Speech and Signal Processing, Vol. ASSP-32, pp.479-488, June 1984. [5] S.P. Lloyd, "Least Squares Quantization in PCM", IEEE Trans.Inform.Theory Vol.IT-28, pp.129-137, March 1982. [6] Y. Linde, A. Buzo and R.M. Gray, "An algorithm for vector quantizer design", IEEE Trans.Commun., Vol.COM-28, pp.89-95, Jan.1980. [7] J.E. Shore, "Minimum Cross-Entropy Spectral Analysis", IEEE Trans.Acoust., Speech and Signal Processing, Vol.ASSP-29, pp.230-237, April 1981. [8] R.M.Gray and A.H.Gray, Jr., "Asymptotically Optimal Quantizers". IEEE Trans.Inform.Theory Vol.IT-23 , pp.143-144, Jan.1977. [9] H. Gish and J.N. Pierce, "Asymptotically Efficient Quantizers", IEEE Trans.Inform.Theory, Vol.IT-14, pp.678-683, Sept. 1968. [10] A. Buzo, F. Kuhlmann, C. Rivera, "Rate distortion bounds for quotient based distortions with application to Itakura-Saito distortion", IEEE Trans. Inform. Theory, to appear.

Fig. 1
Rate (bits/sample) vs. Distortion ($\log_{10}$(average scalar Itakura-Saito)

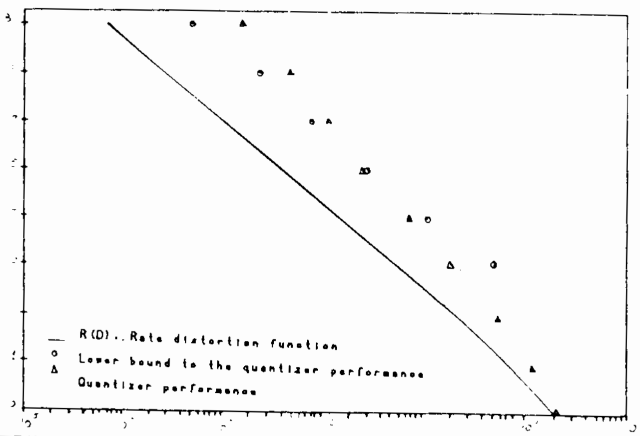

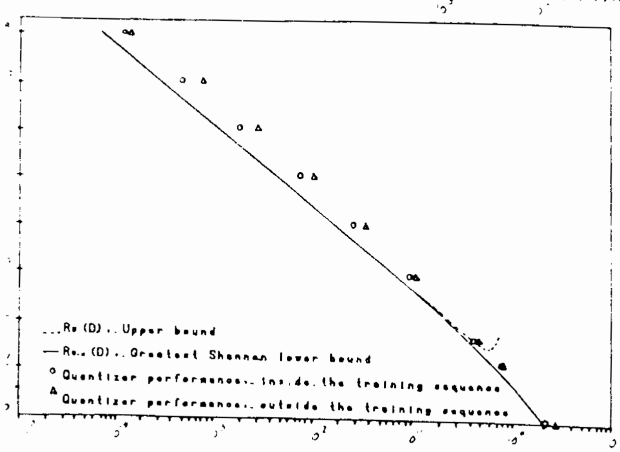

Fig. 2
Rate (bits/sample) vs. Distortion ($\log_{10}$ (average scalar Itakura-Saito)

H. Cinco-Ley, F. Samaniego, et al

THE PRESSURE TRANSIENT BEHAVIOR FOR NATURALLY

FRACTURED RESERVOIRS WITH MULTIPLE BLOCK SIZE.

Society of Petroleum Engineers. September 22-25, 1985

SPE 14168

SPE

Society of Petroleum Engineers

SPE 14168

The Pressure Transient Behavior for Naturally Fractured Reservoirs With Multiple Block Size

by H. Cinco-Ley and F. Samaniego V., *Pemex and UNAM*, and F. Kucuk, *Schlumberger*

SPE Members

ABSTRACT

A new analytical model is presented to study the pressure-transient behavior of a naturally fractured reservoir composed of a fracture network and matrix blocks of multiple size. Matrix blocks are considered to be uniformly distributed--through a reservoir of infinite extent. A general model for fluid transfer between matrix and fractures is established; this model justifies the use of both the Warren and Root model and the transient matrix flow model for double porosity systems.

The multiple block size situation is handled through the use of a distribution function $f(h_{ma})$ that represents the fraction of matrix pore volume contained in blocks of size h_{ma}. It is demonstrated that classical parallel semilog straight lines can be present under these circumstances and the transition zone may exhibit the characteristic half slope straight line when there is no flow restriction between matrix and fractures; --however, the transition between the end of the second and the third semilog straight line appears to be longer. It is found that the behavior of this type of systems is dominated by matrix of smaller size and the matrix blocks size computed from well testing by using the semilog straight line intersection method corresponds to the weighted harmonic average; that is, in discrete form $1/\bar{h}_{ma} = \sum_{i=1}^{NB} fi/h_{mai}$ where NB is the number of block sizes.

On the other hand, the λ value from well test analysis corresponds to the arithmetic weighted average, that is $\lambda = \sum_{i=1}^{NB} f_i \lambda_i$. These findings are important when applying the transient pressure result to waterflooding project design.

INTRODUCTION

A significant portion of the world hydrocarbons reserves are contained in naturally fractured reservoirs. An optimum development an exploitation of these reservoirs requires a complete characterization of the system. One of the most important methods to achieve this goal is the pressure transient testing[1,2] which is used to determine the degree of communication between wells and the fracturing characteristics of the reservoir among other things. Several models have been developed for the analysis of the data collected through this kind of testing; these models include the anisotropic medium, the multiple zone medium, the single fracture system and the so called "double porosity reservoir". The double porosity reservoir has received special attention through the publication of many papers[3-45].

In general, a double porosity reservoir is considered to be composed of matrix blocks and fractures uniformly distributed throughout the medium. Although the matrix possesses a permeability such that fluid is transferred to the fractures, the flow of fluid towards the well is assumed to occur via - the fracture network only. Models with different matrix block geometries have been studied including slabs, cylinders, -- spheres, cubes and parallelepipeds.

It has been demonstrated that the pressure behavior in these system is drastically affected by the way the fluid is transferred from matrix into fractures. Based on this aspect, the double porosity reservoirs can be classified as: a) matrix pseudo-steady-state flow model (Warren and Root) and b) matrix transient flow model (de Swaan and Kazemi). The former characterizes the behavior by using two dimensionless parameters ω and λ, the fracture storage ratio and the interflow parameter, and the later uses three parameters, ω, η_{maD} and A_{fD}; η_{maD} represents the dimensionless hydraulic diffusivity of the matrix and A_{fD} is a parameter related to fracture area per unit of rock volume. One of the main assumptions of these models is that matrix blocks are of the same size and shape in the entire reservoir.

References and illustrations at end of paper.

The purpose of the present work is to develop an analytica model to study the pressure behavior of a double porosity reservoir composed of matrix blocks of multiple size. Special emphasis is given to the effect of a flow restriction between matrix and fractures because this situation appears to justify the application of the pseudo-steady-state matrix flow.

RESERVOIR FLOW MODEL

Let us consider a naturally fractured reservoir composed of matrix blocks of multiple size uniformly distributed throughout the medium. Let $f(h_{ma})$ be the frequency function for matrix blocks of size h_{ma} in such a way that

$$\int_{h_{min}}^{h_{max}} f(h_{ma})\, dh_{ma} = 1 \tag{1}$$

or in discretized form

$$\sum_{i=1}^{NB} f_i(h_{mai}) = 1 \tag{2}$$

where NB is the total number of block sizes.

The function f_i represents the pore volume stored in matrix blocks of size h_{mai} expressed as a fraction of the total pore volume of the matrix in the reservoir.

The model studied in this work is shown in Figure 1, where the fracture network has an equivalent permeability k_{fb}, a total compressibility c_{tf} and porosity ϕ_{fb}. The subscript b indicates that the parameter is defined by using the bulk volume (matrix and fractures). On the other hand, the matrix blocks have a permeability k_{ma}, a porosity ϕ_{ma} and a total compressibility c_{tma}. These parameters are the intrinsic properties defined by using the matrix rock volume.

A parameter, defined in a earlier work[34], that deserves special attention since is directly related to imbibition rate calculations is the fracture area per unit of rock volume A_{fb} (or per unit of matrix volume A_{fma}), that is, the area of interaction between fractures and matrix per unit of rock volume.

Slab matrix blocks

$$A_{fb} = \frac{2}{h_{ma}+h_f} = \frac{2}{h_{ma}}\frac{V_{ma}}{V_b} \tag{3}$$

$$A_{fma} = \frac{2}{h_{ma}} \tag{4}$$

Cube matrix blocks

$$A_{fb} = \frac{6\,h_{ma}^2}{(h_{ma}+h_f)^3} \tag{5}$$

$$A_{fma} = \frac{6}{h_{ma}} \tag{6}$$

both h_{ma} and h_f are defined in Fig. 2 and V_b and V_{ma} are the bulk volume and the matrix volume, respectively.

For a reservoir with multiple matrix block size A_{fb} and A_{fma} are:

$$A_{fb} = \int_{h_{min}}^{h_{max}} f(h_{ma})\, A_{fb}(h_{ma},h_f)\,dh_{ma} \tag{7}$$

and

$$A_{fma} = \int_{h_{min}}^{h_{max}} f(h_{ma})\, A_{fma}(h_{ma})\,dh_{ma} \tag{8}$$

which in discretized form become:

$$A_{fb} = \sum_{i=1}^{NB} f_i A_{fbi} \tag{9}$$

and

$$A_{fma} = \sum_{i=1}^{NB} f_i A_{fmai} \tag{10}$$

In the following, matrix blocks are assumed to be slabs. Other block geometries can be considered in a straight-forward manner. Also, a finite number of matrix block sizes are present in the reservoir.

Let us now assume that the flow in the reservoir occurs under the following conditions.

- Fluid flows towards a well only via the fracture network.
- Flow in the fractures obeys Darcy's Law.
- Pressure gradients are small throughout the reservoir.
- Gravity effects are negligible.
- The fracture network behaves as a homogeneous and isotropic porous medium.

The transient flow phenomenum in this type of reservoirs is described in cylindrical coordinates for radial flow in terms of dimensionless variables by:

$$\frac{1}{r_D}\frac{\partial}{\partial r_D}\left(r_D\frac{\partial p_{fD}}{\partial r_D}\right) - 8(1-\omega)\sum_{i=1}^{NB} f_i \eta_{maDi}\int_0^{t_D}\frac{\partial p_{fD}(\tau)}{\partial \tau}\sum_{n=0}^{\infty} e^{-(2n+1)^2\pi^2\eta_{maDi}(t_D-\tau)}\,d\tau = \omega\frac{\partial p_{fD}}{\partial t_D} \tag{11}$$

where the dimensionless parameters are defined as follows:

Dimensionless radius

$$r_D = \frac{r}{r_w} \tag{12}$$

Dimensionless fracture pressure drop

$$p_{fD} = \frac{k_{fb}\, h\, \Delta p_f}{\alpha\, qB\mu} \tag{13}$$

Dimensionless time

$$t_D = \frac{\beta\, k_{fb}\, t}{(\phi c_t)_t \mu r_w^2} \qquad (14)$$

Fracture storativity ratio

$$\omega = \frac{\phi_{fb} c_{tf}}{(\phi c_t)_t} \qquad (15)$$

Dimensionless matrix hydraulic diffusivity

$$\eta_{maDi} = \frac{k_{ma}\,(\phi c_t)_t\, r_w^2}{k_{fb}\,(\phi c_t)_{ma}\, h_{mai}^2} \qquad (16)$$

See Appendix A for derivation of Eq. 11

According to these equations the multiple block size characteristics of the medium are handled through the use of the functions f_i and η_{maDi}; this last parameter considers the matrix block size. Notice that values are required for f_i and η_{maDi} for different block sizes for the problem to be completely defined.

All t_D, ω and η_{maDi} are defined by using $(\phi c_t)_t$ which is given by:

$$(\phi c_t)_t = \phi_{fb} c_{tf} + \phi_{mab} c_{tma} \qquad (17)$$

and α and β are unit conversion constants given in Table 1.

PRESSURE SOLUTIONS FOR THE FLOW MODEL.

The pressure behavior caused by a well producing at constant rate in a naturally fractured reservoir with multiple block size is given by:

$$p_{fD}(r_D, t_D) = L^{-1}\left(\frac{1}{S^{3/2}[\omega+(1-\omega)g(f_i,\eta_{maDi},s)]^{\frac{1}{2}}} \cdot \frac{K_0\left(r_D s^{\frac{1}{2}}\, [\omega+(1-\omega)g(f_i,\eta_{maDi},s)]^{\frac{1}{2}}\right)}{K_1\left(s^{\frac{1}{2}}[\omega+(1-\omega)g(f_i\eta_{maDi},s]^{\frac{1}{2}}\right)} \right) \qquad (18)$$

where

$$g(f_i,\eta_{maDi},s) = 2\sum_{i=1}^{NB} f_i \sqrt{\frac{\eta_{maDi}}{s}}\ \tanh\sqrt{\frac{s}{(\frac{\eta_{maDi}}{2})}} \qquad (19)$$

See Appendix B for derivation of Eq. 18.

An analytical inversion in Eq. 18 yields a rather complex expression which can be difficult to evaluate; however, short, intermediate and long time behavior may be readily examined.

Short Time Behavior

At very small values of time t_D the matrix blocks contribution is negligible and the fluid is produced due to the expansion of the fluid in the fracture network. Under these conditions $s \to \infty$; the function $g(f_i, \eta_{maDi}, s)$ goes to zero and Equation 39 becomes:

$$\bar{p}_{fD} = \frac{K_0[r_D s^{\frac{1}{2}} \omega^{\frac{1}{2}}]}{s^{3/2}\omega K_1[s^{\frac{1}{2}}\omega^{\frac{1}{2}}]} \qquad (20)$$

this equation is similar to the solution for radial flow in a homogeneous system; that is, if large values of r_D are considered, inversion of Equation 20 yields the well known Line Source Solution:

$$p_{fD}(r_D,\omega,t_D) = \frac{1}{2}\, E_1\left[\frac{r_D^2}{4(t_D/\omega)}\right] \qquad (21)$$

The pressure drop at the wellbore for practical values of t_D is:

$$p_{wD}(\omega,\ t_D) = \tfrac{1}{2}[\ln(\frac{t_D}{\omega})+0.80907] \qquad (22)$$

this equation describes the behavior of a semilog straight line. Both Equations 21 and 22 give the reservoir pressure of the so called fracture network dominated flow period.

Long Time Behavior

At large values of time the expansion of the total system (fractures+matrix) contributes to fluid production and the flow in the matrix reaches a pseudo-steady-state like condition. Under this situation the g function becomes unity and Equation 18 simplifies to give:

$$\bar{p}_{fD}(r_D,s) = \frac{K_0[r_D s^{\frac{1}{2}}]}{s^{3/2} K_1(s^{\frac{1}{2}})} \qquad (23)$$

the Laplace inversion of this equation is the solution for radial flow in a homogeneous infinite reservoir which for large values of r_D produces the line source solution:

$$p_{fD}(r_D,t_D) = \tfrac{1}{2}E_1(\frac{r_D}{4t_D}) \qquad (24)$$

For practical values of time, the pressure at the wellbore is given by:

$$p_{wD} = \tfrac{1}{2}[\ln t_D + 0.80907] \qquad (25)$$

which also is the equation for a semilog straight line. Notice that Equation 22 and 25 are similar, the only difference is the parameter ω. These two equations correspond to the two parallel semilog straight lines.

Intermediate Time Behavior

At intermediate values of time, provided that ω is very small, the pressure behavior is dominated by linear flow in matrix blocks. Under these circumstances the function g is given by

$$g(f_i,\eta_{maDi},s) = 2\sum_{i=1}^{NB} f_i\,(\sqrt{\frac{\eta_{maDi}}{s}}) \qquad (26)$$

the Laplace inversion for times of interest and r_D=1 (wellbore) for Eq. 18 is:

$$p_{wD} = \frac{1}{4}\ln t_D - \frac{1}{2}\ln(2\sum_{i=1}^{NB} f_i\sqrt{\eta_{maDi}}) + 0.2602 \qquad (27)$$

this equation shows that there is an intermediate semilog straight line whose slope is equal to one half of the slope of the parallel semilog straight lines.

Approximate Solutions

For practical values of dimensionless time, some simplifications can be made. For instance the denominator of Equation 18 can be simplified by considering that

$$xK_1(x) \approx 1 \text{ when } x \to o$$

hence:

$$\bar{p}_{fD}(r_D,s) \approx \frac{K_o[\, r_D s^{\frac{1}{2}}(\omega+(1-\omega)2\sum_{i=1}^{NB} f_i \sqrt{\frac{\eta_{maDi}}{s}} \tanh(\sqrt{\frac{s}{\eta_{maDi}}}\frac{}{2}))^{\frac{1}{2}}]}{s}$$

(28)

furthermore, the pressure at the wellbore may be expressed as:

$$\bar{p}_{wD} = -\frac{1}{s} \cdot \left[\ln(\frac{s^{\frac{1}{2}}}{2}(\omega+(1-\omega)2\sum_{i=1}^{NB} f_i \frac{\overline{\eta_{maDi}}}{s}\tanh(\frac{\overline{\frac{s}{\eta_{maDi}}}}{2}))^{\frac{1}{2}})+\gamma\right]$$

(29)

$$\text{since } K_o(x) \approx -(\ln(\tfrac{x}{2})+\gamma) \text{ when } s \to o$$

γ is the Euler's constant (0.5772...)

From the computational point of view Eq. 29 appears to have advantage over Eq. 18 since evaluation of Bessel functions is not required.

Extension to the case of matrix-fracture flow restriction.

Mineral deposition at the fracture face can reduce the interaction between matrix and fractures in naturally fractured reservoirs. This situation delays the flow from matrix into fractures and can be handled as a skin damage (Fig. 3). Appendix C shows that a general model can be developed to consider both transient matrix flow model and pseudo-steady-state matrix flow. It is shown analytically that the use of the Warren and Root Model is justified by this situation and the parameter γ can be expressed in terms of a skin factor, A_{fD} and η_{maD} as follows:

$$\lambda = \frac{A_{fD}\eta_{maD}}{S_{maD}} \qquad (30)$$

where S_{maD} is a dimensionless parameter introduced to handle the matrix-fracture flow restriction. This variable is defined as:

$$S_{maD} = \frac{k_{ma} x_d}{k_d h_{ma}} \qquad (31)$$

k_{ma}, k_d, x_d and h_{ma} are the matrix permeability the damaged zone permeability, the thickness of damaged zone and the matrix block size, respectively. Figure 4 illustrates this type of model.

Equation 18 can be extended to take into account flow restriction between multiple size matrix blocks and fractures (Fig. 5) by redefining the function g as follows:

$$g(f_i, \eta_{maDi}, S_{maDi}, s) = 2\sum_{i=1}^{NB} f_i \frac{\sqrt{\frac{\eta_{maDi}}{s}}\ \tanh((s/\eta_{maDi})^{\frac{1}{2}}/2)}{1+\ \frac{s}{\eta_{maDi}} S_{maDi}\ \tanh((s/\ _{maDi})^{\frac{1}{2}}/2)}$$

(32)

A model defined in this way allows to study the behavior of multiple matrix block size reservoirs in general fashion because considers both the transient matrix flow model (S_{maD}=0) and a pseudo-steady-state flow like model.

It can be shown that the parallel semilog straight lines do exist for this case. Furthermore, if ω is very small and $\eta_{maDi}/S_{maDi} << 1$, the transition period exhibit a stabilized pressure drop similar to the single matrix block size case. The stabilized pressure drop is given by:

$$p_{wD} = \ln(2(1/\sum_{i=1}^{NB} f_i A_{fDi}\ \eta_{maDi}/S_{maDi})^{\frac{1}{2}}) - \gamma$$

(33)

or:

$$p_{wD} = \ln(2(1/\sum_{i=1}^{NB} f_i\ \lambda_i)^{\frac{1}{2}}) - \gamma$$

(34)

Evaluation of Solutions

Solutions were evaluated by using the Stehfest numerical Laplace inverter[44] in a programmable calculator (HP41CV). It was found that ten terms in the series of the numerical inverter provided excellent results.

DISCUSSION OF RESULTS

Several cases were run to study the effect of different parameters on the pressure transient behavior of a well producing at constant rate. One, two, three and five block sizes were considered in addition to the restricted matrix-fracture flow situation. The matrix block size is included in the dimensionless matrix hydraulic diffusivity η_{maD} in such a way that different values of this parameter must be provided to study a multiple block size case.

First, a single matrix block size case was studied. The differences between the transient flow model and the model with flow restriction of the matrix-fracture interaction are shown in a semilog graph in Figure 6 ($\eta_{maD} = 10^{-8}$ and S_{maD}=1). Notice that the first model yields a lower dimensionless pressure drop exhibiting a straight line during the transition period between the two semilog straight lines; the slope of the transition straight line is one half the slope of the parallel semilog straight lines. The matrix-fracture low restriction model exhibits a rather flat transition zone; this behavior resembles the behavior of the Warren and Root model. In addition, it can be observed that the lower the value of ω the flatter the pressure curve in the transition zone.

Figure 7 presents a semilog graph for the behavior of naturally fractured reservoirs with different values of S_{maD} for $\eta_{maD} = 10^{-8}$ and $\omega = .01$. A high value of S_{maD} gives a higher pressure drop during the transition zone. The minimum value of the slope during the transition zone depends on η_{maD}; that is, the higher the S_{maD} value the lower the minimum slope of the transition zone. This fact is also illustrated in figure 8 where a graph of $t_D\, dp_D/dt_D$ (semilog slope) versus t_D is presented. In general, the presence of skin between fractures and matrix causes the fracture network dominated flow period to last longer because matrix-fracture interaction is delayed.

The results for a case where two matrix block sizes are acting ($\eta_{maD1} = 10^{-7}$, $\eta_{maD2} = 10^{-8}$, $\omega = 10^{-2}$) are shown in Fig. 9. Five cases are presented for different values of the block size distribution function f_i. It can be noticed as shown by the approximations of the solutions, that the transition zone exhibit a straight line portion whose slope is one half the slope of th parallel semilog straight lines. The pressure behavior is independent of the block size distribution function for small and large values of time. Furthermore, the pressure curves are closer to the curve representing the behavior of the smaller blocks ($\eta_{maD} = 10^{-7}$).

The curves in Figure 9 are smooth and it seems to be dif icult to detect from the shape the multiple block size nature of the reservoir; however, as indicated by Figure 10, the semilog slope curve shows a strong effect, that is, these curves exhibit two flat portions during the transition zone; again, the curves tend to be closer to the curve-representing the smaller matrix blocks. It should be pointed out that the cases considered in Figures 9 and 10 include two block sizes, being the size of the larger blocks around three times the size of the smaller matrix blocks.

The effect of a high contrast between block sizes is presented in Figures 11 and 12. Notice, as in the previous case, the curves tend to be closer to the curve representing the case of the smaller block size. Although the pressure curves (Fig. 11) are rather smooth to characterized these cases, the semilog slope curves (Fig. 12) appear to have a strong character.

The effect of the number of block sizes on pressure behavior is illustrated in Figure 13. Curves for one, two, three and five block sizes which are evenly distributed are presented. Although each case has a different curve, the shape of the pressure behavior curves is similar being difficult to identify each situation. The semilog slope curves are presented in Fig. 14, we can see that the curves for three and five are quite similar; however, for one and two block sizes the curves are completely different. It appears that as the number of block sizes; increases, for uniform distribution function f, the behavior approaches a smooth curve for both pressure and semilog slope.

The effect of the shape of the block size distribution function is shown in Figures 15 and 16. Here, five different block sizes are considered ($\eta_{maDi} = 10^{-8}$, $5x10^{-8}$, 10^{-7}, $5x10^{-7}$ and 10^{-6}) and the interaction between matrix blocks and matrix is not restricted ($S_{maDi} = 0$). Several sets of distribution functions were studied, they include the even distribution case and cases where a particular block size is the dominant one (see upper left corner in Figures 15 and 16). It can be observed that different cases exhibit pressure curves of similar shape; the pressure behavior is given by rather smooth curves all of them showing the straight line portion in the transition period. The curves for the semilog slope (Fig. 16) are different for the cases included in this study, and they exhibit oscillations indicating the multiple block size nature of the reservoir.

Figure 17 shows the pressure behavior for a reservoir composed of matrix blocks of two sizes ($\eta_{maDi} = 10^{-8}$, 10^{-6}) with matrix-fracture flow restriction ($S_{maDi} = 10$, 1). The curves for different sets of block size distribution function f_i exhibit similar shapes during the transition period; however, the semilog slope curves (Fig. 18) show again different shape for different cases.

From the results for the cases examined in this work we can say that a naturally fractured reservoir with multiple block size may exhibit the classical parallel semilog straight lines. The behavior of this system differs from the behavior for a single matrix block size system only in the transition period and it is difficult to identify the multiple block size nature of the reservoir by using the pressure alone, because the pressure behavior is a kind of average of the corresponding behavior of the components of the system and generally represented by a rather smooth curve.

On the other hand, the pressure derivative function ($t_D dp_D/dt_D$) does show oscillation, related to the different matrix block sizes of a reservoir. In general, it can be ovserved that the smaller matrix blocks (high η_{maDi}) dominates the wellbore pressure behavior during the transition period because small blocks have a high degree of interaction with fractures as a result of a large fracture area per unit of rock volume exhibited by this situation.

An interesting situation occurs when the reservoir has a wide range of matrix block sizes. Under this condition, the first semilog straight line does not exist. This is due to the fast matrix-fracture interaction exhibited by the very small blocks. For these cases, the transition period of the pressure cause is rather smooth approaching the correct semilog straight line a symptotically, resembling the behavior of a well intersected by a single fracture.

APPLICATIONS TO WELL TEST ANALYSIS.

The results obtained in this work can be applied to improve the analysis of pressure transient data for naturally fractured reservoirs with double porosity behavior. Several are the parameters of the reservoir estimated by well test analysis such as the fracture storativity ratio ω, the interflow parameter λ, the matrix block size h_{ma} and the fracture area per unit of rock volume A_{fb}.

The theory presented in this work, for the behavior of a naturally fractured reservoir with multiple block size, allows a better physical interpretation of the results obtained through the application of methods for single matrix block size models. From the results obtained in the previous section we can say that both ω and A_{fb} obtained from single matrix block size model can be interpreted as so for the multiple block size model; however, the physical meaning of both λ and h_{ma} obtained from single matrix block size model has to be modified when considering a multiple block size model.

From Equations 29, 30, 32 and Appendix C, the estimated value for λ through well test analysis appears to be:

$$\lambda = \sum_{i=1}^{NB} f_i \lambda_i \tag{35}$$

where λ_i is the interflow parameter for the ith matrix block size. Equation 35 indicates that the value for λ estimated from well test analysis corresponds to the arithmetic weighted average.

The matrix block size for a single matrix block size reservoir can be estimated in well test analysis from the time of intersection of the transition semilog straight line and the final semilog straight line. For a multiple block size reservoir, in accordance to Equations 25 and 27, a parameter calculated in this fashion yields:

$$h_{ma} = \left[\sum_{i=1}^{NB} \frac{f_i}{h_{mai}} \right]^{-1} \tag{36}$$

this equation indicates that the matrix block size estimated from single matrix block size model represents the harmonic weighted average. In this type of average, the smaller size blocks have an important influence.

It can not be over emphasized that it is difficult to identify a multiple block size case by analysing the pressure alone, the semilog slope (pressure derivative function t dp/dt) seems to be a powerful tool when analyzing data in this type of reservoirs.

CONCLUSIONS

From the theory and results presented in this work the following remarks are pertinent:

1) An analytical model is presented to study the pressure transient behavior of a naturally fractured reservoir with multiple size matrix blocks.

2) The use of the Warren and Root model for double porosity systems can be justified by considering a damaged zone between matrix blocks an fractures.

3) The pressure behavior of a well in a multiple block size system may exhibit the classical behavior of single block size double porosity systems.

4) The first semilog straight line does not exist in the behavior of a well in a naturally fractured reservoir with a wide range of block sizes including very small matrix blocks.

5) The parameters ω and A_{fb} calculated from single matrix block size model are correct for a multiple block size reservoir.

6) The parameter λ calculated from the single matrix block size model corresponds to the arithmetic weighted average for a multiple block size reservoir.

7) The matrix block size h_{ma} estimated from the single matrix block size model corresponds to the harmonic weighted average for a multiple block size reservoir.

8) The multiple block size nature of a reservoir can not be identified by analyzing the pressure alone.

9) The pressure derivative functions is a powerful tool to identify the multiple block size nature of a naturally fractured reservoir.

ACKNOWLEDGMENTS

The development of the present work was supported by Schlumberger Well Services and UNAM.

NOMENCLATURE

A_{fma} = Fracture area per unit of matrix volume
A_{fb} = Fracture area per unit of bulk volume
A_{fD} = Dimensionless fracture area
B = Formation volume factor.
c = Fluid compressibility
c_{tf} = Fracture system total compressibility
c_t = Total compressibility
f = Block size distribution function
h = Formation thickness
h_{ma} = Matrix block size
k = Permeability
p = Pressure
p_D = Dimensionless pressure
p'_D = Dimensionless pressure derivative
p_i = Initial reservoir pressure
Δp = Pressure change
q = Well flow rate
r = Distance to production well
r_w = Wellbore radius
S = Van Everdingen and Hust skin factor
S_{maD} = Dimensionless damage parameter for matrix fracture flow restriction.
s = Laplace transform variable
t = Time
t_D = Dimensionless time
V = Volume
x = Distance, thickness
γ = Euler constant (0.577216)

λ = Interporosity flow coefficient

η = Hydraulic diffusivity

μ = Fluid viscosity

ϕ = Porosity

ω = Dimensionless fracture storativity

SUBSCRIPTS

b = bulk, beginning

d = damaged zone

D = Dimensionless

f = fracture

fb = fracture referred to bulk volume

i = ith matrix block

ma = matrix

surf = surface

t = total

uma = unitary step pressure drop at matrix surface

REFERENCES

1. Matthews, C. S. and Russell, D.G.: Pressure Build-up and Flow Tests in Wells, Monograph Series, Society of Petroleum Engineers of AIME, Dallas (1967) 1.

2. Earlougher, R.C., Jr.: Advances in Well Test Analysis, Monograph Series, Society of Petroleum Engineers of AIME Dallas (1977) 5.

3. Pollard, P.: "Evaluation of Acid Treatments from Pressure" Build-up Analysis, Trans., AIME (1959) 216, 38-42.

4. Pirson, R.S. and Pirson S. J.: "An Extension of the Pollard Analysis Method of Well Pressure Build-up and Drawdown Tests", paper SPE 101 presented at the SPE Annual Fall Meeting, Dallas, Oct. 8-11, 1961.

5. Barenblatt, G.I. and Zheltov, Yu. P.: "Fundamental Equations of Filtration of Homogeneous Liquids in Fissured Rocks", Soviet Physics Doklady (1960) Vol. 5, 522-525.

6. Barenblatt, G.I., Zheltov, Iu. P. and Kochina, I.N.: "Basic Concepts in the Theory of Seepage of Homogeneous Liquids in Fissure Rocks (strata)", (in Russian), PMM (1960) Vol. 24, No. 5 852-864.

7. Warren, J.E. and Root, P.J.: "The Behavior of Naturally Fractured Reservoirs", Soc. Pet. Eng. J. (Sept. 1963) 245-255; Trans. AIME, Vol. 228.

8. Warren, J.E. and Root, P.J.: "Discussion on Unsteady-State Behavior of Naturally Fractured Reservoirs," Soc. Pet. Eng. J. (March 1965) 64-65; Trans., AIME, 234.

9. Odeh, A.S.: "Unsteady-State Behavior of Naturally Fractured Reservoirs", Soc. Pet. Eng. J. (March 1965) 60-66.

10. Adams, A.R., Ramey, H.J., Jr. and Burgess, R.J.: "Gas Well Testing in a Fractured Carbonate Reservoir", J. Pet. Tech. (Oct. 1968) 1187-1194; Trans., AIME, 243.

11. Kazemi, H.: "Pressure Transient Analysis of Naturally Fractured Reservoirs with Uniforme Fracture Distribution", Soc. Pet. Eng. J. (Dec. 1969) 451-458.

12. Gringarten, A.C. and Witherspoon, P.A.: "A Method of Analyzing Pumping Test Data from Fractured Aquifer", Proc. Symp. Percolation Fissured Rock, Ing. Soc. Rock Mech.,

13. de Swaan, O.A.: "Analytic Solutions for Determining Naturally Fractured Reservoir Properties by Well Testing", Soc. Pet. Eng. J. (June 1976) 117-122; Trans. AIME, 261.

14. Crawford, G.E., Hagedorn, A.R. and Pierce, A.E.: "Analysis of Pressure Buildup Tests in Naturally Fractured Reservoirs" J. Pet. Tech. (Nov. 1976) 1295-1300.

15. Strobel, C. J., Gulati, M.S., and Ramey, H.J., Jr.: "Reservoir Limit Tests in a Naturally Fractured Reservoir -- A Field Case Study Using Type Curves", J. Pet. Tech. (Sept. 1976), 1097-1106.

16. Mavor, M.L. and Cinco-Ley, H.: "Transient Pressure Behavior of Naturally Fractured Reservoirs", paper SPE 7977 presented at the SPE 1979 California Regional Meeting, Ventura, Ca., April 18-20, 1979.

17. Streltsova, T.D.: "Hydrodynamics of Groundwater Flow in a Fractured Formations", Water Resources, Res. 12 (3) 1976, 405-414.

18. Ershaghi, I., Rhee, S.W., and Yang h-T: "Analysis of Pressure Transient Data in Naturally Fractured Reservoirs With Spherical Flow", paper SPE 6018 presented at the SPE 51st Annual Fall Technical Conference and Exhibition, New Orleans, Oct. 3-6, 1976.

19. Uldricht, D.O. and Ershaghi, I.: "A Method for Estimating the Interporosity Flow Parameter in Naturally Fractured Reservoirs", paper SPE 7142 presented at the SPE 1978 California Regional Meeting, San Francisco, April 12-14, 1978.

20. Najurieta, H.L.: "Ensayos de Interferencia en Yacimientos Naturalmente Fracturados", Congreso Panamericano de Ingenieria de Petroleo, Mexico, D.F., March 19-73, 1979.

21. Najurieta, H.L.: "Interference and Pulse Testing in Uniformly Fractured Reservoirs", Paper SPE 8283 presented at the 54th Annual Fall Technical Conference and Exhibition Las Vegas, Nevada, Sept. 23-28, 1979.

22. Najurieta, H.L.: "A Theory for Pressure Transient Analysis in Naturally Fractured Reservoirs", J. Pet. Tech. (July 1980) 1241-1250.

23. Kucuk, F. and Sawyer, W.K.: "Transient Flow in Naturally Fractured Reservoirs and its Application to Devonian Gas Shales", paper SPE 9397 presented at the SPE 55th Annual Fall Technical Conference and Exhibition, Dallas, Texas, Sept. 21-24, 1980.

24. Gringarten, A.C.: "Flow Tests Evaluation of Fractured Formations", presented at the Symposium on Recent Trends in Hydrology, Berkeley, Ca., Feb. 8-9, 1979.

25. Da Prat, G., Ramey, H.J., Jr. and Cinco-Ley, H.: "A Method to Determine the Permeability-Thickness Product for a Naturally Fractured Reservoirs".

26. Bourdet, D. and Gringarten, A.C.: "Determination of Fissured Volume and Block Size in Fractured Reservoirs by Type-Curve Analysis", paper SPE 9293 presented at the SPE 55th Annual Technical Conference and Exhibition, Dallas, Texas, Sept. 21-24, 1980.

27. Raghavan, R. and Ohaeri, C.U.,: "Unsteady Flow to a Well Produced at Constant Pressure in a Fractured Reservoir" paper SPE 9902 presented at the SPE 1981 California Regional Meeting, Bakersfield, March 25-26, 1981.

28. Gringarten, A.C., Burgess, T.M., Viturat, D., Pelissier, J. and Aubry M.: "Evaluating Fissured Formation Geometry from Well Test Data: a Field Example", paper SPE 10182 presented at the SPE 56th Annual Fall Technical Conference and Exhibition, San Antonio, Texas, Oct. 5-7, 1981.

29. Stewart, G., Wittmann, S.T., and Van Golf-Racht, T.: "The Application of the Repeat Formation Tester to the Analysis of Naturally Fractured Reservoirs", paper SPE 10181 presented at the SPE 56th Annual Fall Technical Conference and Exhibition, San Antonio, Texas, Oct. 5-7, 1981.

30. Da Prat, G., Cinco-Ley, H. and Ramey, H.J. Jr.: "Decline Curve Analysis Using Type Curves for Two-Porosity Systems", Soc. Pet. Eng. J. (June 1981) 354-362.

31. Gringarten, A.C.: "Interpretation of Tests in Fissured Reservoirs and Multilayered Reservoirs with Double Porosity Behavior: Theory and Practice", paper SPE 10044 presented at the SPE International Petroleum Exhibition and Technical Symposium, Beijing, China, March 26-28, 1982.

32. Streltsova, T.D.: "Well Pressure Behavior of a Naturally Fractured Reservoirs", paper SPE 10782 presented at the SPE 1982 California Regional Meeting, San Francisco, Ca., March 24-26, 1982.

33. Serra, K.V. Reynolds, A.C. and Raghavan, R: "New Pressure Transient Analysis Methods for Naturally Fractured Reservoirs", paper SPE 10780 presented at the SPE 1982 California Regional Meeting, San Francisco, Ca., March 24-26, 1982.

34. Cinco-Ley, H. and Samaniego-V., F.: "Pressure Transient Analysis for Naturally Fractured Reservoirs", paper SPE 11026 presented at the SPE 57th Annual Fall Technical Conference and Exhibition, New Orleans, LA, Sept. 26-29, 1982.

35. Chen, Chih-Cheng, Yeh, N.S., Raghavan, R. and Reynolds, A. C., Jr.: "Pressure Response at Observation Wells in Fractured Reservoir", paper SPE 10839 presented at the SPE/DOE Unconventional Gas Recovery Symposium of SPE of AIME, Pittsburgh, PA, May 16-18, 1982.

36. Da Prat, G.: "Well Test Analysis for Naturally Fractured Reservoirs", Proceedings, Stanford Geothermal Workshop, Stanford, Ca., Dec. 1982.

37. Ohaeri, C.U.: "Pressure Buildup Analysis for a Well Produced at a Constant Pressure in a Naturally Fractured Reservoir", paper SPE 12009 presented at the 58th Annual Technical Conference and Exhibition, San Francisco, Ca., 5-8, 1983

38. Reynolds, A.C., Jr. and Chang, W.C.: "Well Test Analysis for Naturally Fractured Reservoirs", paper SPE 12012 presented at the 58th Annual Technical Conference and Exhibition, San Francisco, Ca., Oct. 5-8, 1983.

39. Lai, C.H., Bolvarson, G.L., Tsang, C.F. and Witherspoon, P.A.: "A New Model for Well Test Data Analysis for Naturally Fractured Reservoirs", paper SPE 11688 presented at the 1983 California Regional Meeting, Ventura, Ca., March 23-25, 1983.

40. Ershaghi, I. and Aflaki, R.: "Problems in Characterization of Naturally Fractured Reservoirs From Well Test Data", paper SPE 12014 presented at the 58th Annual Technical Conference and Exhibition, San Francisco, Ca., Oct. 5-8, 1983.

41. Bourdet, J.A., Ayoub, J.A., Whittle, T.M., Pirard, Y.M. and Kniazeff, V.: "Interpreting Well Tests in Fractured Reservoirs", World Oil, Oct. 1983.

42. House, O.P., Horne, R.N. and Ramey, H.J., Jr.: "Infinite Conductivity Vertical Fracture in a Reservoir with Double Porosity Behavior", paper SPE 12778 presented at the 1984 California Regional Meeting, Long Beach, Ca., April 11-13, 1984.

43. Wijesinghe, A.M. and Culham, W.E.: "Single-Well Pressure Testing Solutions for Naturally Fractured Reservoirs with Arbitrary Fracture Connectivity", paper SPE 13055 presented at the 59th Annual Technical Conference and Exhibition, Houston, Texas, Sept. 16-19, 1984.

44. Stehfest, H.: "Numerical Inversion of Laplace Transforms, Communications of the ACM (January, 1970), 13, No. 1, 47-49.

45. Moench, A.F.: "Double-Porosity Models for a Fissured Groundwater Reservoir with Fracture Skin", Water Resovr. Res., Vol. 20, No. 7 (July, 1984) 831-846.

APPENDIX A

DERIVATION OF FLOW MODEL FOR MULTIPLE BLOCK SIZE RESERVOIR.

The transient flow phenomenum through a double porosity system is described for radial flow by the equation:

$$\frac{1}{r}\frac{\partial}{\partial r}\left(r\frac{\partial p_f}{\partial r}\right)+\frac{\mu q^*_{ma-f,b}}{k_{fb}}=\frac{\phi_{fb}c_{tf}\mu}{k_{fb}}\frac{\partial p_f}{\partial t} \tag{A-1}$$

where $q^*_{ma-f,b}$ is the matrix-fracture flow rate per unit of rock volume and is given by:

$$q^*_{ma-f,b}=\sum_{i=1}^{NB} f_i\left[-\frac{k_{ma}}{\mu}(\nabla p(h_{mai}))_{surf}\right]A_{fbi} \tag{A-2}$$

Equation (A-2) can be written as:

$$\frac{1}{r}\frac{\partial}{\partial r}\left(r\frac{\partial p_f}{\partial r}\right)-\frac{k_{ma}}{k_{fb}}\sum_{i=1}^{NB} f_i(\nabla p(h_{mai}))_{surf}A_{fbi}=\frac{\phi_{fb}c_{tf}}{k_{fb}}\frac{\partial p_f}{\partial t} \tag{A-3}$$

here $(\nabla p(h_{mai}))_{surf}$ is the pressure gradient at the face of a matrix block of size h_{mai}.

In order to obtain general a solution it is necessary to use dimensionless variables. By using Equations 12 through 14 of main text we obtain:

$$\frac{1}{r_D}\frac{\partial}{\partial r_D}\left(r_D\frac{\partial p_{fD}}{\partial r_D}\right)-\frac{k_{ma}}{k_{fb}}r_w^2\sum_{i=1}^{NB} f_iA_{fbi}\frac{2\pi k_{fb}h}{q\mu}(\nabla\Delta p_{ma}(h_{mai}))_{surf}=\frac{\phi_{fb}c_{tf}}{(\phi c_t)_t}\frac{\partial p_{fD}}{\partial t_D} \tag{A-4}$$

The relationship between the matrix pressure gradient and the fracture pressure is:

$$(\nabla\Delta p_{ma}(h_{mai}))_{surf}=\int_0^t\frac{\partial\Delta p_f(\tau)}{\partial\tau}(\nabla\Delta p_{ma}(h_{mai}))(t-\tau)_{surf,\ unit}\,d\tau \tag{A-5}$$

where $(\nabla\Delta p_{ma}(h_{mai}))_{surf,unit}$ is the pressure gradient in the matrix block face caused by a unit pressure drop in the fractures. For the strata case:

$$(\nabla\Delta p_{ma}(h_{mai}))_{surf,\ unit}=\frac{4}{h_{ma}}\sum_{n=0}^{\infty}e^{-\left(\frac{(2n+1)^2\pi^2k_{ma}(\phi c_t)_tr_w^2t_D}{k_{fb}(\phi c_t)_{ma}h_{mai}^2}\right)} \tag{A-6}$$

Hence, Equation A-4 becomes:

$$\frac{1}{r_D}\frac{}{r_D}\left(r_D\frac{p_{fD}}{r_D}\right)-\frac{k_{ma}}{k_{fb}}r_w^2\sum_{i=1}^{NB}f_iA_{fbi}\int_0^{t_D}\frac{4}{h_{mai}}\frac{\partial p_{fD}(\tau)}{\partial\tau}\sum_{n=0}^{\infty}e^{-\left(\frac{(2n+1)^2\pi^2k_{ma}(\phi c_t)_tr_w^2}{k_{fb}(\phi c_t)_{ma}h_{mai}^2}\right)(t_D-\tau)}\,d\tau$$

$$=\frac{\phi_{fb}c_{tf}}{(\phi\ ct)_t}\frac{\partial p_{fD}}{\partial t_D} \tag{A-7}$$

By taking into consideration Equation 3 of main text we have

$$\frac{1}{r_D}\frac{\partial}{\partial r_D}\left(r_D\frac{\partial p_{fD}}{\partial r_D}\right)-\frac{8k_{ma}r_w^2}{k_{fb}}\frac{V_{ma}}{V_b}\sum_{i=1}^{NB}\frac{f_i}{h_{mai}^2}\int_0^{t_D}\frac{\partial p_{fD}(\tau)}{\partial\tau}\cdot\sum_{n=0}^{\infty}e^{-\frac{(2n+1)^2\pi^2k_{ma}(\phi c_t)_tr_w^2}{k_{fb}(\phi c_t)_{ma}h_{mai}^2}(t_D-\tau)}d\tau$$

$$=\frac{\phi_{fb}c_{tf}}{(\phi c_t)_t}\frac{\partial p_{fD}}{\partial t_D} \tag{A-8}$$

If Equations 15 and 16 are used, Eq. A-8 yields Eq. 11 of main text.

APPENDIX B

DIMENSIONLESS PRESSURE CONSTANT RATE IN AN INFINITE MULTIPLE BLOCK SIZE DOUBLE POROSITY RESERVOIR.

The boundary and initial condition of Equation 11 of main text for this case are:

Initial conditions

$$p_{fD}(r_D,\ t_D=0)=0,1<r_D<\infty \tag{B-1}$$

Boundary conditions

$$\left(r_D\frac{\partial p_{fD}}{\partial r_D}\right)_{r_D=1}=-1,\ t_D>0 \tag{B-2}$$

$$\text{and}\ \lim_{r_D\to\infty}p_{fD}(r_D,t_D)=0\quad t_D>0 \tag{B-3}$$

Equation 11 can be solved by using the Laplace Transform method. Let us consider that:

$$L\{p_{fD}(t_D)\}=\bar{p}_{fD}(s) \tag{B-4}$$

Hence Equations 11, B-1, B-2 and B-3 become

$$\frac{1}{r_D}\frac{\partial}{\partial r_D}\left(r_D\frac{\partial\bar{p}_{fD}}{\partial r_D}\right)-8(1-\omega)\sum_{i=1}^{NB}f_i\eta_{maDi}s\,\bar{p}_{fD}\sum_{n=0}^{\infty}\frac{1}{s+(2n+1)^2\pi^2\eta_{maDi}}=s\omega\bar{p}_{fD} \tag{B-5}$$

$$\left(r_D\frac{\partial\bar{p}_{fD}}{\partial r_D}\right)_{r_D=1}=-1 \tag{B-6}$$

$$\text{and}\ \lim_{r_D\to\infty}\bar{p}_{fD}(r_D,s)=0 \tag{B-7}$$

It can be shown that

$$\sum_{n=0}^{\infty}\frac{1}{s+(2n+1)^2\pi^2\eta_{maDi}}=\frac{1}{4}\frac{1}{\sqrt{\eta_{maDi}s}}\tanh\left(\frac{\sqrt{\frac{s}{\eta_{maDi}}}}{2}\right) \tag{B-8}$$

Equation B-5 can be expressed as:

$$\frac{1}{r_D}\,\frac{\partial}{\partial r_D}\left(r_D\,\frac{\partial \bar{p}_{fD}}{\partial r_D}\right) - s\bar{p}_{fD}\left[\omega+(1-\omega)2\sum_{i=1}^{NB} f_i\sqrt{\frac{\eta_{maDi}}{s}}\tanh\left(\frac{\sqrt{\frac{s}{\eta_{maDi}}}}{2}\right)\right]=0 \tag{B-9}$$

The solution for this equation with boundary conditions B-6 and B-7 is:

$$\bar{p}_{fD}(r_D,s)=\frac{K_0\left[r_D s^{\frac{1}{2}}\left(\omega+(1-\omega)2\sum_{i=1}^{NB} f_i\sqrt{\frac{\eta_{maDi}}{s}}\cdot\tanh\left(\frac{\sqrt{\frac{s}{\eta_{maDi}}}}{2}\right)\right)^{\frac{1}{2}}\right]}{s^{3/2}\left[\omega+(1-\omega)2\sum_{i=1}^{NB} f_i\sqrt{\frac{\eta_{maDi}}{s}}\tanh\left(\frac{\sqrt{\frac{s}{\eta_{maDi}}}}{2}\right)\right]^{\frac{1}{2}} K_1\left[s^{\frac{1}{2}}\left(\omega+(1-\omega)2\sum_{i=1}^{NB} f_i\sqrt{\frac{\eta_{ma}}{s_{Di}}}\tanh\left(\frac{\sqrt{\frac{s}{\eta_{maDi}}}}{2}\right)\right)^{\frac{1}{2}}\right]} \tag{B-10}$$

APPENDIX C

PRESSURE BEHAVIOR MODEL FOR A NATURALLY FRACTURED RESERVOIR WITH MATRIX-FRACTURE FLOW RESTRICTION.

Let us consider a fractured porous medium composed of two parts: matrix blocks and fractures. Let us also assume that matrix blocks are of equal size and that the flow interaction between matrix and fractures is restricted by the presence of a low permeability medium (mineral deposition). This flow restriction causes a flow rate dependent pressure drop between matrix surface and fractures.

The reservoir contains matrix blocks uniformly distributed in the reservoir (Fig. 3). All assumptions regarding the flow conditions in the reservoir presented in the main text for a multiple block size condition are also valid in this single block size model.

For this case, Equation 11 describes the flow behavior if we take NB=1. The relationship between matrix pressure and fracture pressure can be found by considering Fig. 4, where k_d and x_d represent the damaged zone permeability and thickness, respectively. By assuming that the flow in this region occurs under steady-state flow conditions (i.e. the pressure changes are instantaneous and storage capacity of this zone is negligible) we can write:

$$\Delta p_f = (\Delta p_{ma})_{surf} + \frac{\mu x_d}{A_{fb} k_d}\, q^*_{ma-f,b} \tag{C-1}$$

or

$$\Delta p_f = (\Delta p_{ma})_{surf} + \frac{\mu x_d}{A_{fb} k_d}\int_0^t \left(\frac{\partial \Delta p_{ma}(\tau)}{\partial \tau}\right)_{surf} q^*_{ma-f,unit}(t-\tau)\,d\tau \tag{C-2}$$

In dimensionless form Equation C-2 becomes:

$$p_{fd} = (p_{mad})_{surf} + \frac{S_{maD}}{\eta_{maD}}\int_0^{t_D}\left(\frac{\partial p_{maD}(\tau)}{\partial \tau}\right)_{surf} F(\eta_{maD}, t_D-\tau)\,d\tau \tag{C-3}$$

where F is defined as:

$$\text{Strata: } F(\eta_{maD}, t_D-\tau) = 4\eta_{maD}\sum_{n=0}^{\infty} e^{-(2n+1)^2\pi^2\eta_{maD}(t_D-\tau)} \tag{C-4}$$

$$\text{Spheres: } F(\eta_{maD}, t_D-\tau) = 4\eta_{maD}\sum_{n=0}^{\infty} e^{-4n^2\pi^2\eta_{maD}(t_D-\tau)} \tag{C-5}$$

S_{maD} is a dimensionless variable to consider flow restriction and is defined as:

$$S_{maD} = \frac{k_{ma} x_d}{k_d h_{ma}} \tag{C-6}$$

Application of the Laplace Transform to the partial differential equation yields

$$\frac{1}{r_D}\,\frac{\partial}{\partial r_D}\left(r_D\frac{\partial \bar{p}_{fD}}{\partial r_D}\right) = \omega\,\bar{p}_{fD}s + (1-\omega)A_{fD}\, f(\eta_{maD}, s)(\bar{p}_{maD})_{surf.}s \tag{C-7}$$

$$\text{where } f(\eta_{maD}, s) = L\left[F(\eta_{maD}, t_D)\right]$$

The transform of Equation C-3 is:

$$\bar{p}_{fD} = (\bar{p}_{maD})_{surf.} + \frac{S_{maD}}{\eta_{maD}} f(\eta_{maD}, s)(\bar{p}_{maD})_{surf.}s \tag{C-8}$$

hence:

$$(\bar{p}_{maD})_{surf.} = \frac{\bar{p}_{fD}}{1+\frac{S_{maD}}{\eta_{maD}} f(\eta_{maD}, s)s} \tag{C-9}$$

Equation C-7 can be written as:

$$\frac{1}{r_D}\,\frac{\partial}{\partial_r}\left(r\,\frac{\partial \bar{p}_{fD}}{\partial r_D}\right) = \left[\omega + \frac{(1-\ )A_{fD} f(\eta_{maD}, s)}{(1+\frac{S_{maD}}{_{maD}} f(\eta_{maD}, s)s}\right]\bar{p}_{fD}s \tag{C-10}$$

The solution of this equation for constant production rate in an infinite reservoir is given by Equation 18 of main text for NB=1, where the function g has to be defined as:

$$g(\eta_{maD}, S_{maD}, A_{fD}) = \frac{A_{fD} f(\eta_{maD}, s)}{1 + \frac{S_{maD}}{\eta_{maD}} f(\eta_{maD}, s)s} \qquad \text{(C-11)}$$

wehre f is given by:

strata:

$$f(\eta_{maD}, s) = \left(\frac{\eta_{maD}}{s}\right)^{1/2} \tanh\left(\frac{\left(\frac{s}{\eta_{maD}}\right)^{1/2}}{2}\right) \qquad \text{(C-12)}$$

spheres:

$$f(\eta_{maD}, s) = \left(\frac{\eta_{maD}}{s}\right)^{1/2} \left[\mathrm{Coth}\left(\frac{\left(\frac{s}{\eta_{maD}}\right)^{1/2}}{2}\right) - 2\left(\frac{\eta_{maD}}{s}\right)^{1/2}\right] \qquad \text{(C-13)}$$

Short Time Solution

For small values of time ($s \to \infty$):

$$\omega + (1-\omega) g(\eta_{maD}, S_{maD}, A_{fD}) \approx \omega \qquad \text{(C-14)}$$

Thus, the Laplace inversion of the solution for the wellbore is:

$$p_{wD} = \frac{1}{2}\left[\ln\left(\frac{t_D}{\omega}\right) + 0.80907\right] \qquad \text{(C-15)}$$

Long Time Solution

For large values of time ($s \to 0$):

$$\omega + (1-\omega) g(\eta_{maD}, S_{maD}, A_{fD}) \approx 1 \qquad \text{(C-16)}$$

inversion of the solution for the wellbore yields:

$$p_{wD} = \frac{1}{2}\left[\ln t_D + 0.80907\right] \qquad \text{(C-17)}$$

Notice that Equations C-15 and C-17 represent the two classical parallel semilog straight lines.

Intermediate Time Solution

If ω is very small and $S_{maD}/\eta_{maD} >>> 1$:

$$\omega + \frac{(1-\omega) A_{fD} f(\eta_{maD}, s)}{1 + \frac{S_{maD}}{\eta_{maD}} f(\eta_{maD}, s)s} \approx \frac{A_{fD}\eta_{maD}}{S_{maD} s} \qquad \text{(C-18)}$$

Thus, the solution for pressure drop is:

$$\bar{p}_{fD} = \frac{1}{s} K_o\left[\left(\frac{r_D A_{fD} \eta_{maD}}{S_{maD}}\right)^{1/2}\right] \qquad \text{(C-19)}$$

By inverting this equation we obtain:

$$p_{fD} = K_o\left[\left(\frac{r_D A_{fD} \eta_{maD}}{S_{maD}}\right)^{1/2}\right] \qquad \text{(C-20)}$$

For $r_D = 1$ and practical values of A_{fD}, η_{maD} and S_{maD}

$$p_{wD} = \ln\left[2\left(\frac{S_{maD}}{A_{fD}\eta_{maD}}\right)^{1/2}\right] - \gamma \qquad \text{(C-21)}$$

These last equations indicate that for intermediate values of time the pressure drop stabilizes like in the Warren and Root model.

A comparison of Equation (C-21) and Equation 16 in reference 26 shows that the parameter λ is:

$$\lambda = \frac{A_{fD}\eta_{maD}}{S_{maD}} \qquad \text{(C-22)}$$

This equation establishes the relationship between Warren and Root model and the model presented in this work.

A similar study was developed by Moench[45] who reached the same conclusions. He also examined the solution for observation wells.

TABLE 1 - SI PREFERRED UNITS, CUSTOMARY UNITS, AND UNIT CONVERSION CONSTANTS USED IN THESE SYSTEMS

Parameter or Variable	SI Preferred Units	Customary Units
k	μm^2	md
h	m	ft
q_o	m^3/d	STB/D
μ	Pa·s	cp
B	m^3/m^3	RB/STB
ϕ	fraction	fraction
c_t	Pa^{-1}	psi^{-1}
p	kPa	psi
t	hours	hours
α	1,842	141.2
β	3.6×10^{-9}	2.637×10^{-4}

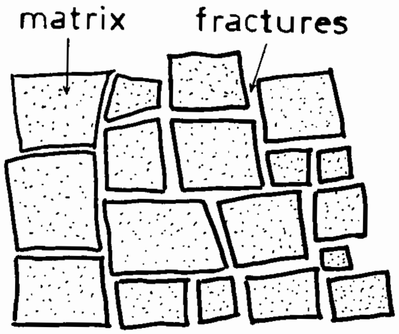

Fig. 1—Naturally fractured reservoir with multiple matrix block size.

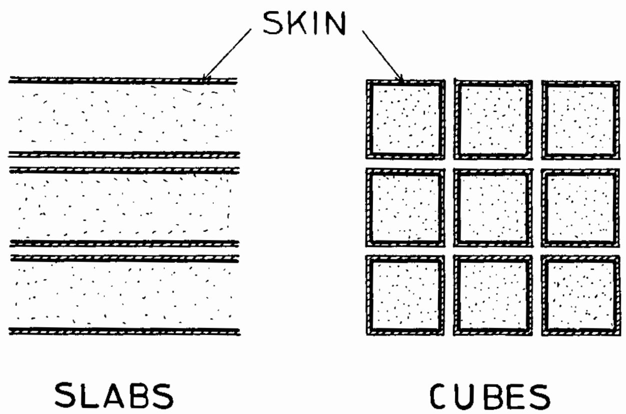

Fig. 3—Naturally fractured reservoir with a skin between matrix and fractures.

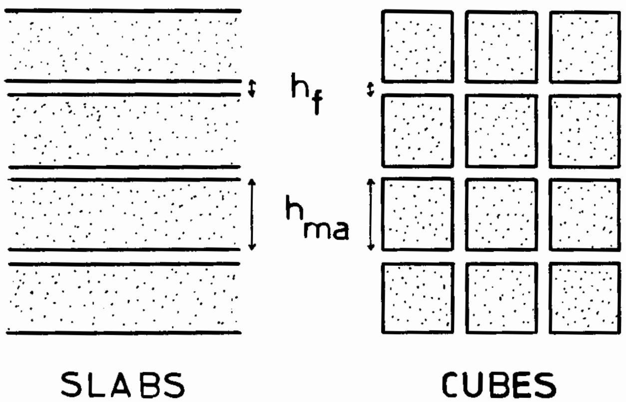

Fig. 2—Representation of a naturally fractured reservoir.

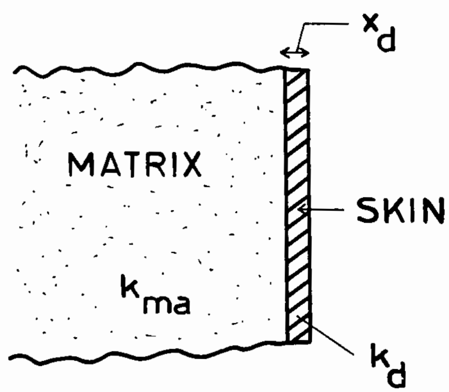

Fig. 4—Model for a naturally fractured reservoir with skin between matrix and fractures.

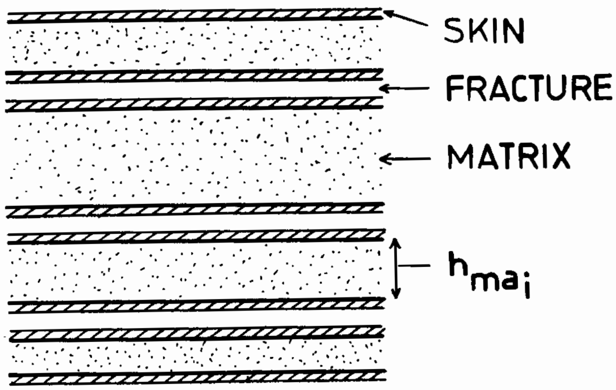

Fig. 5—Model for a naturally fractured reservoir with multiple block size and skin between matrix and fractures.

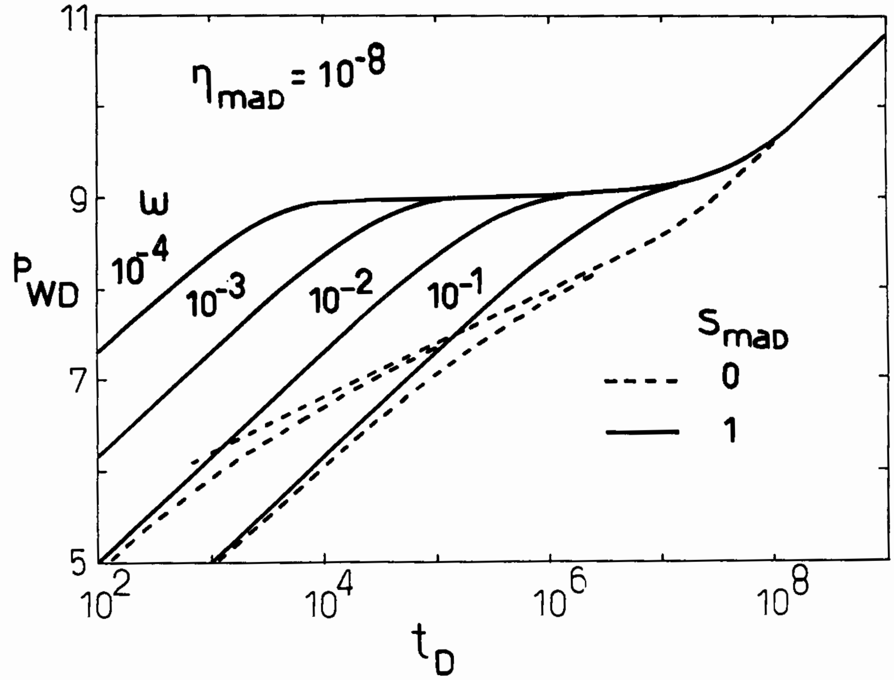

Fig. 6—P_{wD} vs. log t_D for a naturally fractured reservoir with and without skin between matrix and fractures.

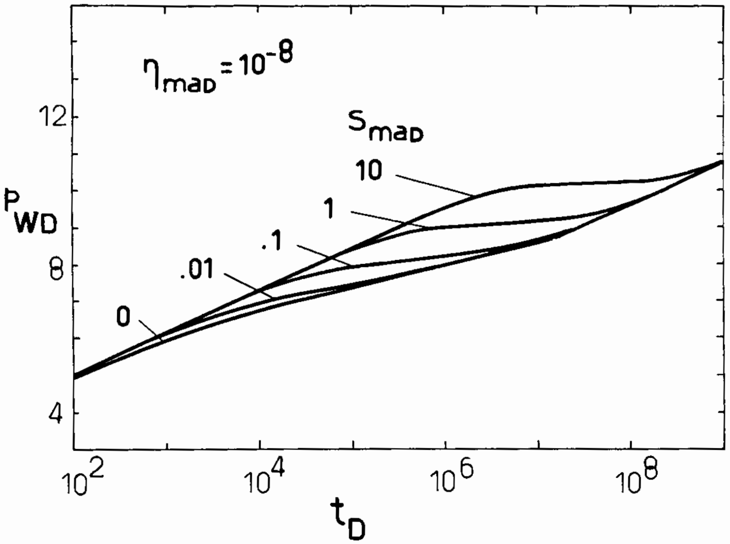

Fig. 7—P_{wD} vs. t_D for a naturally fractured reservoir with skin between matrix and fractures.

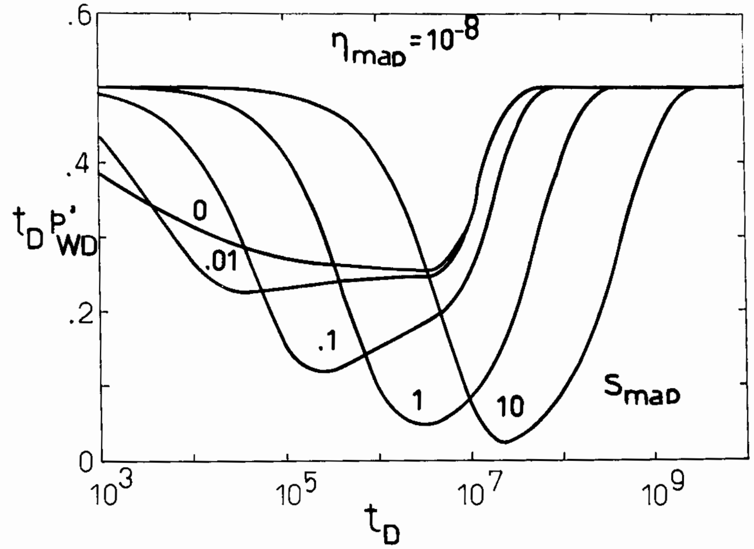

Fig. 8—$t_D dp_{wD}/dt_D$ vs. t_D for a naturally fractured reservoir with skin between matrix and fractures.

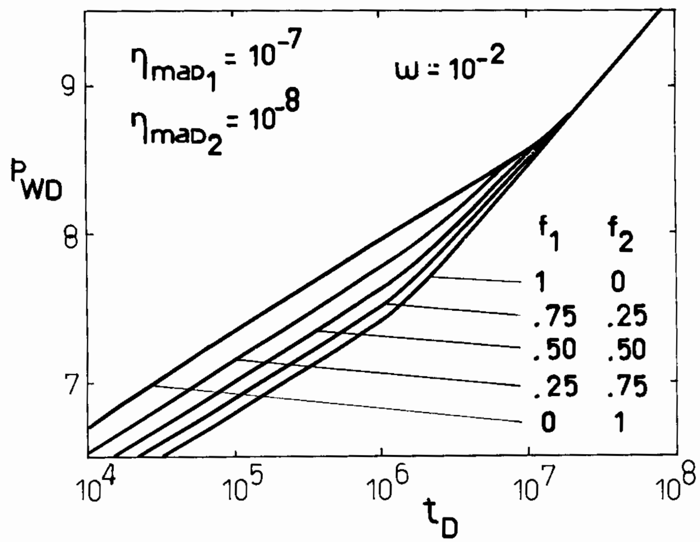

Fig. 9—p_{wD} vs. t_D for a naturally fractured reservoir with two block sizes.

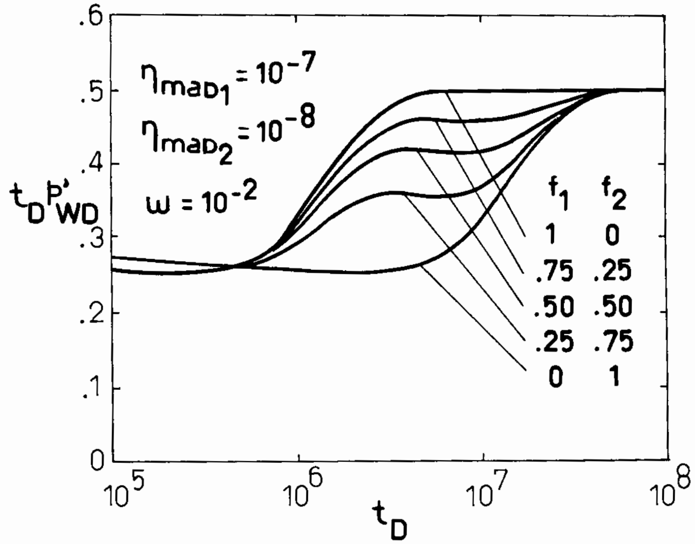

Fig. 10—t_D dp_{wD}/dt_D vs. t_D for a naturally fractured reservoir with two matrix block sizes.

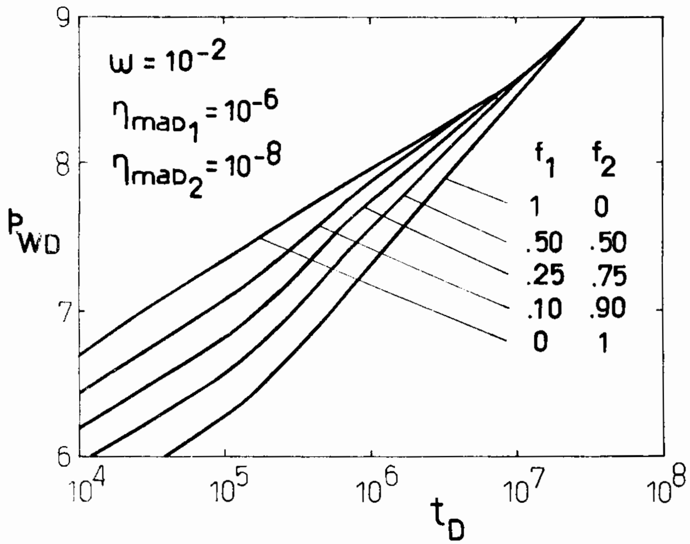

Fig. 11—p_{wD} vs. t_D for a naturally fractured reservoir with two matrix block sizes.

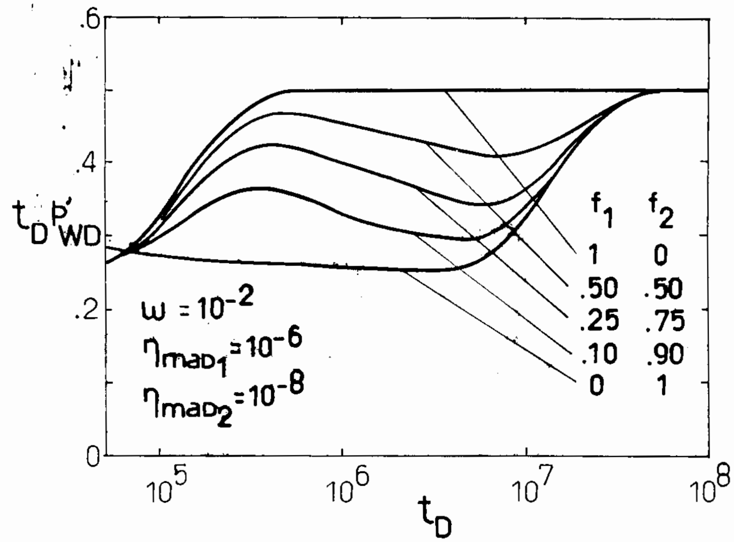

Fig. 12—$t_D\, dp_{wD}/dt_D$ vs. t_D for a naturally fractured reservoir with two matrix block sizes.

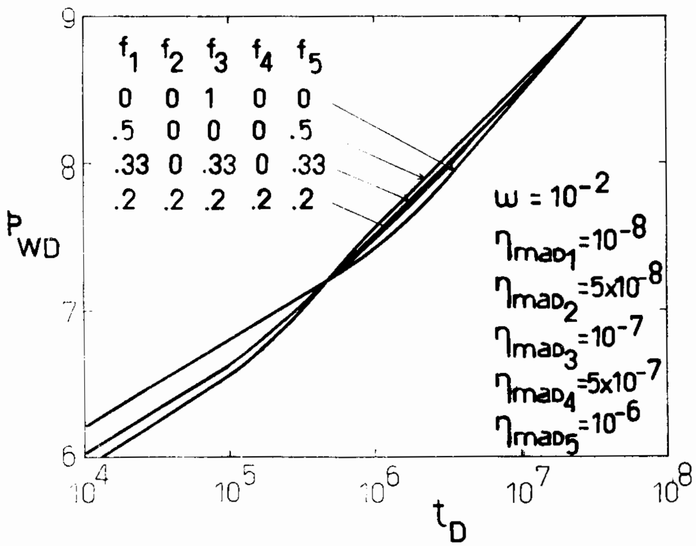

Fig. 13—p_{wD} vs. t_D for a naturally fractured reservoir with different number of block sizes.

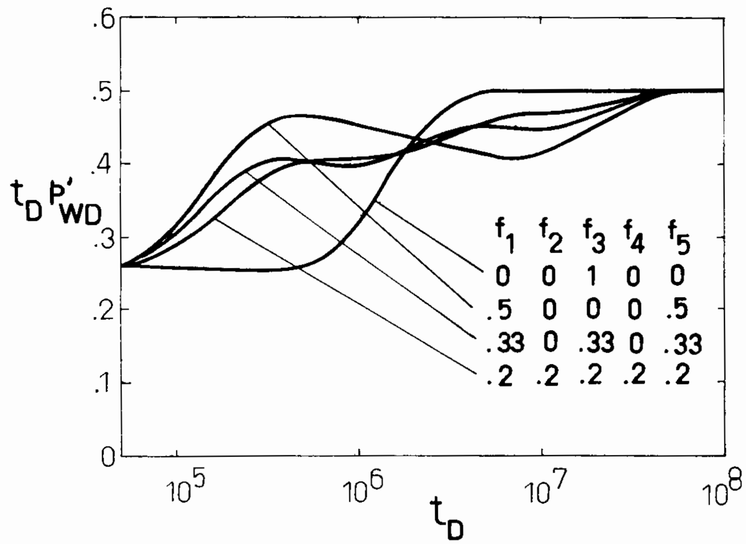

Fig. 14—$t_D\, dp_{wD}/dt_D$ vs. t_D for a naturally fractured reservoir with different number of block sizes.

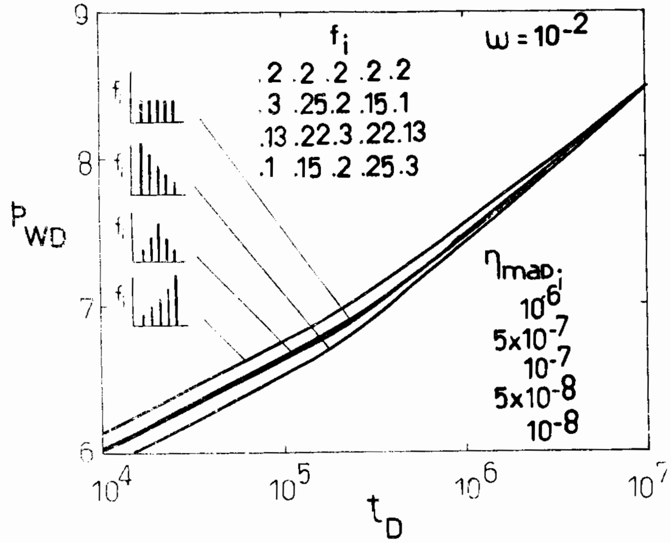

Fig. 15—p_{wD} vs. t_D for a naturally fractured reservoir with five matrix block sizes.

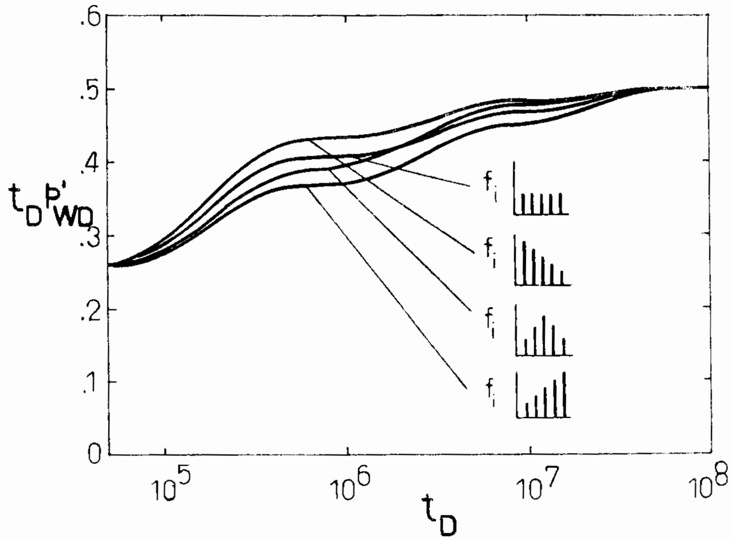

Fig. 16—$t_D\, dp_{wD}/dt_D$ vs. t_D for a naturally fractured reservoir with five matrix block sizes.

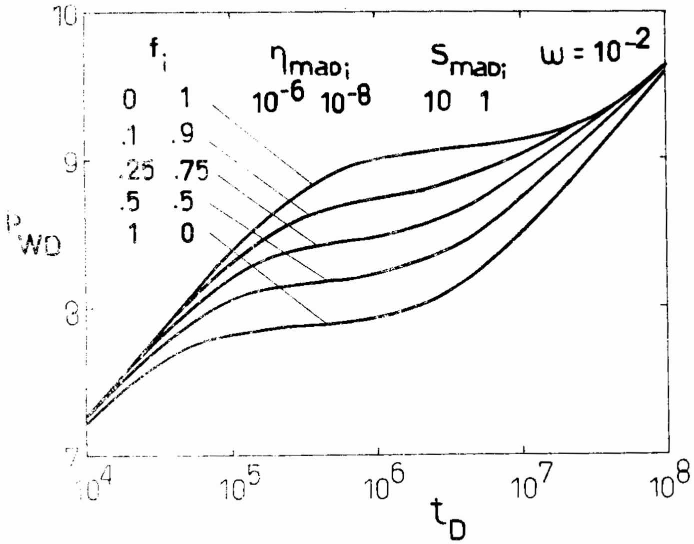

Fig. 17—p_{wD} vs. t_D for a naturally fractured reservoir with two block sizes and skin.

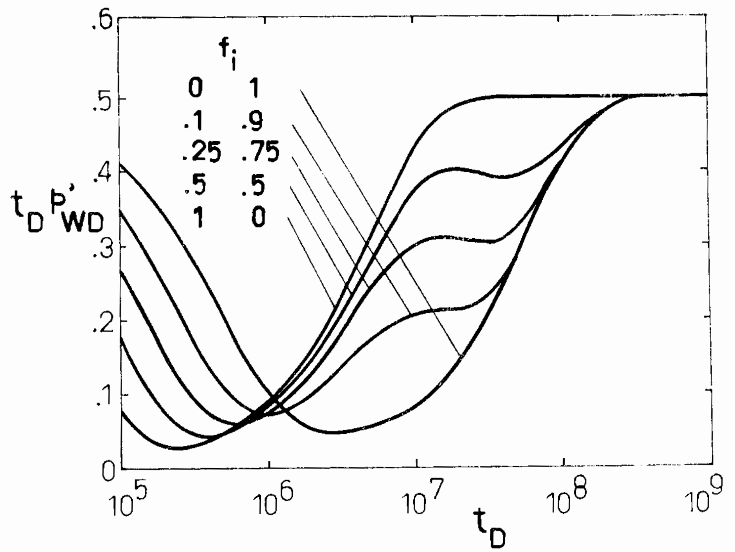

Fig. 18—$t_D\, dp_{wD}/dt_D$ vs. t_D for a naturally fractured reservoir with two block sizes and skin.

G. Echávez, F.I. Arreguín

HIGH HEAD STILLING BASIN REDUCES EXCAVATION COSTS

Water Power and Dam Construction December 1985.

High head stilling basin reduces excavation costs

By G. Echávez and F. I. Arreguín
Research Professors*

An aerated stilling basin, designed to reduce excavation costs and operate under high heads without cavitation problems is proposed. Model studies carried out on two open-channel spillways are described.

HIGH capital costs and new developments in the design of hydraulic structures make it increasingly necessary for engineers to opt for less expensive and flexible designs.

The stilling basin proposed here (see Fig. 1) has an aeration step, a ramp, two rows of baffle blocks and, at the end, a combined weir that gives the required tailwater for each discharge. It functions in such a way that the hydraulic jump starts for all discharges, between the end of the ramp and the first row of blocks. Stabilization is improved by the ramp and the blocks, and cavitation problems are avoided since the flow is aerated, and it is accomplished by keeping adequate water depth in the stilling basin with a combined weir downstream.

Model investigation

Two open channel spillways were used in the research. They were 2.7 and 0.21 m high, and can be considered as 1:30 and 1:400 scale models, respectively. After several tests the step height, ramp length, location of the first row of blocks, and geometry of the weir at the downstream end of the spillway were established. The results obtained from the two models were close enough to be taken as being equal.

Step height. A 1.8 m-high step was proposed to ensure good aeration in all the spillway width. It seems possible to reduce this height and to relate it with the water depth, y_1, at the toe of the spillway. In the cases tested the following ratio was used, where [illegible] is the step height.

[illegible]

for y_1 corresponding to the design discharge. In particular cases, for very narrow or very wide spillways this height may be reduced or increased accordingly.

Ramp. This is necessary to stabilize the hydraulic jump. Since the jet of water is very sensitive to pressure gradients normal to the flow, it is essential to prevent the beginning of the hydraulic jump from moving upstream, becoming submerged, and precluding its functioning as an aerator. For the authors' research a ramp with a length of 21 m, that is 10.7 y_1, for the design discharge, and a 0.121 slope was used.

Baffle blocks. After tests with one, two and three rows of rectangular blocks, it was found that the best results were obtained with two rows of staggered blocks. The geometry and spacing of the blocks was estimated using Burec criteria[1], but taller blocks should preferably be used to prevent the water from jumping over them. The final geometry is shown in Fig. 2.

*Faculty of Engineering, National Autonomous University of Mexico, University City, Mexico

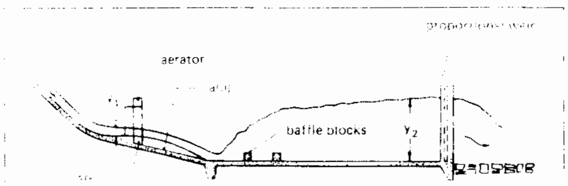

Fig. 1. Stilling basin with an aerator.

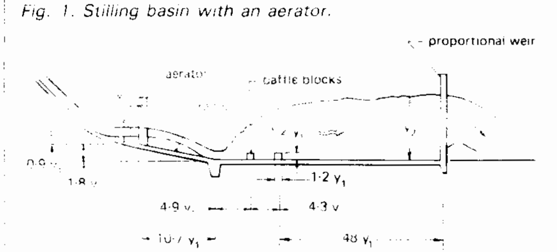

Fig. 2. Final arrangement of the stilling basin with an aerator.

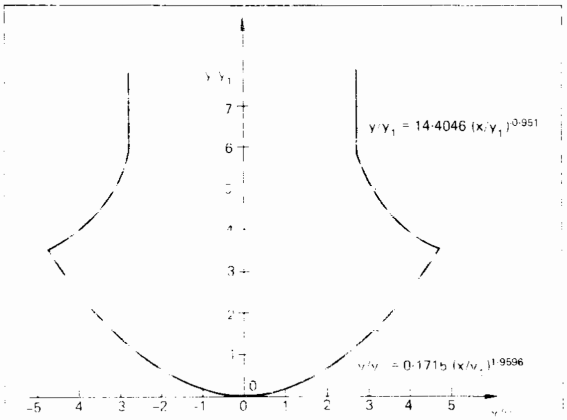

Fig. 3. Geometry of the control weir.

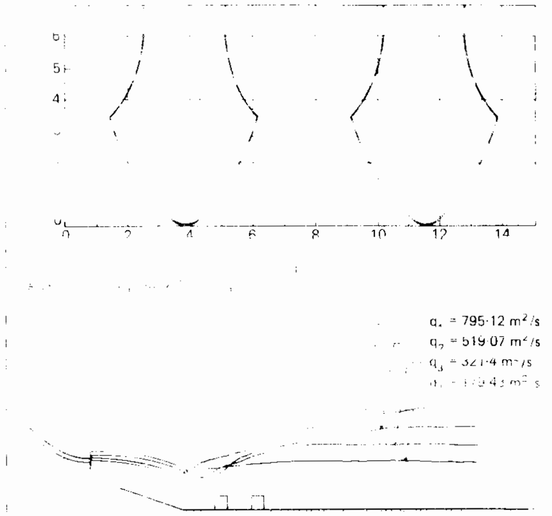

Fig. 5. Water profile for five discharge rates.

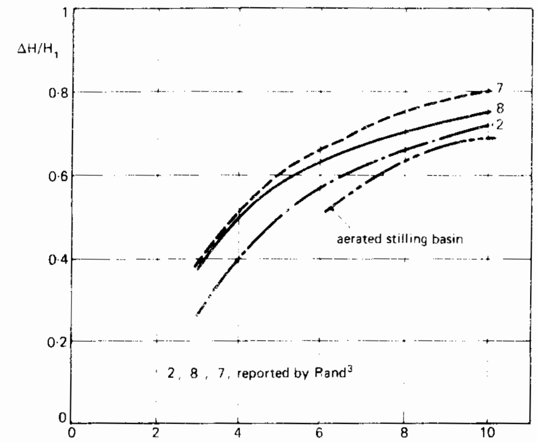

Fig. 6. Energy loss in the aerated stilling basin and as reported by Rand[3].

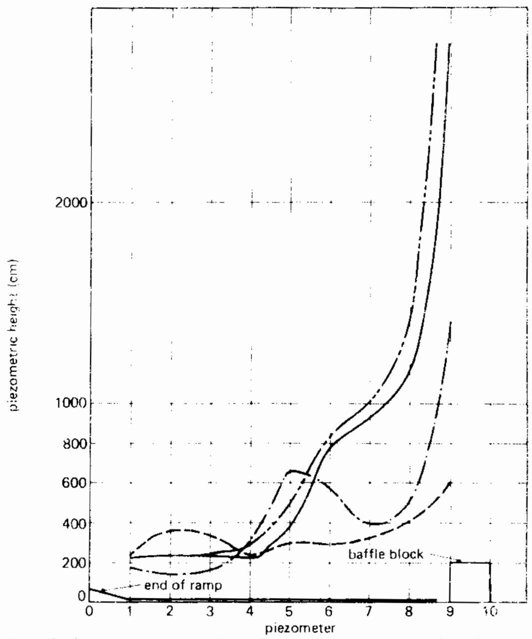

Fig. 8. Pressure distribution along the centreline of a block.

Downstream weir. With this weir the proper y_2 versus q ratio is maintained to keep the hydraulic jump in place for all discharges. Although the influence of the jet striking the floor and the drag on the blocks is difficulty to evaluate, a preliminary geometry, using the proportional weir theory[2], was established analytically. This geometry works well up to a given depth but for greater depths the hydraulic jump is swept downstream. To avoid this it was necessary to narrow the weir crest, so finally the geometry shown in Fig. 3 was obtained experimentally. For wide stilling basins, for example where $b/y_1 = 30$, it is recommended that two identical weirs be provided, as shown in Fig. 4, to keep the hydraulic jump bi-dimensional.

One advantage of this arrangement is that the stilling basin drains itself after operation, avoiding the creation of a large pool of water and the pressures and inconvenience associated with it.

With the geometry previously mentioned, the hydraulic jump remains almost in the same place for all discharge rates. In Fig. 5 the water profile for five discharges is shown, and Fig. 6 is a graph showing the efficiency of this stilling basin as compared with values reported by Rand[3].

One of the problems associated with this kind of stilling basin is the structural design of the blocks and the zone adjacent to them: Figs. 7 and 8 show the pressure distribution along a line between blocks and at the centreline of one of them.

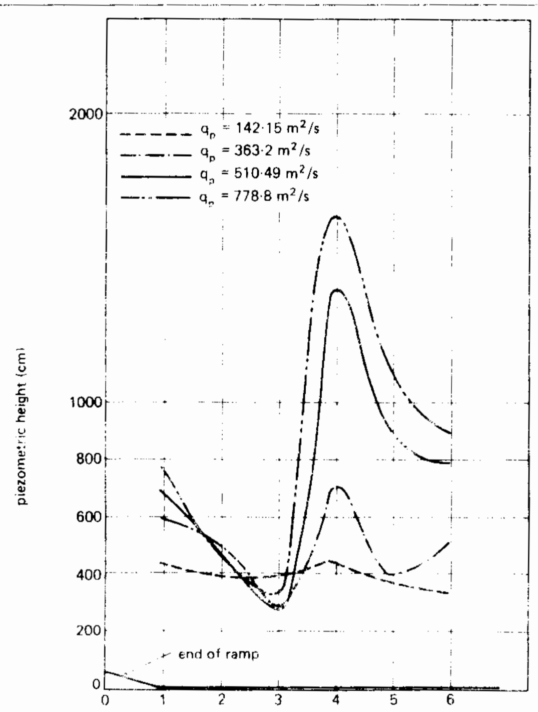

Fig. 7. Pressure distribution between blocks.

Conclusions

The aerated stilling basin with baffle blocks which has been described does not have cavitation problems and can be used for velocities higher than those generally considered safe until now[4], that is 15 m/s.

Although the basin functions adequately it will be necessary to continue model studies, to improve performance. The general design, however appears acceptable in view of the advantages demonstrated, which can be summarised as follows:

- The basin requires much less excavation than the traditional high-head stilling basins.
- It is cavitation free so it can be used in high-head water works.
- Energy is dissipated adequately.
- The basin drains after discharge.
- The drainage pipe of the spillway can surface in the vertical wall of the step.

References

1. United States Department of the Interior Bureau of Reclamation, "Design of Small Dams", Edition 5a; January 1976.
2. AZEVEDO A. "The Design of Proportional and Logarithmic Thin Plate Weirs", *Journal of Hydraulic Research, IAHR*, Vol. 6 No 2, 1968.
3. RAND W. "Efficiency and Stability of Forced Hydraulic Jump", *Journal of the Hydraulic Division, ASCE*, HY4; July 1967.
4. HAMILTON W. S. "Preventing Cavitation Damage to Hydraulic Structures", Part Two, *Water Power and Dam Construction*, December 1983.

O. Gelman, S. Macías

TOWARD A CONCEPTUAL FRAMEWORK FOR INTERDISCIPLINARY DISASTER RESEARCH

Ekistics 309

Toward a conceptual framework for interdisciplinary disaster research

Ovsei Gelman and Santiago Macías

Dr Gelman is Research Professor at the Engineering Institute of the Mexican National Autonomous University, Mexico and Professor of Postgraduate Studies at the Engineering and Administrative Faculties of the same university. Santiago Macías is Research Assistant at the Engineering Institute and Assistant Professor at the Engineering Faculty, also at the Mexican National Autonomous University. *A preliminary version of this paper was published in* Quaderno, *nos. 83-86, Dipartimento di Sociologia dei Disastri, Istituto di Sociologia Internazionale, Italy, in 1982.*

Introduction

Reliable information and economic studies about disasters are scarce. However, some gross estimates allow them to be considered a "formidable obstacle to economic and social development."[1] The direct losses — in terms of cost in the US alone — caused by 30 common natural calamities constituted about 1 percent of the GNP in 1979[2]; and the damage caused by natural hazards between 1964 and 1970 in the countries of Centroamerican Common Market, reached, according to the estimate by the Mexican office of CEPAL, 2.3 percent of their General Domestic Product without taking into account the indirect and secondary effects.[3]

The situation is aggravated by the increasing magnitude and frequency of disasters which are usually attributed to the growth and concentration of population in large cities and the consequent complexity and deterioration of services necessary for their maintenance. However, considerable human loss is caused by the exceptionally high vulnerability[4] of human settlements in developing countries, resulting from the poverty or marginality of the population and the overall socioeconomic conditions, which make the frequently used concept of "natural disaster" meaningless. Natural events become disasters only when human settlements are not prepared to withstand them; very often, because of lack of precautionary planning.

Conditions in Mexico combine both of these factors, natural and social: geographically, the country is located in a zone prone to a variety of natural hazards — earthquakes, hurricanes, torrential rains; and socioeconomically, it is a developing nation with a rather high rate of population growth and a much higher rate of population concentration in several cities.

Over recent decades, substantial effort has been made, particularly in the field of engineering, to reduce the negative impacts of natural hazards. Antiearthquake precautions in human settlements have been improved by the introduction of construction codes and by the strengthening of the surveillance in their application. Major technological works such as the deep drainage system in Mexico City and other special hydraulic structures appear to be substantial measures in reducing floods.[5] Furthermore, increased attention has been paid to the study of the destructive phenomena and their effects. But the practical application of many high quality studes[6,7,8] has been frequently impeded by the fact that they were too specialized, by the lack of a unified terminology and the absence of a general conceptual framework. These weaknesses make the transference of methods and results from one area to another[9] nearly impossible, particularly when the studies do not solve problems, therefore implying the need for adaptations and interpretations in order to be of any use in dealing with disaster conditions.

Frequently, disaster responses have been oriented toward the immediate necessities of rescue and relief,[10] and are restricted to corrective actions during the occurrence of a disaster. This points out the necessity to give more attention to preventive and planned measures.

It has been pointed out[11,12,13] that to fortify human settlements facing disasters, it is not enough to better any of the existing means and to implement new ones. It is also necessary to plan, organize and coordinate a set of activities that has to take place systematically before, during and after the disaster.

The planning of these activities and their execution, as well as the evaluation of their success and their adaptation to changing conditions, mean the necessity to prepare a conceptual framework which will also permit the fixing of priorities and the coordination of studies and actions in order to establish and improve upon policies and strategies for the safeguarding of human settlements facing disasters.

A conceptual framework

The elaboration of a conceptual framework, ie a system of basic concepts that permits the posing of problems, and a set of adequate methods to resolve them, is a crucial stage in the process of planning, developing and implementing any study in general. It is particularly so when dealing with interdisciplinary research on disasters.

The development of a conceptual framework is based on certain paradigms,[14] ie cognitive tools, in order to recognize reality as well as identify, choose and study its relevant fragments in order to represent them by constructs and, consequently in the case of research, to substitute these with models. Thus the paradigms determine the whole cognitive process, searching to describe

Desastres, vol. 4 (New York, UNDRO, United Nations, 1979).
11. O. Gelman and J. L. Montaño, "Planteamiento general del diseño e implantación de un sistema de protección y restablecimiento de los asentamientos humanos en caso de desastre," *Memorias del IV Congreso de la Academia Nacional de Ingeniería* (Mérida, Yucatán, Mexico, Oct. 1978).
12. O. Gelman and J. L. Rangel, "Los desastres vistos bajo el enfogue sistémico: El diseño de un sistema de salvaguarda," *Memorias del Simposium: Los Asentamientos Humanos y la Falla de San Andrés* (Tijuana, BC, Mexico, Sept. 1979).
13. O. Gelman and J. L. Rangel, "Desarrollo de un sistema de protección y restablecimiento para una ciudad frente a desastres," *Memorias del V Congresso de la Académia Nacional de Ingeniería* (Morelia, Michoacan, Mexico, Sept. 1979).
14. T. Kuhn, *The Structure of Scientific Revolutions*(Chicago, University of Chicago Press, 1962).
15. O. Gelman and N. Lavrenchuck, "Specifics of analysis of scientific theories within the framework of the general systems theory," *Collection: Philosophical Problems of Logical Analysis of Scientific Knowledge*, Issue 3 (Yerevan, Armenian Academy of Sciences, 1974).
16. O. Gelman, "Metodología de la ciencia e ingeniería de sistemas: Algunos problemas, resultados y perspectivas," *Memorias del IV Congreso de la Academia Nacional de Ingeniería* (Mérida, Yuc., Mexico, Oct. 1978).
17. S. Toulmin, *Foresight and Understanding* (Bloomington, Indiana University Press, 1961).
18. J. L. Rangel and O. Gelman, "Desarrollo del enfoque sistémico y concretización de algunos elementos básicos para definir y analizar el sistema educativo en México," *Informe Interno* (Instituto de Ingeniería, UNAM, 1980).
19. O. Gelman and G. Negroe, "Papel de la planeación en el proceso de conducción," *Boletín IMPOS*, no. 61, year XI (1981).
20. J. Dworkin, "Global trends in natural disasters," *Working Paper 26 - Natural Hazards Research* (Boulder, Colorado, 1974).
21. O. Gelman and G. Negroe, "Planeación como un proceso de conducción," *Revista de la Academia Nacional de Ingeniería*, vol. 1, no. 4 (1982).
22. O. Gelman and S. Macías, "Aplicación del enfoque sistémico para el estudio interdisciplinario de desastres," *Extended Abstracts of the 1983 World Conference on Systems* (Caracas, Venezuela, July 1983).
23. O. Gelman and S. Macías, "Desastre provocado por la erupción del volcán Chichonal: Estudio de campo," *Series del Instituto de Ingeniería*, no. 465 (Mexico, March 1983).
24. O. Gelman and S. Macías, "Estudio del desastre provocado por la erupción del volcán Chichonal," *Boletín Preparación para casos de desastre en las Américas* (1983).
25. O. Gelman and S. Macías, "Disaster provoked by the volcano Chichonal eruptions: A field study," *Natural Hazards Research workshop* (Boulder, Colorado, July 1983).
26. O. Gelman, H. Merino and M. A. Sanchez, "Plan general de emergencias," Chapter 9 in *El sistema hidraúlico del Distrito Federal. Un servicio público en transición* (DDF, Mexico, 1982).
27. O. Gelman "Uso de modelos en el pronóstico de fenómenos destructivos para su prevención y mitigación," *Boletín Informativo* (SAHOP, Mexico, June, 1982).
28. O. Gelman and S. Macías, "Aspectos metodológicos de la elaboración y uso de modelos en el pronóstico de fenomenos destructivos," *Boletín IMPOS*, Year XII, vol. 68 (Oct.-Nov.-Dec. 1982).
29. O. Gelman and S. Macías, "Forecast of destructive events for their prevention and mitigation," *Natural Hazards Research Workshop* (Boulder, Colorado, July 1983).
30. O. Gelman and S. Macías, "Salvaguarda de los sistemas urbanos frente a desastres: El caso de México," *Extended Abstracts of the 1983 World Conference on Systems* (Caracas, Venezuela, July 1983).
31. O. Gelman and S. Macías, "Sistema de protección y restablecimiento de la Ciudad de México frente a desastres," *Ingeniería*, vol. 53, no. 3 (Mexico, 1983).
32. O, Gelman, G. Guerrero, S. Macías, G. Perea, C. Rodríguez and M.A. Sanchez, "Plan de atención de emergencias de la Ciudad de México frente a inundaciones, dentro del contexto del SIPROP," *Tercer Simposium Internacional sobre Emergencias Urbanas: Huracanes, Inundaciones y sus efectos en los asentamientos humanos* (La Paz, BC, Mexico, Nov. 1981).
33. O. Gelman, "Planes de emergencia en el contexto de la protección y restablecimiento de la Ciudad de México frente a desastres," *Emergency 82: International Congress for Emergency, Disaster Preparedness and Relief* (Geneva, Oct. 1982).
34. O. Gelman and S. Macías, "Metodología para la elaboración de planes de emergencia," *Primer Congreso Internacional sobre la aplicación de planes de emergencia a los asentamientos humanos*, held in Cancún, QR, Mexico, June 1982. (Dipartimento di Sociologia dei Disastri, Istituto di Sociologia Internazionale, Gorizia, Italia), *Quaderno*, no. 83-2 (1983).
35. O. Gelman and S. Macías, "Earthquake relief in the context of protection and reestablishment of integral measures: The case of Mexico City," *Proceedings of the International Symposium on Earthquake Relief in Less Industrialized Areas* (Zurich, March 1984).
36. O. Gelman, "Los desastres naturales y ser humano," *Simposio: La Salud y los desastres de la I Reunión Internacional Médico Militar* (Mexico, March 1984).

A. Grinberg, R. Colás, D.M.K. Grinberg

STRESS-STRAIN IRREGULARITIES OBSERVED DURING TENSILE TESTING OF A FERRITIC STAINLESS STEEL

Proceedings of the 7th International Conference on the Strength of Metals and Alloys

Montreal, Canada, 12-16 August 1985

Volume I

Pergamon Press

Stress-Strain Irregularities Observed During Tensile Testing of a Ferritic Stainless Steel

A. Grinberg*, R. Colás and D. M. K. Grinberg***

**División de Estudios de Posgrado, **División de Ingeniería Mecánica y Eléctrica, Facultad de Ingeniería, U.N.A.M. 04510 México, D.F.*

ABSTRACT

During tensile testing, stress-strain irregularities were found in a 17% chromium stainless steel (AISI 430F) that was specially heat treated to develop a dual structure. These irregularities were put in evidence when plotting the work hardening coefficient as a function of stress and in a logarithmic stress vs. strain plot. Scanning electron metallography and microhardness studies were conducted in some of the specimens that have shown the irregular behaviour. These studies put in evidence that both phases were deformed at strains as low as 0.1 and, at the same time, the volume fraction of a precipitated phase increased. Moreover, it was found that the chromium content in the precipitates varied from 20 to 50% depending on the parent phase and the testing conditions.

KEYWORDS

Stainless steel, tensile testing, mechanical instabilities, mechanically induced phase transformations, warm working.

INTRODUCTION

In the recent years extense research has been carried out on the deformational behaviour of low alloy dual-phase steels (1-3). In them the contribution of each phase is deduced from logarithmic stress vs. strain plots (1,2) or from metallographic observations (3). One characteristic of these steels is the supression of the yield point phenomena.

In this paper we explain some stress-strain irregularities observed in an AISI type 430F stainless steel that shows dynamic strain ageing (4) after being heat treated to develop a dual-phase structure.

EXPERIMENTAL PROCEDURE

Tensile specimens (4 mm diameter, 40 mm long) from an AISI 430F stainless steel (16.5% Cr, 0.1% C, 0.07% N, 0.2% Ni, 0.53% Si, 0.8%Mn, 0.1% Mo, 0.015% P, 0.25% S) were annealed for four hours at 850°C in nitrogen atmosphere in order to develop a dual-phase, around 15% martensite, structure (5,6). The resulting ferritic grain size was around 30 μm, the martensitic of around 10 μm.

The specimens were deformed in an Instron 1125 testing machine at different temperatures and strain rates. The tests were carried out either in air on in a nitrogen atmosphere whether an Instron environmental chamber, with temperature stability of ±0.5°C, or an Instron three zone furnace, with a temperature stability of ±2°C, was used.

The resultant load vs. displacement chart was digitized with the aid of a Hewlett Packard 9825 desk top computer and converted into stress vs. strain curves up to the UTS. The work hardening coefficient (Θ=dσ/dε) was calculated by succesive interpolations of five points parabola.

Metallographic examinations and chemical analysis were carried out in a scanning electron microscope at 25 kV. The proportion of the different phases was calculated by point counting; microhardness tests were conducted on a Leitz tester.

RESULTS AND DISCUSSION

Stress-Strain Relationships

Due to their physical meaning (7,8) Θ vs. σ curves, Fig. 1, were used to document the temperature and strain rate dependence of the mechanical properties. In the figure the dashed line corresponds to Considere's criterion (Θ=σ). It can be seen that the curves from tests at the higher temperatures deviate from the linear (expected) behaviour implying a change in the regime of deformation (9). Two of the curves from Fig. 1 are represented in the logarithmic way in Fig. 2; it can be seen that the relationship proposed by Ludwik ($\sigma=\sigma_0+k\varepsilon^n$) is not followed, as would be expected from a dual-phase steel (1). Moreover, the stress level at which the curves deviate from linearity in Fig. 1 (arrows) corresponds to the one at which the logσ vs. logε bends down.

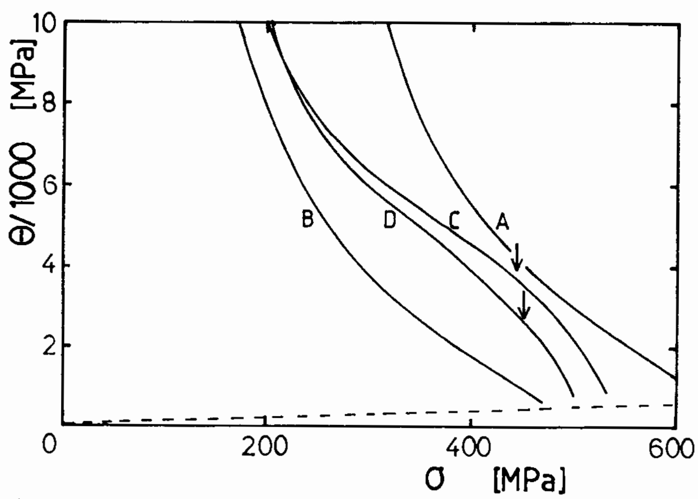

Fig. 1. Θ vs. σ curves for the present material. A) T=22°C, $\dot{\varepsilon}=4.2\cdot10^{-2}$ s^{-1}, B) T=400°C, $\dot{\varepsilon}=4.2\cdot10^{-2}$ s^{-1}, C) T=475°C, $\dot{\varepsilon}=8.3\cdot10^{-5}$ s^{-1}, D) T=600°C, $\dot{\varepsilon}=2.1\cdot10^{-3}$ s^{-1}.

Rashid (1) has shown that on dual-phase steels the strain at the onset of necking (ε_p) corresponds to the value of the exponent of Ludwik's equation (n_i) measured close to this strain. In our case the value of n_i is almost twice

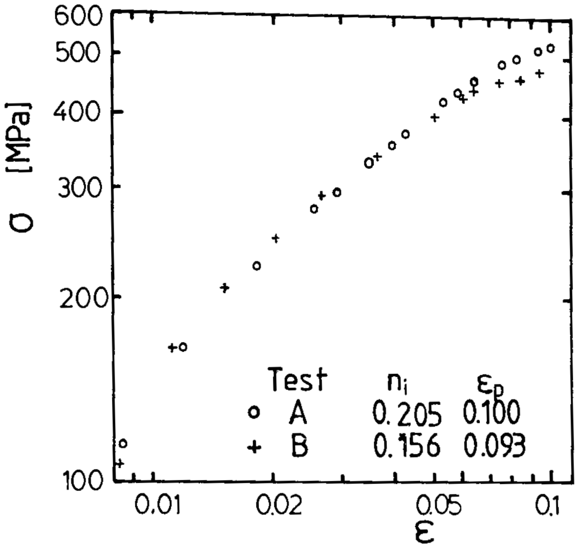

of the strain at the UTS, and this might be due to dynamic strain ageing (4).

Fig. 2. Log σ vs. log ε plot for
A) T=475°C, $\dot{\varepsilon}= 8.3\cdot 10^{-5}s^{-1}$
B) T=475°C, $\dot{\varepsilon}= 2.1\cdot 10^{-3}s^{-1}$

Metallography

Fig. 3 (a) shows the undeformed portion of a specimen tested at T=475°C and $\dot{\varepsilon}=8.3\cdot 10^{-5}\ s^{-1}$. Fig. 3 (b) shows the deformed region of the same specimen. The structure consists, in both cases, of ferrite plus a second phase plus abundant precipitation and sulphur inclusions which were dissolved by the etchant. Table 1 shows the proportion and hardness of the different phases. From Table 1 we observe that the volume fraction of the second phase (γ) tends to decrease and the precipitated phase (σ) tends to increase as straining progresses.

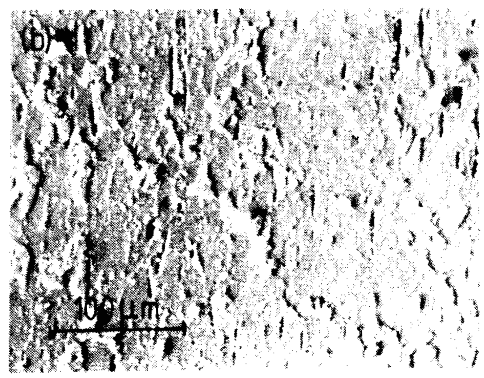

Fig. 3. Scanning electron micrographs from a specimen deformed at T=475°C and $\dot{\varepsilon}=8.3\cdot 10^{-5}\ s^{-1}$ showing the (a) undeformed and (b) deformed regions.

The hardness of the different phases is plotted in Fig. 4 as a function of a parameter that takes into account the time and temperature involved in the deformation. This figure shows that in both major phases the hardness is higher after deformation indicating that both phases were deformed at strains as low as 0.1, and this might be due to the hard ferrite in the composite (10).

The very hard value of hardness of around 600 VHN observed in some of the samples indicates that the second phase has transformed to martensite as a

TABLE 1 Relative Phase Percentage and Vickers Hardness as a Function of Rate and Temperature of Deformation

	α-phase		γ-phase		σ-phase	
	Undeformed	Deformed	Undeformed	Deformed	Undeformed	Deformed
A	82.3 % 339 VHN	84.5 % 471 VHN	11.5 % 402 VHN	8.7 % 613 VHN	6.0 % ---	6.8 % ---
B	77.4 % 185 VHN	75.7 % 284 VHN	14.7 % 413 VHN	16.8 % 561 VHN	7.9 % ---	7.5 % ---
C	79.3 % 162 VHN	79.4 % 228 VHN	13.6 % 369 VHN	12.2 % 407 VHN	7.1 % ---	8.4 % ---

A : $T = 600°C$; $\dot{\varepsilon} = 2.1 \times 10^{-3} s^{-1}$
B : $T = 475°C$; $\dot{\varepsilon} = 8.3 \times 10^{-5} s^{-1}$
C : $T = 600°C$; $\dot{\varepsilon} = 2.1 \times 10^{-5} s^{-1}$

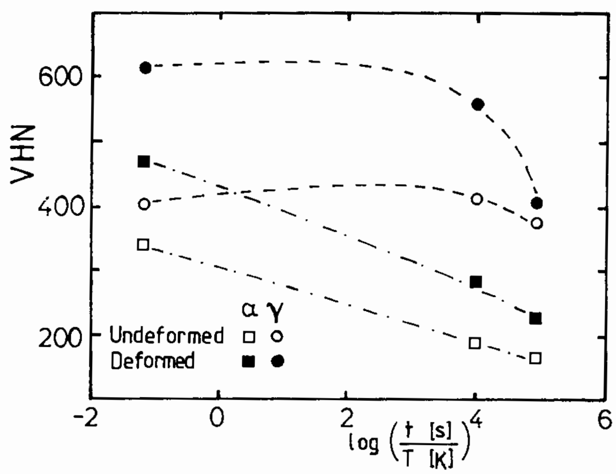

Fig. 4. Microhardness in the two major phases as a function of a temperature compensated time parameter.

Fig. 5. Higher amplification of Fig. 3 (b).

result of the concurrent deformation (3). This idea is further reinforced by Fig. 5 which shows very similar features to the martensite found in low carbon dual-phase steels (3). X-ray diffraction studies are being carried out in order to prove this idea.

In table 2 the chromium content of the different phases is reported. Althought all the values are within the scatter band, the chromium content is higher in the matrix, denominated alpha, than in the second phase, denominated gamma, indicating the limits of the α+γ region in the phase diagram (5,6). It is more important to observe the variation of chromium in the precipitates, denominated sigma, Fig. 6. By comparing this last plot with Fig. 4 we deduce that at low values of the temperature compensated time parameter the precipitates ar:

TABLE 2 Chromium Distribution

Sample	α-phase	σ in α-phase	γ-phase	σ in γ-phase
A	17.1 %	21.4 %	15.1 %	25.1 %
B	16.1 %	35.9 %	15.0 %	45.2 %
C	17.7 %	47.5 %	16.4 %	43.7 %

The values are averaged over the deformed and undeformed regions

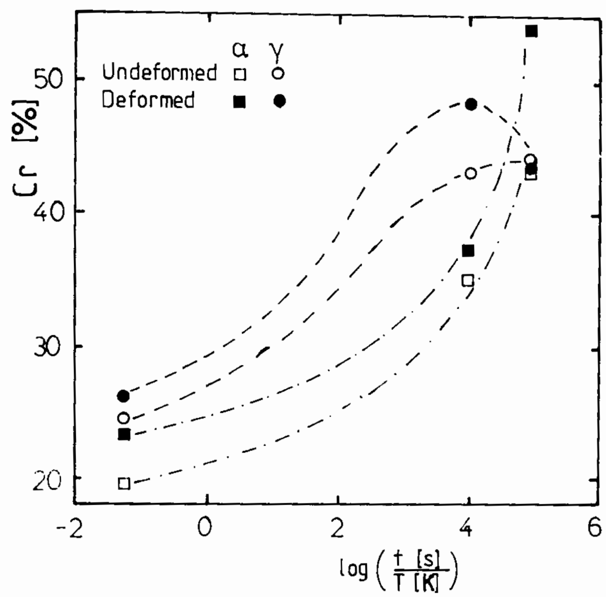

Fig. 6. Chromium content in the precipitates present in the two major phases as a function of the temperature compensated time parameter.

small with a low chromium content and a high strength, and that coarsening is accompanied by chromium enrichement. Research in TEM is being conducted on this point.

CONCLUSIONS

1. Instabilities develop in our stainless dual-phase steel at strains lower than that of necking.

2. The abundant precipitation might be responsible for dynamic strain ageing and the lower than expected ductility.

3. The hard phase is deformed at strains as low as 0.1.

4. The increase in hardness in the second phase can be attributed to deformation, martensitic transformation and precipitation, whereas in the ferrite it can be only attributed to deformation and precipitation.

5. The chromium concentration in the sigma phase precipitates ranges from 20 to 50%.

AKNOWLEDGEMENT

The authors recognize the help given by A.A. Gasca and R.E. Rubinovich from the Consejo de Recursos Minerales for their help with the scanning electron microscope.

REFERENCES

1. M.S. Rashid: "Formable HSLA and Dual-Phase Steels", ed. A.T. Davenport, The Metallurgical Society of AIME, New York, 1979, 1.
2. D.K. Matlock, F. Zia-Ebrahimi and G. Krauss: Proceedings of ASM Materials Science Seminar on Deformation, Processing and Structure, 1982.
3. J.M. Rigsbee and P.J. Van der Arend: ibid Ref. 1, 58.
4. E. Pink and A. Grinberg: Mater. Sci. Eng., 51, 1, 1981; Acta Metall., 30, 2153, 1982.
5. L. Brewer and S-G. Chang: "Metals Handbook, vol. 8: Metallography, Structures and Phase Diagrams", ASM, Metals Park, 1973, 422.
6. W. Schmidt and O. Jarleborg: "Ferritic Stainless Steels with 17% Chromium", Climax Molibdenum GMBH, 1977.
7. F.R. Nabarro, Z.S. Basinski and D.B. Holt: Adv. Phys., 13, 193, 1964.
8. H. Mecking: "Work Hardening in Tension and Fatigue", ed. A.W. Thompson, The Metallurgical Society of AIME, New York, 1978, 25.
9. R. Colás: To be published in Scripta Metall., 1985.
10. F.E. Al-Jouni: Ph.D. Thesis, University of Sheffield, England, 1983.

E. Juárez-Badillo

GENERAL TIME VOLUME CHANGE EQUATION FOR SOILS

Proceedings of the Eleventh International Conference

on Soil Mechanics and Foundation Engineering

San Francisco, California 12-16 August 1985

Publications Committee of XI ICSMFE

General time volume change equation for soils

Equation générale de variation de temps volume pour sols

E. JUAREZ-BADILLO, Research professor, Graduate School of Engineering, National University of Mexico; Technical Adviser of the General Director of Technical Services, Ministry of Communications and Transports, Mexico

SYNOPSIS Traditionally the time volume change behaviour of soils under isotropic and confined conditions has been divided into instantaneous and delay deformations. This time a general unifying equation for soils is presented. The time volume change behaviour of soils is described by 2 parameters: the "coefficient of volume viscosity δ" and the "characteristic time t*".

"παντα ρει" (Heraclitus)

INTRODUCTION

A general compressibility equation for soils has already been presented by the author (1981) using some general philosophic principles. These philosophic ideas have also been used to obtain a general permeability change equation for soils (1983a). This time the same philosophic ideas are used to obtain the evolution of such volume changes with time. It includes the instantaneous and delay volume changes in dry coarse soils (sands and gravels) and the delay or secondary compression of fine saturated soils (silts and clays). Primary compression or consolidation due to the retardation caused by the dissipation of pore pressure in saturated fine soils has already been the subject of previous papers (Juarez-Badillo, 1983b, 1985; Juarez-Badillo and Chen, 1983).

BASIC CONSIDERATIONS

Let us consider a sample of dry coarse soil subject to an isotropic stress σ_1 for a very long time. Let now the stress σ_1 be increased "instantaneously" to σ_2. The problem is to find the infinitesimal changes in volume dV taking place in the infinitesimal times dt. Let V_i be the initial volume for t = 0 and V_f be the final volume for $t = \infty$. The relation between dV and dt should produce an equation satisfying the following philosophic principle:

"The equation relating V and t may exist only through a non dimensional parameter and should, independently of critical points, satisfy the extreme boundary conditions, namely: $V = V_i$ for $t = 0$ and $V = V_f$ for $t = \infty$".

The connection between dV and dt can be obtained through the following steps which are thought to be philosophically supported:

1) The real domain for t is complete, that is, from 0 to ∞, while the real domain for V is incomplete and inverse, that is, from V_i to V_f. We need to find a function f(V) with real domain complete and straight, that is f(V) = 0 for t = 0 and $f(V) = \infty$ for $t = \infty$. Fig 1 illustrates the obtention of f(V) that results to be

$$f(V) = \frac{1}{V - V_f} - \frac{1}{V_i - V_f} \tag{1}$$

2) Now f(V) and t are ready to be connected. For philosophic reasons, which includes the philosophic principle enunciated above, the relationship should be

$$\frac{df(V)}{f(V)} = \delta \frac{dt}{t} \tag{2}$$

where δ is a non dimensional parameter of proportionality, called the non linear "coefficient of volume viscosity".

GENERAL EQUATION

Let V_1 be the known volume for $t = t_1$ ($t_1 \neq 0$). Integrating eq (2) between the limits (t_1, V_1) and (t, V) we get

$$\ln f(V) \Big]_{V_1}^{V} = \delta \ln t \Big]_{t_1}^{t}$$

$$\therefore \quad \frac{f(V)}{f(V_1)} = \left(\frac{t}{t_1}\right)^{\delta} \tag{3}$$

Introducing eq (1) into eq (3) we obtain

$$\frac{\dfrac{1}{V - V_f} - \dfrac{1}{V_i - V_f}}{\dfrac{1}{V_1 - V_f} - \dfrac{1}{V_i - V_f}} = \left(\frac{t}{t_1}\right)^{\delta} \tag{4}$$

1/A/28

Multiplying numerator and denominator of the first term by $V_i - V_f$, this eq (4) may be written as

$$\frac{V_i - V_f}{V - V_f} = 1 + \left(\frac{V_i - V_f}{V_1 - V_f} - 1\right)\left(\frac{t}{t_1}\right)^{\delta} \qquad (5)$$

In practice, a simpler and more convenient way of writing eq (5) is using alternatively the symbols

$$\begin{aligned} V_i - V &= \Delta V = x \\ V_i - V_f &= (\Delta V)_T = x_T \end{aligned} \qquad (6)$$

where $\Delta V = x$ is the volume change at time t and $(\Delta V)_T = x_T$ is the volume change at $t = \infty$.

Introducing eqs (6) into eq (5) we obtain

$$\frac{x_T}{x_T - x} = 1 + \left(\frac{x_T}{x_T - x_1} - 1\right)\left(\frac{t}{t_1}\right)^{\delta} \qquad (7)$$

$$\therefore \quad \frac{x}{x_T - x} = \frac{x_1}{x_T - x_1}\left(\frac{t}{t_1}\right)^{\delta}$$

$$\therefore \quad \frac{x_T - x}{x} = \frac{x_T - x_1}{x_1}\left(\frac{t_1}{t}\right)^{\delta}$$

and therefore we arrive at the useful equation

$$\frac{x_T}{x} = 1 + \left(\frac{x_T}{x_1} - 1\right)\left(\frac{t_1}{t}\right)^{\delta} \qquad (8)$$

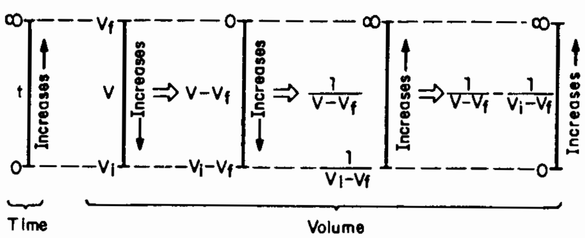

Fig.1 Scheme for the obtention of

$$f(V) = \frac{1}{V - V_f} - \frac{1}{V_i - V_f}$$

If the degree of compression U is defined as $U = \frac{x}{x_T}$, then eq (8) may be written as

$$\frac{1}{U} = 1 + \left(\frac{1}{U_1} - 1\right)\left(\frac{t_1}{t}\right)^{\delta} \qquad (9)$$

A further simpler form for eq (9) is defining the "characteristic time t*" as the time for which $U_1 = 0.5$. In this way eq (9) may be written in the very simple form

$$\frac{1}{U} = 1 + \left(\frac{t^*}{t}\right)^{\delta} \qquad (10)$$

In order to feel the progress of compression with time Fig. 2 shows the graphs of eq (9) for the special case that $t_1 = t_{0.9}$ for $U_1 = 0.9$. Different values of δ are shown. The Terzaghi's linear solution for onedimensional consolidation is shown for comparison. Fig. 3 shows the same curves for the case that $t_1 = t_{0.1}$ for $U_1 = 0.1$ and Fig . 4 shows also the same curves for $t_1 = t_{0.5}$ for $U_1 = 0.5$. From Figs. 2, 3 and 4 it appears obvious that they are not very convenient plots to deal with in practice.

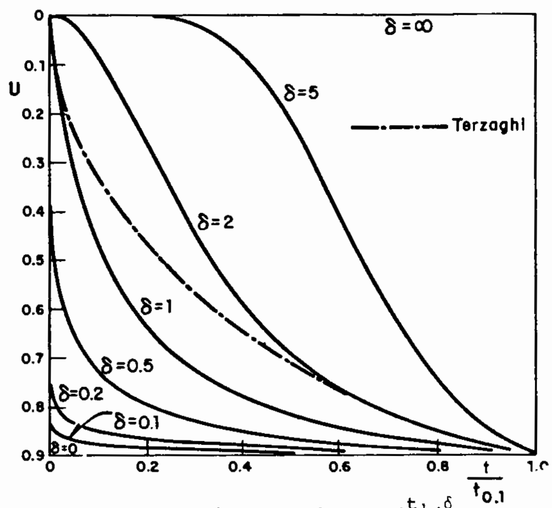

Fig.2 Graphs of $\frac{1}{U} = 1 + \left(\frac{1}{U_1} - 1\right)\left(\frac{t_1}{t}\right)^{\delta}$ for $U_1 = 0.9 (t_1 = t_{0.9})$

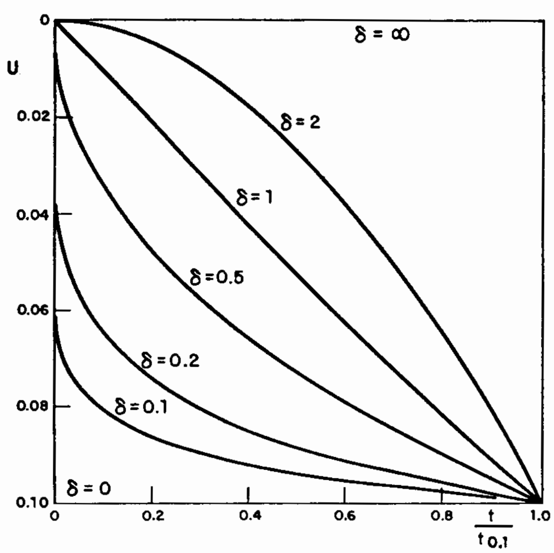

Fig.3 Graphs of $\frac{1}{U} = 1 + \left(\frac{1}{U_1} - 1\right)\left(\frac{t_1}{t}\right)^{\delta}$ for $U_1 = 0.1 (t_1 = t_{0.1})$

1/A.28

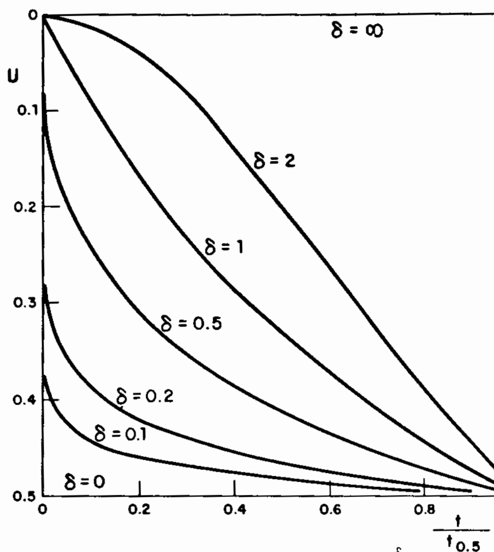

Fig.4 Graphs of $\frac{1}{U} = 1 + \left(\frac{1}{U_1} - 1\right)\left(\frac{t_1}{t}\right)^{\delta}$ for $U_1 = 0.5 (t_1 = t_{0.5})$

Fig. 5 (a and b) shows the same curves than Fig. 2 but in a semi-log plot, that is, the time in log scale.

If the "time factor τ" is defined by

$$\tau = \left(\frac{t}{t^*}\right)^{\delta} \tag{11}$$

then eq (10) may be written as

$$\frac{1}{U} = 1 + \frac{1}{\tau} \tag{12a}$$

or in the form

$$\frac{U}{1-U} = \tau \tag{12b}$$

Fig. 6 presents the graph of eq (12) as well as the values of τ for different values of U.

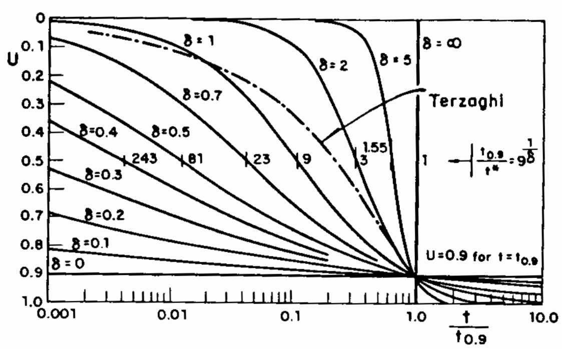

Fig.5a Graphs of $\frac{1}{U} = 1 + \left(\frac{1}{0.9} - 1\right)\left(\frac{t_{0.9}}{t}\right)^{\delta}$

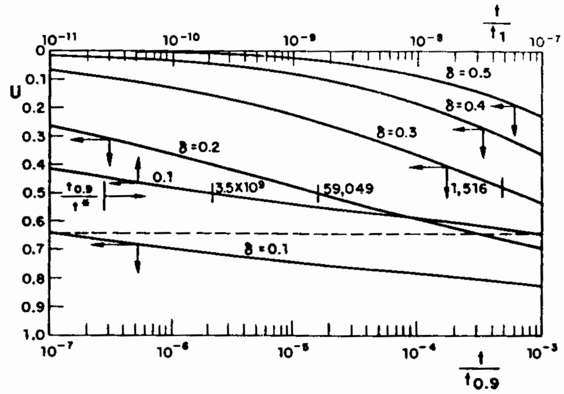

Fig.5b Graphs of $\frac{1}{U} = 1 + \left(\frac{1}{0.9} - 1\right)\left(\frac{t_{0.9}}{t}\right)^{\delta}$

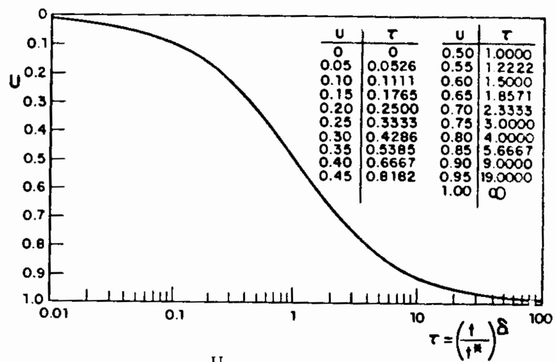

U	τ	U	τ
0	0	0.50	1.0000
0.05	0.0526	0.55	1.2222
0.10	0.1111	0.60	1.5000
0.15	0.1765	0.65	1.8571
0.20	0.2500	0.70	2.3333
0.25	0.3333	0.75	3.0000
0.30	0.4286	0.80	4.0000
0.35	0.5385	0.85	5.6667
0.40	0.6667	0.90	9.0000
0.45	0.8182	0.95	19.0000
		1.00	∞

Fig.6 Graph of $\frac{U}{1-U} = \tau$

In order to ascertain in practice the values of δ and t*, some characteristics of the semi-log plots follows.

1) The semi-log plots are anti-symmetric, that is if $U_2 = 1 - U_1$, then $\frac{t_2}{t^*} = \frac{t^*}{t_1}$. From eq (12b) for $U = U_1$ we have

$$\tau_1 = \frac{U_1}{1 - U_1} \tag{13}$$

For $U_2 = 1 - U_1$ we similarly have

$$\tau_2 = \frac{U_2}{1 - U_2} = \frac{1 - U_1}{U_1} = \frac{1}{\tau_1} \tag{14}$$

that is, from eq (11)

$$\left(\frac{t_2}{t^*}\right)^{\delta} = \left(\frac{t^*}{t_1}\right)^{\delta} \tag{15}$$

therefore

$$\frac{t_2}{t^*} = \frac{t^*}{t_1} \tag{16}$$

1/A/28

In the semi-log plots, therefore, symmetrical values of U with respect to U = 0.5, have symmetrical values of t with respect to t*. See Figs. 5 and 6.

2) The middle third of the semi-log plots resembles very close a stright line.

The slope of the curve in Fig. 6 may be found using eqs (12)

$$\frac{dU}{d\log\tau} = 2.3\tau\,\frac{dU}{d\tau} = 2.3\tau\,\frac{U^2}{\tau^2} = 2.3\,\frac{U^2}{\tau}$$

$$\therefore\quad \frac{dU}{d\log\tau} = 2.3U(1-U) \qquad (17)$$

The maximum slope occurs at U = 0.5 (t=t*) and its value is

$$\left(\frac{dU}{d\log\tau}\right)_{max} = \frac{2.3}{4} \qquad (18)$$

Similarly, the slopes of the curves in Fig 5 are as follows. From eq (11) we have

$$\frac{d\tau}{\tau} = \delta\,\frac{dt}{t} \qquad (19)$$

and therefore, we may write from eqs (19) and (17)

$$\frac{dU}{d\log t} = 2.3t\,\frac{dU}{dt} = 2.3\delta\,\tau\,\frac{dU}{d\tau} = 2.3\,\delta\,\frac{U^2}{\tau}$$

$$\therefore\quad \frac{dU}{d\log t} = 2.3\delta U(1-U) \qquad (20)$$

The maximum slope occurs at U = 0.5 (t=t*) and its value is

$$\left(\frac{dU}{d\log t}\right)_{max} = \frac{2.3}{4}\,\delta \qquad (21)$$

The ratio of the slope at any point to the maximum slope is therefore given by

$$\frac{\dfrac{dU}{d\log t}}{\left(\dfrac{dU}{d\log t}\right)_{max}} = 4U(1-U) \qquad (22)$$

The values of this ratio for U = 0, 0.1, 0.2, 0.3, 0.4, 0.5 are: ratio = 0, 0.36, 0.64, 0.84, 0.96, 1.0 respectively. For U = 1/3, ratio = 8/9 = 0.89.

Finally, the ratio of the slope of the stright line passing by the extreme points of the middle third of the graph (secant slope = $\frac{\Delta U}{\Delta\log\tau}$) to the maximum slope is, using eq (12b)

$$\frac{\Delta U}{\Delta\log\tau} = \frac{2/3-1/3}{\log\frac{\tau 2/3}{\tau 1/3}} = \frac{1/3}{\log\frac{2}{\frac{1}{2}}} = \frac{1}{6\log 2} \qquad (23)$$

The ratio is, therefore, from eqs (23) and (18)

$$\frac{\dfrac{\Delta U}{\Delta\log\tau}}{\left(\dfrac{dU}{d\log\tau}\right)_{max}} = \frac{2}{3 \times 2.3\log 2} = 0.96 \qquad (24)$$

The above shows that, in practice, the middle third of the time curve may be considered, without serious error, as a stright line. See Figs. 5 and 6.

The stright line (middle third) of the time curve extends over certain number of cicles in the log scale of time. The number of cicles may be found as follows. For Fig. 6 and from eq (12b) we have that for U = 1/3, τ = 0.5 and for U = 2/3, τ = 2, therefore, the number of cicles given by $\Delta\log\tau$ is

$$\Delta\log\tau = \log\frac{\tau 2/3}{\tau 1/3} = \log 4 = 0.6 \qquad (25)$$

Similarly, for Fig. 5 and from eq (11) we may write

$$\Delta\log t = \log\frac{t2/3}{t1/3} = \frac{1}{\delta}\log\frac{\tau 2/3}{\tau 1/3} = \frac{\log 4}{\delta} = \frac{0.6}{\delta} \qquad (26)$$

For example, for δ =0, 0.1, 0.3, 0.6, 1.0, ∞, the stright lines extends over ∞, 6, 2, 1, 0.6, 0 cicles, respectively. See Fig. 5.

All the above characteristics of the time curves are very useful to determine, in practice, the parameters δ and t* from the experimental data.

Once the values of δ and t* are known the time for a give degree of compression may be found. From eqs (11) and (12b)

$$\left(\frac{t}{t^*}\right)^{\delta} = \frac{U}{1-U} \qquad (27)$$

For example, for U = 0.9

$$\frac{t_{0.9}}{t^*} = 9^{1/\delta} \qquad (28a)$$

Observe that for (1-U) the time is just reciprocal. For the above example, for U = 0.1

$$\frac{t_{0.1}}{t^*} = \left(\frac{1}{9}\right)^{1/\delta} \qquad (28b)$$

Fig 5 shows the values of eq (28a) for the different values of δ.

The rate at which the degree of compression progresses may be found as follows. From eqs (12a) and (12b)

$$\frac{dU}{d\tau} = \frac{U^2}{\tau^2} = (1-U)^2 \qquad (29)$$

From eq (11)

$$d\tau = \delta\left(\frac{t}{t^*}\right)^{\delta}\frac{dt}{t} \qquad (30)$$

Introducing eq (30) into eq (29)

$$\frac{dU}{dt} = (1-U)^2\,\frac{\delta}{t}\left(\frac{t}{t^*}\right)^{\delta} \qquad (31)$$

For t = 0 (U = 0) we get

1/A/28

$$\text{If} \quad \delta < 1 \quad \left[\frac{dU}{dt}\right]_{t=0} = \infty$$

$$\text{If} \quad \delta = 1 \quad \left[\frac{dU}{dt}\right]_{t=0} = \frac{1}{t^*} \tag{32}$$

$$\text{If} \quad \delta > 1 \quad \left[\frac{dU}{dt}\right]_{t=0} = 0$$

From expressions (32) we see that only for the case $\delta < 1$ we may expect to have "instantaneous" or "simultaneous" deformation with the "instantaneous" increase in stress. However the amount of this instantaneous deformation depends on the value of δ and on the time we take to register it. See Figs. 2, 3 and 4. For $\delta = 1$ the rate of deformation is finite and therefore any deformation needs some time to take place. For $\delta > 1$ the rate of deformation is zero.

The above theory, developed for soils under isotropic stresses is thought to be also true for triaxial conditions if the principal directions of stress and of strain do not change and if the ratio of the principal stresses are kept constant, as for example, in confined onedimensional compression.

The determination, in practice, of the parameters δ and t^* depends on the type of the experimental data. Using the semi-log plots we will refer to the three thirds by (c), (s), (c), that is, curve, stright line, curve. Data with points in the three thirds: (csc). Data with only in two thirds: (cs) and (sc). Data with only in one third: (c_1), (s) and (c_2). The best experimental data is (csc). The worse experimental data is (s) if it is a "short" stright line.

For obtaining δ and t^* from an experimental curve, the author has found convenient to proceed as follows. The procedure is general but, for simplicity, imagine we have an (cs) type data.

Let t_3, x_3 be an initial point (See eq (8)). Let t_1, x_1 be an intermediate point. Let t_2, x_2 be a final point. The last two points located in the initial and final zones of the stright line. Observe that the values of the x may be any quantities proportional to the volume changes.

1) Guess a value for x_T making use of the characteristics of the semi-log plot. Find the value of x = a for the point where the stright line starts. Then, $x_T = 3a$.

2) Compute δ using points 1 and 2 (they are usually better points than point 3). Points 1 and 2 satisfy eq (10)

$$\frac{1 - U_1}{U_1} = \left(\frac{t^*}{t_1}\right)^{\delta} \tag{33}$$

$$\frac{1 - U_2}{U_2} = \left(\frac{t^*}{t_2}\right)^{\delta} \tag{34}$$

Dividing eq (33) by eq (34)

$$\frac{1 - U_1}{U_1}\,\frac{U_2}{1 - U_2} = \left(\frac{t_2}{t_1}\right)^{\delta} \tag{35}$$

Solving eq (35) for δ and writing the U,s in terms of the x,s we get

$$\delta = \frac{\log \dfrac{x_2}{x_1}\,\dfrac{x_T - x_1}{x_T - x_2}}{\log \dfrac{t_2}{t_1}} \tag{36}$$

3) Check the value of x_T using the initial point 3. This point should satisfy eq (8)

$$\frac{x_T}{x_3} = 1 + \left(\frac{x_T}{x_1} - 1\right)\left(\frac{t_1}{t_3}\right)^{\delta} \tag{37}$$

4) Repeat steps 1 to 3 in case eq (37) is not satisfied, changing the value of x_T in the correct direction (a grater x_T results in grater calculated x_3).

5) Compute t^* using preferable point 2. From eq (10)

$$\left(\frac{t^*}{t_2}\right)^{\delta} = \frac{x_T - x_2}{x_2} \tag{38}$$

6) Introduce x_T, δ and t^* in eq (10). The time equation is ready for use

$$\frac{x_T}{x} = 1 + \left(\frac{t^*}{t}\right)^{\delta} \tag{39}$$

Equation (39) written in terms of volumes and in terms of heights (for onedimensional consolidation) are as follows

$$V = V_i - \Delta V = V_i - \frac{(\Delta V)_T}{1 + \left(\frac{t^*}{t}\right)^{\delta}} \tag{40a}$$

$$H = H_i - \Delta H = H_i - \frac{(\Delta H)_T}{1 + \left(\frac{t^*}{t}\right)^{\delta}} \tag{40b}$$

For the case of (sc) type data use the antysimmetrical points. For (csc) type data use the extreme points of the stright line for points 1 and 2 and check two points 3 located at the extremes of the intire experimental curve.

For the case of (s) type data, the parameters may be determined if it is a "complete stright line". Intervals for x_T, δ and t^* may be found otherwise.

For this case let x_1 and x_2 the values of x for the initial and final points of the stright line. The stright line is complete if $x_2 = 2x_1$. If $x_2 < 2x_1$ it is incomplete. In this last case x_T shoud satisfy the unequality

1/A/28

$$1.5x_2 \le x_T \le 3x_1 \qquad (41)$$

Assuming for x_T the extreme values given by eq (41), the corresponding values for δ and t^* may be found using eqs (36) and (38).

If the value of δ is known, x_T may be found solving eq (35) for x_T. It results

$$\frac{x_T}{x_2} = \frac{\left(\frac{t_2}{t_1}\right)^{\delta} - 1}{\left(\frac{t_2}{t_1}\right)^{\delta} - \frac{x_2}{x_1}} \qquad (42)$$

The value of x_T found should satisfy unequality (41).

PRACTICAL APPLICATION

The above theory is now applied to some experimental data.

One of the earliest "Time curve for a typical load increment on sand" is Fig 10.4 in Taylor's book (1948) (Not included here). Comparison with Fig. 2, indicates approximate values of δ = 0.1 and t^* = 1 sec.

Fig. 7 presents the experimental (Vesic and Clough, 1968) and theoretical curves for "medium, uniform, slightly micaceous sand, composed of sub-angular quartz grains" between 0.1 to 1.0 mm sizes, Chattahoochee River sand, during isotropic compression. "The volumetric strains are plotted as percentages of total volumetric strains under the particualr load increments (degrees of consolidation) versus time". The deformation in question "predominantly breakdown of particles" situates these curves on the second phase (virgin) of the compression curves (Juarez-Badillo, 1981). An inspection of the curves obliged the author to make an allowance of 10 sec for primary consolidation for the first 3 increments of load, and to make an allowance of 3% for further compression for the last increment of load. With these "corrections" eq (10) was applied using δ = 1 and the characteristic times t^* indicated for each laod increment. It is to be observed that t^* increases with the level of stress.

Fig. 8 (a and b) present the experimental (Zepeda and Diaz, 1982) and theoretical time curves for Mexico City pumice sand, between 0.84 to 4.76 mm sizes, under the particular load increments indicated. The loads were sustained from 2 to 17 hrs. Tests were made on a very dense state of the sand and on a very loose state. The experimental data includes the types: (csc), (cs) (sc) and (s). The values of $x_T = (\Delta H)_T$, δ and t^* were ascertained as indicated above, using eqs (36), (37) and (38) and eq (40b) was used to plot the theoretical curves. The check was almost intirely within 0.01 mm with few zones (at the beginning of the curves) where the check was within 0.02 mm. It was necessary, however, to make 2 small "corrections" to H_i, as indicated in Figs. 9 and 10.

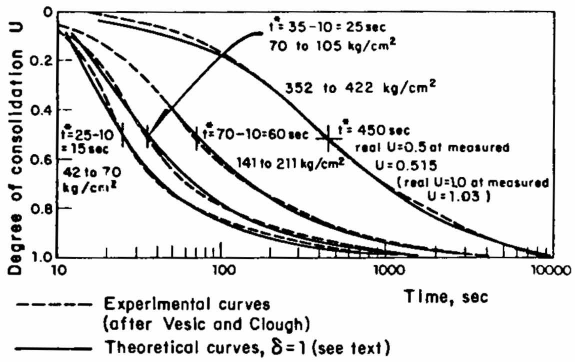

Fig.7 Progress of volumetric strain with time during isotropic compression. Chattahoochee River sand

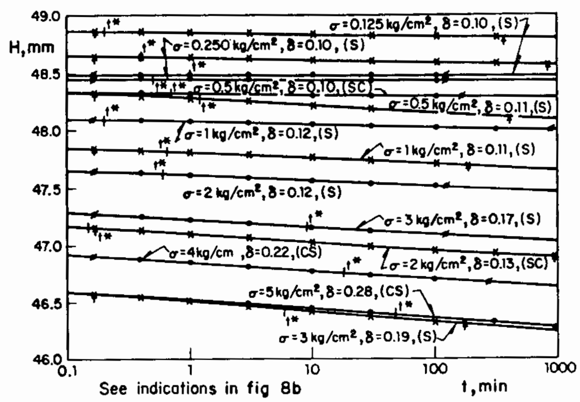

Fig.8a Time Volume change of Mexico City pumice sand

Table 1 presents the time parameters of all these time curves. Figs. 9 and 10 present the compression curves for both, very dense and very loose states. Note that for stresses below 1 or 2 kg/cm² the experimental data was of the (s) type, and they were "short" stright lines with $x_2 < 2x_1$. However, by interpolation in Figs. 9 and 10 it was possible to choose the "correct" values for x_T, δ and t^*. Fig. 11 shows the variation of δ with the level of stress. Zepeda reported he believed there was breakdown of particles at all increments of load. The author believes there was not breakdown of particles for stresses below 2 kg/cm², due to the constant small value of δ = 0.1. The feeling of the author, at present, is that, for granular soils, δ is small and constant ($\delta \doteq 0.1$), before the breaking of particles and that δ is large and constant ($0.5 < \delta \le 1$) when the level of stress is already in the virgin. curve where a generalized breakdown of particles exists. In these experiments it appears that the "critical zone" where there is partial breaking of particles extends from 2 to 8 kg/cm^2. Fig 11 also shows that for the very dense state the values of δ were somewhat smaller than for the very loose state. Observe also from Table 1 that t* appears to be constant (~ 0.5 min) before the breakdown of particles.

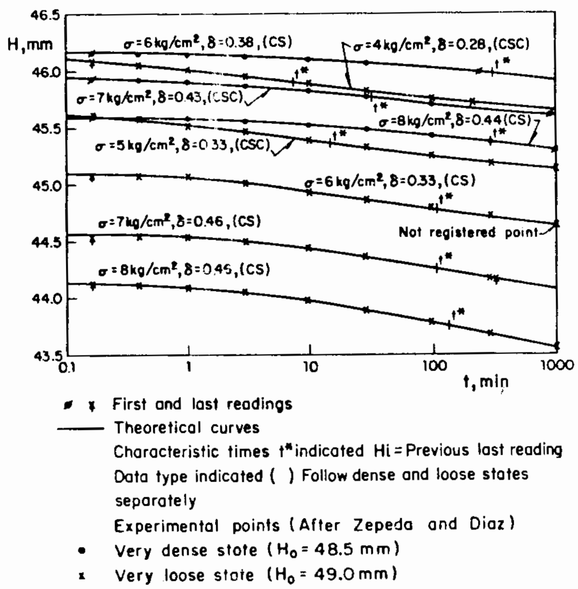

Fig.8b Time Volume change of Mexico City pumice sand

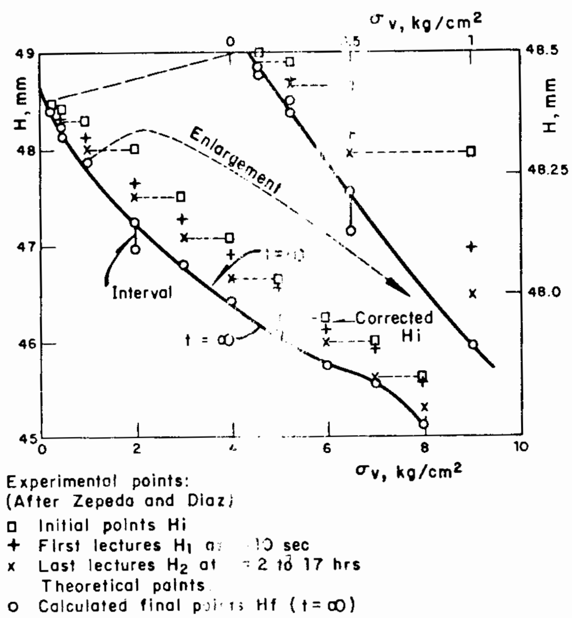

Fig.9 Compression of Mexico City pumice sand. Very dense state

Table 1. Time parameters for Mexico City pumice sand tests

State	σ, kg/cm^2	Time of loading min	H_i mm	x_T mm	H_f mm	δ	t* min
Very dense	0.125	120	48.50	0.03	48.47	0.10	1.0
	0.25	120	48.48	0.08	48.40	0.10	0.5
	0.5	160	48.43	0.22	48.21	0.10	0.7
	1	850	48.29	0.40	47.89	0.12	0.2
	2	120	48.00	0.75	47.25	0.12	0.6
	3	120	47.51	0.70	46.81	0.17	9
	4	270	47.08	0.65	46.43	0.22	18
	5	1000	46.66	0.55	46.11	0.28	47
	6	240	46.20	0.45	45.75	0.38	310
	7	940	45.99	0.45	45.54	0.43	33
	8	1000	45.62	0.50	45.12	0.44	300
Very loose	0.125	340	49.00	0.28	48.72	0.10	0.2
	0.25	790	48.81	0.35	48.46	0.10	0.4
	0.5	380	48.57	0.55	48.02	0.11	1.2
	1	180	48.21	0.80	47.41	0.11	0.65
	2	925	47.69	1.05	46.64	0.13	0.15
	3	170	46.89	0.90	45.99	0.19	6
	4	215	46.30	0.80	45.50	0.28	7.5
	5	1000	45.74	0.75	44.99	0.33	15
	6	1010	45.14	0.70	44.44	0.41	110
	7	340	44.61	0.70	43.91	0.46	110
	8	1000	44.17	0.85	43.32	0.46	140

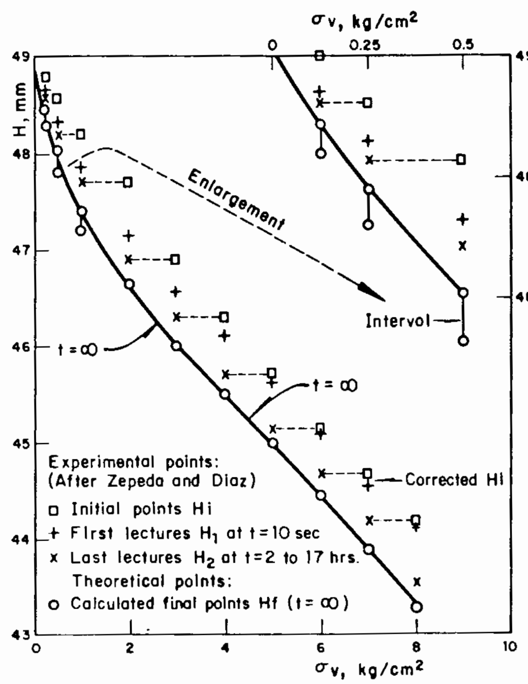

Fig.10 Compression of Mexico City pumice sand. Very loose state

A similar experimental work (Porras and Diaz, 1984) was made on Guadalajara pumice sand (Jal) in a medium dense dry and saturated

1/A/28

states. The load increments were sustained one day but the "short" stright lines were more abundant making somewhat difficult their analysis. However the author found that the values of δ for the saturated sand were, in the average, 1.5 times the corresponding values of δ for the dry sand.

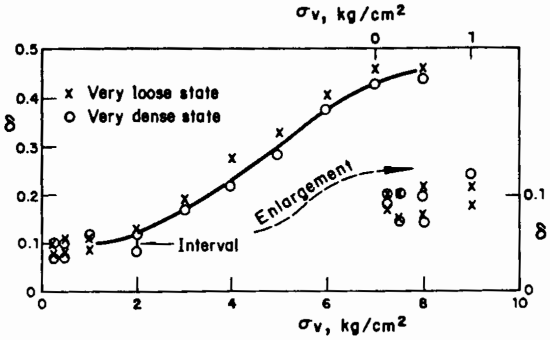

Fig.11 Variation of δ for Mexico City pumice sand

Fig. 12 presents the time curve for a long time oedometer test made on a typical sample of Mexico City clay. The sample was 15 mm height. A vertical pressure of 0.96 kg/cm² was sustained 250 days. The previous load was 0.74 kg/cm² sustained 8 days. The increment load ratio was therefore 0.30. Eq (40b) was applied with H_i = 12.12 mm, $(\Delta H)_T$ = 0.84 mm, δ = 0.73 and t^* = 7.2 days. After 90 days the experimental points presented some inconsistencies and bacterial growth was very noticeable. A second test was made in identical conditions and its behaviour was practically identical but with higher inconsistencies after 90 days. It should be observed that, for this test, primary consolidation was almost unnoticeable. Probably it was very small and took place in less than 0.1 day making the "secondary compression" data very consistent.

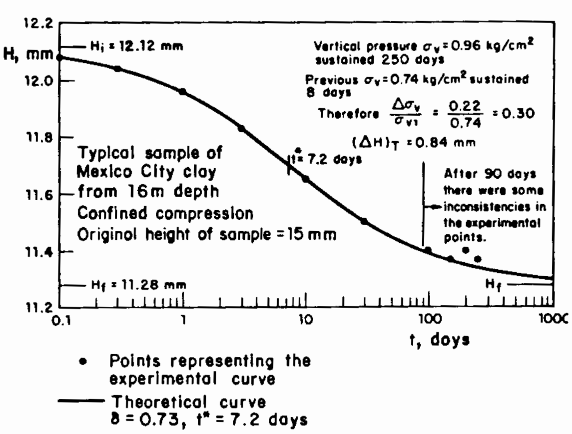

Fig 12. Time volume change of Mexico City clay

A "coefficient of secondary compression" that may prove to be useful in practice due to its similarity with the ones already in use (Mesri, 1973) is the following. From eq (21)

$$\varepsilon_\alpha^* = \left(\frac{dH}{d\log t}\frac{1}{H}\right)_{t=t^*} = \frac{2.3}{4}\delta\frac{(\Delta H)_T}{H^*} \tag{43}$$

where H^* is the value of H for $t = t^*$

In terms of volumes, eq (43) would read

$$\varepsilon_\alpha^* = \frac{2.3}{4}\delta\frac{(\Delta V)_T}{V^*} \tag{44}$$

For the test on Mexico City clay of Fig. 12 we have, therefore

$$\varepsilon_\alpha^* = \frac{2.3}{4}\,0.73\,\frac{0.84}{11.70} = 0.030 \tag{45}$$

Note, however, that this parameter is not enough to completely specify secondary behaviour.

Several time curves were made available to the author by his colleague Leonardo Zeevart (1983) using 20 mm thick samples of typical Mexico City clay, with load increment ratios from 0.30 to 0.75 in the recompression branch and from 0.15 to 0.40 in the normally consolidation branch. The loads were sustained from 4 to 24 hours. An inspection of these curves clearly showed that in the recompression branch primary consolidation took place for $U \doteq 0.3$. In the normally consolidation branch the author could not determine the termination of primary consolidation.

Mesri (1973) has published a very extensive experimental data on onedimensional tests using Organic (liquid limit w_L = 70) and Inorganic (w_L = 54) Paulding clays. Thixotropic hardening has not been considered in the above theory. Therefore, remoulded samples are not considered. Only sedimented samples behaviour on the normally consolidated branch will be considered (K_o is not constant in the recompression and swelling branches). The data is mainly presented in terms of C_α and $\varepsilon_{\alpha p}$ defined by

$$\varepsilon_{\alpha p} = \frac{C_\alpha}{1+e_p} = \frac{\Delta e}{\Delta\log t}\,\frac{1}{1+e_p} \tag{46}$$

where e_p = void ratio at the beginning of the linear portion of the e-log t curve.

For our analysis let us substitute expression (46) for the equivalent expression

$$\varepsilon_{\alpha p} = \left(\frac{dH}{d\log t}\right)_{t=t^*}\frac{1}{H_p} \tag{47}$$

where H_p is the value of H for $e = e_p$.

Comparison of eqs (43) and (47) leads to

$$\varepsilon_\alpha^* = \varepsilon_{\alpha p} \frac{H_p}{H^*} \tag{48}$$

The tests were made on 25.4 mm thick samples, using load increment ratios $\frac{\Delta\sigma}{\sigma} = 1$. The loads were from 0.25 to 32 kg/cm^2. The level of stress was reached "with only sufficient time allowed for excess pore pressure dissipation". Let us assume, in order to continue with the analysis, that this ocurred for U = 1/3.

Fig. 13 presents a scheme illustrating primary and final compression curves in clays using the above assumption. The data was suggested by Organic Paulding clay. Approximate values of its coefficient of compressibility γ and of its void ratio e_8 for $\sigma = 8$ kg/cm^2 may be found using the expressions (Juarez-Badillo, 1975)

$$\gamma = 0.0016(w_L - 10) = 0.10 \tag{49}$$

and

$$e_8 = 7.5\gamma = 0.75 \tag{50}$$

The primary compression curve would, therefore, be (σ in kg/cm^2)

$$\frac{V}{V_8} = \left(\frac{\sigma}{8}\right)^{-0.10} \tag{51}$$

or in terms of void ratios

$$\frac{1+e}{1.75} = \left(\frac{\sigma}{8}\right)^{-0.10} \tag{52}$$

The void ratio for $\sigma = 4$ kg/cm^2 is, from eq (52), e = 0.875, that is $(\Delta e)_p = 0.125$, and, therefore, $(\Delta e)_T$, = 0.375, and for the total compression curve, we get, for $\sigma = 8$ kg/cm^2, $e_8 = 0.5$. The equation for this curve is, therefore,

$$\frac{1+e}{1.5} = \left(\frac{\sigma}{8}\right)^{-0.10} \tag{53}$$

The value of $\frac{H_p}{H^*}$, entering in eq (48), is given by (See Fig. 13)

$$\frac{H_p}{H^*} = \frac{H_i - (\Delta H)_p}{H_i - \frac{3}{2}(\Delta H)_p} = \frac{1 - \frac{(\Delta H)_p}{H_i}}{1 - \frac{3}{2}\frac{(\Delta H)_p}{H_i}} \tag{54}$$

where, for our case

$$\frac{(\Delta H)_p}{H_i} = 1 - \left(\frac{\sigma_2}{\sigma_1}\right)^{-\gamma} = 1 - 2^{-\gamma} \tag{55}$$

Introducing eqs (54) and (55) into eq (48) we obtain

$$\varepsilon_\alpha^* = \varepsilon_{\alpha p} \frac{2}{3 - \left(\frac{\sigma_2}{\sigma_1}\right)^{\gamma}} \tag{56}$$

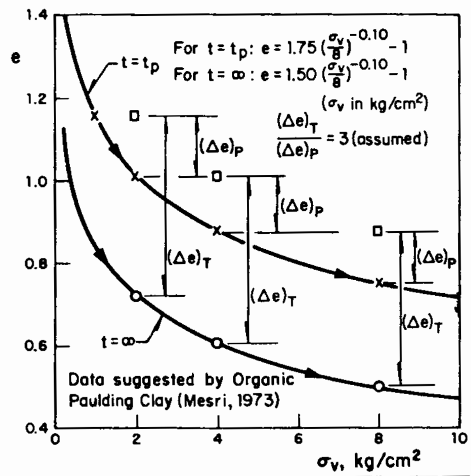

Fig.13 Scheme illustrating primary and final compression curves in clays

The value of $\frac{(\Delta H)_T}{H^*}$ entering in eq (43) is given by

$$\frac{(\Delta H)_T}{H^*} = \frac{3(\Delta H)_p}{H_i - \frac{3}{2}(\Delta H)_p} = \frac{3}{\frac{H_i}{(\Delta H)_p} - \frac{3}{2}} \tag{57}$$

Mesri has reported that for Organic Paulding clay, $\varepsilon_{\alpha p} = 0.013$, and that for Inorganic Paulding clay, $\varepsilon_{\alpha p} = 0.0035$ (Fig. 5 in Mesri paper).

Applying eqs (49), (55), (56), (57) and (43) to Organic Paulding clay we get

$$\begin{aligned} \gamma &= 0.10 \\ \varepsilon_\alpha^* &= 0.0135 \\ \delta &= 0.10 \end{aligned} \tag{58}$$

Similarly, applying the same equations to Inorganic Paulding clay we get

$$\begin{aligned} \gamma &= 0.07 \\ \varepsilon_\alpha^* &= 0.0036 \\ \delta &= 0.04 \end{aligned} \tag{59}$$

Observe that there is no practical difference between ε_α^* and $\varepsilon_{\alpha p}$. Observe also that these parameters can not be used in practice without the t* parameter.

Mesri et al (1975) have published a very extensive experimental data on secondary compression of typical samples of Mexico City clay. The samples were 19 mm high. The applied pressures were up to 30 kg/cm^2. "The samples were loaded in increments to a final

1/A/28

pressure using a load increment ratio of unity and a load increment duration just sufficient for completion of primary consolidation determined by Taylor's method (Taylor, 1948)". For undisturbed samples, first sustained loading, they report a constant value $\varepsilon_{\alpha p} = 0.033$ (their Fig. 25) for the virgin branch of the compressibility curve. From the compressibility curve (their Fig. 16) the author obtained a compressibility coefficient $\gamma = 0.43$. Making the assumption that primary consolidation ocurred for $U \leq 1/3$, application of eqs (55), (56), (57) and (43) give

$$\begin{aligned} \gamma &= 0.43 \\ \varepsilon^*_\alpha &= 0.040 \\ \delta &= 0.06 \end{aligned} \tag{60}$$

The value of γ coincides with the value reported by the author (1975). Observe now that ε^*_α is 20% higher than $\varepsilon_{\alpha p}$. Compare also this value of ε^*_α with the one given by eq (45) for Fig. 12. Compare also the small value of $\delta = 0.06$ with the high value $\delta = 0.73$ obtained in Fig. 12. This great difference, might be due to the fact that Fig. 12 is still in the recompression branch of the compressibility curve. Future research should clarify this point.

FINAL DISCUSSION

It has been shown that the time volume change behaviour of soils (when no retardation exists due to pore water pressure dissipation) under isotropic and confined compression (if K_o = constant) may be described by a single equation containing two parameters, the coefficient of volume viscosity δ and the characteristic time t^*. The coefficient δ has to do mainly with the form of the time curve while the time t^* has to do mainly with the rapidity of the phenomenon. See Fig. 2.

This general time equation is identical in form to the general compressibility equation (Juarez-Badillo, 1981). Compare Fig. 3 of the present paper with Fig. 2 of the above mentioned paper. The coefficient δ in the volume time curve has the same significance than the coefficient γ in the volume pressure curve. Similarly, the characteristic time t^* has the same significance in the time curves than the characteristic pressure σ^* has in the pressure curves.

The compressibility equation reads

$$\frac{V_o}{V} = 1 + \left(\frac{\sigma}{\sigma^*}\right)^\gamma \tag{61}$$

while the time equation reads (eq (10))

$$\frac{1}{U} = 1 + \left(\frac{t^*}{t}\right)^\delta \tag{62}$$

If U' is defined by

$$U' = 1 - U \tag{63}$$

then eq (62) may be written as

$$\frac{1}{U'} = 1 + \left(\frac{t}{t^*}\right)^\delta \tag{64}$$

and the similarity of eqs (61) and (64) is evident. This is so because they satisfy the same philosophic requirements. Because of this similarity the time curves of Figs. 5 and 6 may also be interpreted, using eq (63), as the compressibility curves of granular materials before the braking of particles, that is, in the unvirgin curves.

It is the feeling of the author that for granular soils like sands:

1. In the first mechanical phase of the compressibility curve, unvirgin, δ is small and constant, say $\delta = 0.1$ and t^* is small and constant, say $t^* = 1$ to 30 sec (Taylor's figure, Fig. 11 and Table 1).

2. In the transition or critical zone, where partial breakdown of particles exists, δ and t^* increase when the stress increases (Figs. 8 and 11 and Table 1).

3. In the second mechanical phase, virgin curve, where a general breakdown of particles exists, δ is high and constant, say $\delta = 0.5$ to 1.0 and t^* increases when the compressive stress increases (Figs. 7, 8 and 11 and Table 1).

Similarly, it is the feeling of the author that for plastic soils like clays:

4. In the recompression branch δ is constant, apparently with high values (Fig. 12). Is t^* also constant?

5. In the normally consolidated branch δ is constant, apparently with low values (eqs (58), (59) and (60)). Is t^* also constant?

The above comments are mainly made to promote future experimental research. The published data does not allow the determination of t^* in clays. The author believes that a reconsideration of some of the experimental data of the past is highly desirable.

It should be noted that, in clays, primary consolidation will make necessary to introduce a modification in the time scale after the termination of the excess pore pressure dissipation, Fig. 7. Future research will indicate how this should be done.

It is important to realize that primary compression curves are functions of the loading programs while the final ($t = \infty$) compression curves are postulated to be unique for given soil samples under monotonic loading, Figs. 9, 10 and 13.

1/A/28

It should be noted that, according to this theory, the parameter ε_{α}^{*}, eq (43), very similar to the traditional $\varepsilon_{\alpha p}$, eqs (46),(47) and (48), is not a good parameter to study secondary compression. $\frac{(\Delta H)_T}{H^*}$ is constant as far as the load increment ratio is constant and no previous sustained loads have acted (eqs (57) and (55)).

It is suggested that eq (10) is also applicable to solids, liquids and gases. It should be very interesting to know the parameters δ and t* for water. Very surely they both are very small.

CONCLUSIONS

The main conclussion are as follows:

1. A general time volume change equation for soils is presented,eq (10). It consist of two parameters: the coefficient of volume viscosity δ and the characteristic time t*. The parameter δ has to do mainly with the form of the time curve while the parameter t* has to do mainly with the rapidity of the phenomenon, Fig. 2.

2. We may expect to have "instantaneous" or "simultaneous" deformation with the "instantaneous" increase of stress only when $\delta < 1$. However its amount depends on the value of δ and on the time we take to register it, Figs. 2 to 4.

3. The semi-log plot seems most appropriate for the time curves, Figs. 5 and 6. In this plots, the time curves are antisymmetric and its middle third is very close to a stright line.

4. For sands, it appears that, for the unvirgin branch of the compressibility curves, the values of δ and t* are small and constant, while for the virgin branch of the compressibility curves, the values of δ are high and constant and the values of t* increases when the compressive stress increases.

5. For clays, it appears that the values of δ are constants, but different, in the recompression and in the normally consolidation branches of the compressibility curve.

6. In clays there is a high need of experimental data to study the t* parameter.

7. There is a need of experimental data to study the factors that influence the values of the δ and t* parameters in soils.

8. It is suggested that eq (10) is also applicable to solids, liquids and gases.

ACKNOWLEDGEMENTS

The author thanks the National University of Mexico (Graduate School of Engineering and Institute of Engineering) and to the Ministry of Communications and Transports for their support of this work.

The experimental data for Fig. 12 was obtained at the particular soils laboratory of Miguel Aguirre-Menchaca, who kindly made available to the author 2 oedometers for almost a year. The tests were made by Mateo Lopez.

Some useful comments by Miguel Madinaveitia, Neftalí Rodríguez-Cuevas and Leonardo Zeevaert are gratefully acknowledged.

REFERENCES

Juárez-Badillo, E. (1975). Constitutive relationships for soils. Symposium on Recent Developments in the Analysis of Soil Behaviour and their Application to Geotechnical Structures. The University of New South Wales, Kensington, NSW, Australia, July 1975, pp 231-257.

Juarez-Badillo, E. (1981). General compressibility equation for soils. Tenth International Conference on Soil Mechanics and Foundation Engineering, Stockholm, Sweden, pp 171-178.

Juarez-Badillo, E. (1983a). General permeability change equation for soils. International Conference on Constitutive Laws for Engineering Materials, University of Arizona, Tucson, Arizona, Jan. 1983, pp 205-209.

Juarez-Badillo, E. (1983b). General consolidation theory for clays. Report No 8, Soil Mechanics Series, Graduate School of Engineering, National University of Mexico.

Juarez-Badillo, E. (1985). General theory of consolidation for clays. ASTM Symposium on Consolidation Behaviour of Soils, Ft. Lauderdale, Florida, USA, Jan. 1985.

Juarez-Badillo, E. and Chen, B. (1983). Consolidation curves for clays. Journal of Geotechnical Engineering, Vol. 109, No 10, October, 1983, ASCE, pp 1303-1312.

Mesri, G. (1973). Coefficient of secondary compression. Journal of the Soil Mechanics and Foundations Division, ASCE, Vol. 99, No SM1, Jan. 1973, pp 123-137.

Mesri, G., Rokhsar, A. and Bohor, B. F. Composition and compressibility of typical samples of Mexico City clay. Geotechnique, Vol XXV, No 3, Sept. 1975, pp 527-554.

Porras-Lopez, A. (1984). Comportamiento mecánico de una arena pomez saturada. Master Thesis directed by Diaz-Rodríguez, J.A., Graduate School of Engineering, National University of Mexico.

Taylor, D. W. (1948). Soil Mechanics. John Wiley and Sons, New York, p 217.

Vesic, A. S. and Clough, G. W. (1968). Behaviour of granular materials under high stresses. Journal of the Soil Mechanics and Foundations Division, ASCE, Vol. 94, No SM3, May, 1968, pp 661-688.

Zeevaert, L. (1983). Personal communication.

Zepeda-Garrido J. A. (1982). Estudio de las propiedades esfuerzo-deformación de una arena pomez. Master Thesis directed by Diaz-Rodriguez, J. A., Graduate School of Engineering, National University of Mexico.

R. Ortega, et al

ROBUSTNESS OF DISCRETE-TIME DIRECT ADAPTIVE CONTROLLERS

IEEE Transactions on Automatic Control,

Vol. AC-30, No. 12, December 1985

Robustness of Discrete-Time Direct Adaptive Controllers

ROMEO ORTEGA, LAURENT PRALY, AND IOAN D. LANDAU

Abstract—**The problem of preserving stability of discrete-time adaptive controllers in spite of reduced-order modeling and output disturbances is addressed in this paper. Conditions for global stability (convergence of the tracking error with bounded signals) are derived for a discrete-time pole-zero placement adaptive controller where the parameter estimator is modified in terms of normalized signals. Following an input-output perspective, the overall system is decomposed into two subsystems reflecting the parameter estimation and modeling errors, respectively, and its stability is studied using the sector stability and passivity theorems. First the analysis is carried for the class of disturbances and reference inputs that are either decaying or can be exactly nulled by a linear controller of the chosen structure. In this $\mathcal{L}_2$-framework, it is shown that the only substantive assumption to assure stability is the existence of a linear controller such that the closed-loop transfer function verifies certain conicity conditions. The convergence speed and alertness properties of various parameter adaptation algorithms regarding this condition are discussed. The results are further extended to a broader class of $\mathcal{L}_\infty$ disturbances and reference inputs.**

I. Introduction

THE fundamental practical issue which motivates the entire body of feedback design is how to achieve desired levels of performance in the face of plant uncertainties. Two aspects of the problem must be distinguished: choosing a mathematically convenient representation of the modeling error [generically referred to as model-process mismatch (MPM)] and capturing both the uncertainty and performance aspects in a single problem statement. These constitute the essential difficulty of a successful design technique.

Manuscript received February 9, 1984; revised August 28, 1984, May 14, 1985, and June 26, 1985. This paper is based on a prior submission of February 7, 1983. Paper recommended by Past Associate Editor, H. Elliott.

R. Ortega is with the Facultad de Ingenieria, Universidad Nacional Autonoma de Mexico, Mexico P.O. Box 70-256, 04510.

L. Praly is with the Centre d'Automatique et Informatique, Ecole Nationale Superieure des Mines de Paris, Fontainebleau, France.

I. D. Landau is with the Centre National de la Recherche Scientifique, France.

In a very general way, we can distinguish three specific classes of MPM leading to different mathematical problems. Optimal control of *stochastic models* when disturbances arise from small independent linearly combined fluctuations. Adaptive control, where MPM is represented in terms of a set membership statement *for the parameters* of a suitably choosen structure, e.g., an otherwise known linear time-invariant (LTI) system. Robust control theory which characterizes uncertainty by a set membership statement *for the input-output (I/O) operator*, e.g., the process transfer function.

Intense research activity has been devoted to the control of stochastic models with parametric uncertainty. Single-stage optimization schemes for scalar LTI invertible systems have been shown to be globally stable under fairly reasonable assumptions provided the system noise dynamics verifies a positivity condition and the underlying model structure has been suitably chosen. Equivalence of single-stage optimal stochastic and pole-zero placement deterministic adaptive controllers is now well established; see, e.g., [11]. It has been shown in [25] that bounded output disturbances (BOD), and more recently in [4], [21], that reduced-order modeling (ROM) could make the closed-loop adaptive system unstable. Since such violations are the rule and not the exception in practice, these results raised the interest of studying the controllers ability to retain adequate performance when faced with *other classes of MPM besides parametric uncertainty*. We will refer to this case as the mismatched case in contrast to the *matched case* where no disturbances are present and an upper bound on the process order is known.

Since in the mismatched case it is no longer possible to ensure convergence to zero of the tracking error for all BOD and reference sequences, a revised notion of *acceptable performance* is required. Three fundamental, if modest, requirements are the following. 1) Assure tracking error cancelation with bounded signals for all BOD and reference sequences for which a linear robust servobehavior is possible, i.e., the tracking error can be exactly nulled by a linear controller of the same structure. 2) When perfect tracking error cancelation is not possible, preserve its boundedness for "sufficiently small" BOD. 3) Since the key property of an adaptive regulator is to track variations in process

0018-9286/85/1200-1179$01.00

dynamics, gain decreasing estimation schemes should be discarded. Convergence to a constant value of the estimated parameters and the capability of reflecting the MPM level in the stability conditions are further desirable properties.

A. Background

Robustness results of adaptive controllers were first available for the output disturbance problem [25], [18], [19]. Fairly complete results in a state-space setting were obtained in [21] for the case when the reduced-order model residuals are a parasitic system. Ad hoc modifications to the adaptation laws were presented in [18], [19], [21]. Although in the latter the MPM is characterized by a well-defined scalar parameter (the ratio of the dominant versus parasitic frequencies) in none of the aforementioned schemes is it straightforward to establish the validity of the prior information required nor to incorporate *a priori* knowledge about the process. Any attempt to treat "less structured" uncertainties from a *state-space approach* seems doomed from the outset not to yield useful results.

In contrast to adaptive control theory, research in robust control [1], [2], [17] has preceded from an *operator model formulation.* This allows natural accommodation of uncertain model order and provides an adequate framework to incorporate *a priori* knowledge to quantify the MPM. Conic bounded transfer functions to deal with coarsely defined systems are used to characterize uncertainty. In this approach the input–output map is assumed to be in a ball in the frequency domain, whose center is the plant parametric model and the radius defines, by a known frequency function, the error induced by the unstructured uncertainty.

The key to the successful application of the powerful I/O stability theorems [9] in an adaptive context is to find, as was done for the nominal stability analysis of model-reference adaptive controllers [6], a suitable operator-theoretic description of the systems isolating the parametric error. To treat robustness problems, the effects of the *modeling and parameter estimation error must be effectively isolated.* This was first clearly stated in [10] for a class of continuous-time adaptive controllers leading to stability conditions given in terms of passivity requirements of an MPM-related operator. Stabilizability of the process by a fixed gain regulator (with the same structure as the adaptive one), which is an obvious requirement, is used in [10] to ensure boundedness of the regressor vector. The first discrete-time robustness results using an I/O approach were reported in [8]. There, a small gain formulation is proposed to study the robustness of the self-tuning controller. Unfortunately, the results are incomplete, since besides the small gain requirement an intricately signal-dependent assumption has to be made, specifically, it was assumed that the regressor signals are *a priori* known to be bounded. The same flaw is present in [5], [15] where sectoricity theory was proposed for robustness analysis. The $\mathcal{L}_2$ results of [8] have been translated to an $\mathcal{L}_\infty$ framework in [23]; however, the signal-dependent assumption remained unsolved.

Departing from the operator-theoretic approach, a signal-to-noise ratio formulation of the robustness problem was introduced in [28]. It allows one to derive results for both ROM and BOD [24] using a modified version of the adaptation law introduced in [25]. The results obtained are however more of a qualitative rather than quantitative nature.

Some local stability conditions have been reported in [22]. This type of approach, which may lead to more practical results, complements the global one where the goal is to define the limits of the adaptive schemes in its widest possible formulation.

B. Contributions of the Paper

The purpose of our robustness studies is to determine a class of modeling errors (besides parameter uncertainty) for which the adaptive scheme retains acceptable performance (as defined above).

The *framework* proposed in this paper, largely inspired by [10], is of the system theoretic type and is based on conic sectors. Our main technical device is the sector stability theorem [2], [17] which states that the feedback interconnection of two conic bounded operators is globally stable if one is strictly inside a cone and the inverse of the other one outside it. This theorem is applied to the error model derived in [5] which is similar to the ones in [8], [10]. The operator representing the parameter adaptation algorithm (PAA) is in feedback interconnection with an LTI operator. The latter operator is the transfer function from the delayed reference sequence to the system output.

In order to apply the conic sector theory, conic sector conditions must be established for the PAA. In [7], [14] these tools were applied to analyze the stability of the self-tuning controller. The conic sectors derived in those papers are critically dependent on the $\mathcal{L}_\infty$ norm of the regressor vector. The assumption of a bounded regressor vector leaves the results incomplete. To remove this defect we use, as in [25], normalized signals in the PAA and following the approach of [24], we modify the least squares algorithm by regularizing the covariance matrix. In this way, signal-independent conic sectors are established for constant gain (CG) and regularized least squares (RLS) estimation schemes. It is worth mentioning that the regularization in the least squares algorithm is required only for the $\mathcal{L}_\infty$-stability analysis. For the $\mathcal{L}_2$-stability analysis of the weighted least squares PAA, see [31].

$\mathcal{L}_2$-stability, that is tracking error cancellation, may be ensured for reference inputs and disturbances that are either $\mathcal{L}_2$ signals or such that linear robust servobehavior is possible. To treat the more realistic situation of arbitrary reference inputs and BOD, an $\mathcal{L}_\infty$ formulation is required. Analogously to [23], we use exponentially weighted techniques [9] to extend the $\mathcal{L}_2$ result to a $\mathcal{L}_\infty$ framework. In both cases a tradeoff between altertness of the PAA and robustness arises.

Direct application of the sector stability theorem to the normalized error model allows us to derive conditions for the stability of the normalized signals. To be able to conclude stability of the adaptive scheme from stability of the normalized error model, two additional results are needed. First, the conditions ensuring stability of the normalized scheme, which are given in terms of normalized operators, must be translated to the original operators. Second, conditions under which stability of the normalized scheme implies stability of the original one must be established. This is done by referring to multiplier theory [9, p. 202]. The problem basically reduces to proving that the regressor vector is bounded, which ensures that the normalization factor qualifies as a multiplier. Arguments similar to the ones in [24] are used for this part of the proof.

The *main contributions of the paper* are the following. 1) An extension of the I/O approach pioneered in [7], [8], [10] for analyzing the effects of ROM and BOD in discrete-time adaptive controllers. 2) Establishment of a well-defined class of ROM errors and BOD for which robust stability is ensured. 3) Use of a normalized approach to parameter estimation for improved robustness. The latter completes the results of [5], [8], [23].

The paper is organized as follows. The type of MPM and the regulator structure studied are presented in Section II together with the error equations. The implications of the presence of MPM in the PAA selection and the I/O properties of a class of PAA's are discussed in Section III. In Section IV the need to normalize the PAA signals is motivated. The main stability theorems are given in Section V. Some concluding remarks are presented in Section VI.

II. Problem Formulation

In order to carry out the objective presented in Section I-B we must isolate the effects of the modeling and parameter estimation errors. This is done by reconfiguring the adaptive system into two subsystems: the parameter adaptation algorithm (PAA) and an LTI subsystem independent of the parametric error.

In this section we will first define the MPM representation considered in the paper. A standard pole-zero placement adaptive controller is introduced later. Before proceeding to describe the PAA, which is left to Section III, error equations suitable to the robust stability analysis are then established. Assuming linear stabilizability of the process, the stability problem of the adaptive case is reduced to the analysis of a feedback arrangement around the PAA; this arrangement is suitable to the application of I/O stability theorems [2], [9], [17].

A. The Plant

It is assumed that the plant to be controlled is described by

$$A(q^{-1})Y_t = q^{-d}B(q^{-1})U_t + \xi_t \tag{2.1}$$

where A, B are polynomials in q^{-1}. A is monic, U_t, Y_t, ξ_t are the input, output, and disturbance sequences, and d is known. The order of each polynomial and its coefficients are unknown and ξ_t is bounded, i.e., $\xi_t \in \mathcal{L}_\infty$.

B. The Controller Structure

We will pursue a pole-placement all-zero canceling objective with the desired closed-loop poles being the roots of a polynomial C_R. Defining a filtered tracking error

$$e_t \triangleq C_R Y_t - \omega_t \tag{2.2}$$

our objective is to ensure that e_t tends to 0 as t tends to infinity.

Choosing two integers n_S and n_R we use the regulator structure

$$\hat{S}_t U_t = \omega_{t+d} - \hat{R}_t Y_t$$

where $\hat{S}_t$ and $\hat{R}_t$ are polynomial functions in q^{-1} of degrees n_S and n_R, respectively, with time-varying coefficients and ω_t is the reference signal assumed known d steps ahead. In compact notation the control law may be written as

$$\omega_{t+d} = \hat{\theta}_t^T \phi_t \tag{2.3}$$

with

$$\phi_t \triangleq [U_t, U_{t-1}, \cdots, U_{t-n_S}; Y_t, Y_{t-1}, \cdots, Y_{t-n_R}]^T. \tag{2.4}$$

Before proceeding with the process reparameterization, let us introduce the following stabilizability assumption that will justify the choice of the regulator given above.

Assumption A.1: Let S_*, R_* be polynomials of given orders n_S, n_R. Let $\mu \in (0, 1)$ be a scalar. Define the polynomial coefficients vector

$$\theta_* \triangleq [S_0^*, S_1^*, \cdots, S_{n_S}^*, r_0^*, r_1^*, \cdots, r_{n_R}^*]^T$$

and the polynomial

$$C \triangleq S_* A + q^{-d} R_* B. \tag{2.5}$$

With these notations, we assume that there exists a *nonempty* set θ_{LS} defined as

$$\Theta_{LS} \triangleq \{\Theta_* \in \mathbb{R}^n : C(q) \neq 0,\ \forall\, q \in C,\ |q| > \mu^{1/2}\} \neq \emptyset$$

where $n \triangleq n_S + n_R + 2$. □

Remark 2.1: The set θ_{LS} defines the fixed gain regulators which ensure that the systems closed-loop poles are within a disk of radius $\mu^{1/2}$, where μ is a designer chosen parameter to be defined later. The elements of this set, which we will call the linear stabilizing set, the corresponding polynomials and associated signals will be denoted with an asterisk. Notice that for $\mu = 1$ this assumption simply states that the system may be stabilized by a linear regulator of the chosen structure. If Θ_{LS} is empty the plant cannot be stabilized even when it is perfectly known.

C. Error Equations

Combining (2.5) with (2.1) and using (2.4)

$$CY_t = B\theta_*^T \phi_{t-d} + S_* \xi_t \tag{2.6a}$$

$$CU_t = A\theta_*^T \phi_t - R_* \xi_t. \tag{2.6b}$$

Define

$$\psi_t \triangleq (\hat{\theta}_{t-d} - \theta_*)^T \phi_{t-d} \triangleq \tilde{\theta}_{t-d}^T \phi_{t-d} \tag{2.7}$$

where $\tilde{\theta}_t$ is the difference between the actual parameters [see (2.3)] and a vector of stabilizing parameters. From (2.2), (2.3), (2.6), and (2.7) we see that the error model may be expressed as

$$e_t = -H_2 \psi_t + e_t^* \tag{2.8}$$

where

$$e_t^* \triangleq (H_2 - 1)\omega_t + C_R C^{-1} S_* \xi_t \tag{2.9a}$$

$$H_2 \triangleq C_R C^{-1} B. \tag{2.9b}$$

The regressor vector can analogously be written as

$$\phi_{t-d} = -W_1 \psi_t + \phi_{t-d}^* \tag{2.10}$$

where

$$\phi_{t-d}^* \triangleq W_1 \omega_t + W_2 \xi_t \tag{2.11a}$$

$$W_1 \triangleq C^{-1}[A, q^{-1}A, \cdots, q^{-n_R}A; \quad q^{-d}B, q^{-d-1}B, \cdots, a^{-d-n_S}B]^T \tag{2.11b}$$

$$W_2 \triangleq C^{-1}[-q^{-d}R_*, -q^{-d-1}R_*, \cdots, -q^{-d-n_R}R_*; \quad q^{-d}S_*, q^{-d-1}S_*, \cdots, q^{-d-n_S}S_*]. \tag{2.11c}$$

Remark 2.2: Notice that in the matched case there exists S_* and R_* such that $C_* \equiv C_R B$, see (2.5), so that $H_2 = 1$. Furthermore, since $\xi_t = 0$, then $e_t^* = 0$. It is reasonable to expect that the stability conditions in the mismatched case will require "H_2 close to 1" and "small" e_t^*. Our problem is to formalize these notions and to provide conditions to ensure its verification.

In Fig. 1 the complete error model is depicted. H_1 denotes a relation defined by the PAA. One important difference arises with respect to the continuous-time error model developed in [10], namely that defining ψ_t in terms of the delayed signals [see (2.7)], allows us to obtain a transfer function H_2 of relative degree zero, i.e., proper. This will prove to be of fundamental importance in the analysis of the stability conditions implications.

Remark 2.3: It is easy to show that $H_2 = C_R Y_t^* / \omega_{t+d}$; that is, H_2 represents the transfer function of the process in closed-loop with a stabilizing regulator. e_t^* and ϕ_t^* are the corresponding tracking error and regressor signals for that linear scheme. Notice that they can be interpreted as inputs to the error model [10] which are bounded in view of Assumption A.1. Henceforth, the establishment of tracking error convergence conditions for the overall system reduces to ensuring stability for the feedback interconnection of the blocks H_1, H_2. Boundedness of ϕ_t will follow if the former conditions are ϕ_t-independent.

III. The Parameter Adaptation Algorithms

We intend to obtain stability conditions in terms of conic bounds in the presence of MPM. In addition, we will attempt to satisfy performance requirements. Our key technical device to

IEEE TRANSACTIONS ON AUTOMATIC CONTROL, VOL. AC-30, NO. 12, DECEMBER 1985

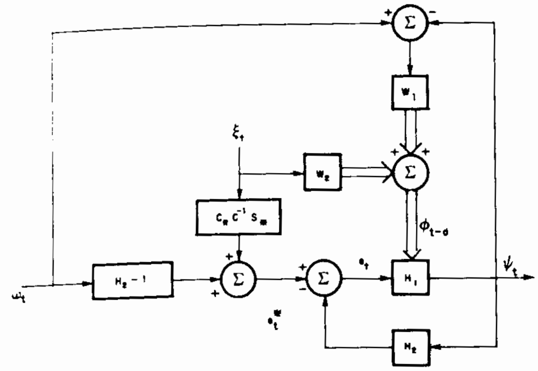

Fig. 1.

study the feedback interconnection is the conic sector stability theorem [17] (see also [2]). It is required then to choose a PAA such that sector conditions may be established for the relation $H_1: e_t \rightarrow \psi_t$.

It will be shown below that to obtain ϕ_t-independent properties for the PAA (see Remark 2.3) normalization of e_t and ϕ_t are compulsory. In the following ($\bar{\ }$) *will be used to denote normalized* variables and corresponding operators and are defined as:

$$\bar{\phi}_{t-d} \triangleq \rho_t^{-1/2}\phi_{t-d},\ \bar{e}_t \triangleq \rho_t^{-1/2}e_t;\ \bar{\psi}_t \triangleq \rho_t^{-1/2}\psi_t \qquad (3.0a)$$

$$\bar{H}_i \triangleq \rho_t^{-1/2}H_i[\rho_t^{1/2}\ \cdot];\qquad i=1,\ 2. \qquad (3.0b)$$

The normalization factor ρ_t is introduced in Section V.

To gain some insight into the problem of the selection of the PAA we will consider first the approaches and motivations of the matched case, that is when no ROM or BOD are present. A class of PAA for which suitable I/O properties have been established is later presented and its properties stated and proved.

A. The Matched Case

Most adaptive schemes reported in the literature use an integral PAA of the form

$$\hat{\theta}_t = \hat{\theta}_{t-1} + F_t\phi_{t-d}e_t^p \qquad (3.1)$$

where F_t is a time-varying matrix (the matrix gain) and e_t^p is an estimate of the prediction error. The increasing complexity of the treated cases required increasing information fed through e_t^p into the PAA. Therefore, the choice of e_t^p may be thought of as reflecting the evolution of the adaptive control theory. It was initially taken equal to the tracking error to solve the unitary delay case. Later it was shown that using this same error, a physically realizable globally stable solution was still possible for $d = 2$, by proper replacement of $\hat{\theta}_t$ by the multiplier operator $P_t(\hat{\theta}_t)$.[1]. This last modification was required to ensure the positive real condition of the error model. The ingenious inclusion of the augmented error model allowed proof of convergence of the tracking error by taking

$$e_t^p = (C_R Y_t - \hat{\theta}_{t-1}^T\phi_{t-d})/(1+\phi_{t-d}^T F_t \phi_{t-d}). \qquad (3.2)$$

However, this new form of e_t^p posed the new stability problem of *ensuring boundedness* of the auxiliary signal, which was later proved for invertible systems [13] by showing that $\Delta\hat{\theta}_t \in \mathcal{L}_2$. Similar results were obtained in [25], [26].

The introduction of the *a posteriori* error representation [6], [11] allows a clear-cut interpretation of the stability proofs, either Lyapunov or Popov based, available in the literature. Due to the structure of the integral PAA it is easy to show that in the matched case e_t^p as given in (3.2) is equal to $-\tilde{\theta}_t^T\phi_{t-d}$, the *a posteriori* error. Since the operator $H_1: e_t^p \rightarrow \tilde{\theta}_t^T\phi_{t-d}$ is passive (for a constant gain matrix), even for unbounded ϕ_t, direct application of the passivity theorem leads to the stability of $\tilde{\theta}_t^T\phi_{t-d}$. The proof is completed by showing that $\tilde{\theta}_t^T\phi_{t-d} \rightarrow 0$ implies $e_t \rightarrow 0$ with bounded ϕ_t. A similar procedure will be required below when we will seek to prove stability of the adaptive scheme from the stability of the normalized signals.

Remark 3.1: It can also be shown that when $d > 1$ an interlaced version of (3.1) avoids the necessity of using the augmented error in (3.2) since for that scheme

$$\frac{e_t}{1+\phi_{t-d}^T F_t \phi_{t-d}} = -\tilde{\theta}_t^T\phi_{t-d}.$$

B. PAA Sector Conditions

Given our objective of uniform asymptotic stability we disregard proportional components in the PAA. In addition, gain decreasing PAA are discarded to *preserve the alertness* of the adaptive scheme. Extrapolating from current usage we consider integral interlaced PAA of the form

$$\hat{\theta}_t = \hat{\theta}_{t-d} + \mathfrak{F}\bar{\phi}_{t-d}\bar{e}_t \qquad (3.3)$$

where $\mathfrak{F}$ takes one of the following forms.

1) Constant gain (CG) PAA: $\mathfrak{F}$ is a scalar

$$\mathfrak{F} \triangleq f > 0. \qquad (3.4a)$$

2) Regularized least squares (RLS) PAA: $\mathfrak{F}$ is a time-varying matrix

$$\mathfrak{F} \triangleq F_t \qquad (3.4b)$$

where (see [24] for further details)

$$F_t = \left(1 - \frac{\lambda_0}{\lambda_1}\right)\left[F_{t-d} - \frac{F_{t-d}\bar{\phi}_{t-d}\bar{\phi}_{t-d}^T F_{t-d}}{\lambda + \bar{\phi}_{t-d}^T F_{t-d}\bar{\phi}_{t-d}}\right] + \lambda_0 I \qquad (3.4c)$$

and $\lambda_0 < \lambda_1$, λ are strictly positive scalars.

The eigenvalues of F_t are all contained in the chosen interval $[\lambda_0, \lambda_1]$.

Equations (3.3) and (3.4) define an operator $\bar{H}_1: \bar{e}_t \rightarrow \bar{\psi}_t$ (see Fig. 2). Besides this operator we will consider for the RLS/PAA, its exponentially weighted counterpart $\bar{H}_1^\alpha: \bar{e}_t^\alpha \rightarrow \bar{\psi}_t^\alpha$ where the superscript α denotes

$$X_t^\alpha \triangleq \alpha^t X_t:\qquad \alpha > 0.$$

The I/O properties of the two operators are summarized in the following lemma. Similar results were obtained earlier in [7], [14], [15], [24]. Notice that $\bar{H}_1^\alpha = \bar{H}_1$ when $\alpha = 1$.

Lemma 3.1 (I/O Properties of the PAA):

1) *CG/PAA:* If $\mathfrak{F}$ is given by (3.4a), then

$$\bar{H}_1 + \frac{1}{2}\,\bar{\sigma}_{CG} \text{ is passive}$$

for all $\bar{\sigma}_{CG}$ such that

$$\bar{\sigma}_{CG} \geq f\|\bar{\phi}_t^T\bar{\phi}_t\|_\infty. \qquad (3.5)$$

2) *RLS/PAA:* If $\mathfrak{F}$ is given by (3.4b), (3.4c), then

$$\bar{H}_1^\alpha \text{ is outside CONE } (-1,\ \sqrt{1-\bar{\sigma}_{RLS}})$$

[1] This section's discussion, although restricted to discrete-time systems, is further simplified by choosing the following structure for the operator: $P_t: P_t(\hat{\theta}_t) \triangleq q^d\hat{\theta}_t q^{-d}$ (see [13]) so that the operator retains the basic concepts of continuous and hybrid schemes.

for α verifying

$$\lambda \max \left[F_t^{-1}\left(F_{t-d}-\frac{F_{t-d}\bar{\phi}_{t-d}\bar{\phi}_{t-d}^T F_{t-d}}{\lambda+\bar{\phi}_{t-d}^T F_{t-d}\bar{\phi}_{t-d}}\right)\right] \cdot \alpha^{2d} \leq 1 \qquad (3.6)$$

and all $\bar{\sigma}_{\text{RLS}}$ satisfying

$$\bar{\sigma}_{\text{RLS}} \geq \frac{\lambda_1 \bar{\phi}_t^T \bar{\phi}_t}{\lambda+\lambda_1 \bar{\phi}_t^T \bar{\phi}_t}. \qquad (3.7)$$

Proof: The proof is given in two parts. The passivity property for the CG/PAA is first established. The conic sector for the RLS/PAA is later derived.

1) Consider the quadratic function

$$V_t \triangleq \frac{1}{2}\tilde{\theta}_t^T f^{-1}\tilde{\theta}_t$$

direct manipulation of (3.3) and (3.4a) gives

$$V_t - V_{t-d} = \bar{\psi}_t \bar{e}_t + \frac{1}{2}\bar{\phi}_{t-d}^T f \bar{\phi}_{t-d}(\bar{e}_t)^2.$$

It can be readily seen that

$$\left\langle \frac{1}{2}\bar{\sigma}_{\text{CG}}\bar{e}_t + \bar{\psi}_t | \bar{e}_t \right\rangle_N \geq -V_{-d} - \cdots - V_{-1}$$

which completes the first part of the proof.

2) Let the matrix F_t' and the scalars V_t, V_t' be defined as

$$F_t' \triangleq F_{t-d} - \frac{F_{t-d}\bar{\phi}_{t-d}\bar{\phi}_{t-d}^T F_{t-d}}{\lambda+\bar{\phi}_{t-d}^T F_{t-d}\bar{\phi}_{t-d}} \qquad (3.8)$$

$$V_t \triangleq \frac{\tilde{\theta}_t^T F_t^{-1}\tilde{\theta}_t}{\lambda}, \quad V_t' \triangleq \frac{\tilde{\theta}_t^T F_t'^{-1}\tilde{\theta}_t}{\lambda}.$$

We have (see the Appendix)

$$V_t \leq \lambda \max (F_t^{-1}F_t') \cdot V_t'$$

and after some algebra (see [30] for example).

$$V_t' - V_{t-d} = (\bar{\psi}_t + \bar{e}_t)^2 - \frac{\lambda}{\lambda+\bar{\phi}_{t-d}^T F_{t-d}\bar{\phi}_{t-d}}\bar{e}_t^2.$$

Now from (3.4c), (3.6) it follows that:

$$\alpha^{2d}\lambda \max (F_t^{-1}F_t') \leq 1, \quad \bar{\phi}_{t-d}^T F_{t-d}\bar{\phi}_{t-d} \leq \lambda_1 \bar{\phi}_{t-d}^T \bar{\phi}_{t-d}.$$

Hence,

$$\alpha^{2d}V_t \leq \alpha^{2(t-d)}V_{t-d} + \alpha^{-2d}\left[(\bar{\psi}_t^\alpha + \bar{e}_t^\alpha)^2 - \frac{\lambda}{\lambda+\bar{\phi}_{t-d}^T F_{t-d}\bar{\phi}_{t-d}}\bar{e}_t^{\alpha^2}\right]$$

Summing from 0 to N leads to the result

$$\sum_{t=0}^{N}(\bar{\psi}_t^\alpha + \bar{e}_t^\alpha)^2 \geq \sum_{t=0}^{N}\frac{\lambda}{\lambda+\bar{\phi}_{t-d}^T F_{t-d}\bar{\phi}_{t-d}}\bar{e}_t^{\alpha^2} - \sum_{t=-1}^{-d}\alpha^{2d}V_t. \qquad \square$$

Remark 3.2: From (3.5), (3.7) we see that the PAA's properties are critically dependent on the boundedness of $\bar{\phi}_t$. This indicates that the normalization factor ρ_t in (3.0) should ensure a finite $\mathcal{L}_\infty$-norm for $\bar{\phi}_t$. We will assume from now on that ρ_t is such that

$$\|\bar{\phi}_t\|_\infty \leq 1. \qquad (3.9)$$

A sequence ρ_t giving this property will be presented in Section V. With (3.9), the radius of the cone for the RLS/PAA does not vanish. It is exactly at this point that our result differs from [5], [8], [15], [23].

Remark 3.3: Another interesting property for our study would be to have $\alpha > 1$ in (3.6). Clearly from (3.4c) we have

$$F_t \geq F_t'.$$

Therefore, in any case

$$\alpha \geq 1. \qquad (3.10)$$

In some circumstances, the stronger property "$\alpha > 1$" is also satisfied. In the Appendix we show that, in the case $d = 1$, this is achieved at least for $\bar{\phi}_t$ persistently spanning in the following sense: there exist $0 < \beta < 1$, $\epsilon > 0$, N_o such that:

$$\sum_{t=0}^{N}\beta^{N-t}\bar{\phi}_t\bar{\phi}_t^T \geq \epsilon I \qquad \forall N \geq N_0. \qquad (3.11)$$

Unfortunately this is a signal-dependent condition. However, it is usually satisfied for λ large enough (slow adaptation) and for all period of time such that $\hat{\theta}_t \in \Theta_{LS}$ provided the reference input is persistently exciting.

IV. Stability of the Normalized Error Model

$\mathcal{L}_2$ and $\mathcal{L}_\infty$-stability results for the normalized system are given below. Discussion on the stability conditions is deferred to the following section, where stability of the adaptively controlled system is derived from the stability of the normalized error model.

A. $\mathcal{L}_2$-Stability

Combining Lemma 3.1 and the sector stability theorem we get the following $\mathcal{L}_2$ result for the normalized system.

Lemma 4.1: Consider the feedback interconnection

$$\bar{\psi}_t = \bar{H}_1\bar{e}_t \qquad (4.1a)$$

$$\bar{e}_t = -\bar{H}_2\bar{\psi}_t + \bar{e}_t^*. \qquad (4.1b)$$

If $\bar{H}_2$ is strictly inside $\mathcal{C} \triangleq$ CONE (C_A, R_A), where

$$(C_A, R_A) = \begin{cases} (1/\bar{\sigma}_{\text{CG}},\ 1/\bar{\sigma}_{\text{CG}}) & \text{for the CG/PAA} \quad (4.2a) \\ (1/\bar{\sigma}_{\text{RLS}},\ \sqrt{1-\bar{\sigma}_{\text{RLS}}}/\bar{\sigma}_{\text{RLS}}) & \text{for the RLS/PAA} \quad (4.2b) \end{cases}$$

for any

$$\bar{\sigma}_{\text{CG}} \geq f \text{ and } \bar{\sigma}_{\text{RLS}} \geq \frac{\lambda_1}{\lambda+\lambda_1} \qquad (4.3)$$

then

$$\bar{e}_t,\ \bar{\psi}_t \in \mathcal{L}_2 \qquad \text{for all } \bar{e}_t^* \in \mathcal{L}_2.$$

Proof: This is a straightforward application of [17, Theorem 2a p. 234]. $\square$

B. $\mathcal{L}_\infty$-Stability

The $\mathcal{L}_\infty$ extension of the previous result using the RLS/PAA follows below.

Lemma 4.2: Consider the feedback system (4.1) for the RLS/PAA. Assume ρ_t is bounded away from zero. Under these conditions, if

$$\bar{H}_2^\alpha \triangleq \alpha^t \bar{H}_2[\alpha^{-t}] \cdot \text{ is strictly inside } \mathcal{C} \text{ [with } \mathcal{C} \text{ as in (4.2b)]}$$

with $\alpha > 1$ satisfying (3.b), then there exists a scalar K_2 such that

$$\bar{\psi}_N^2 \leq \frac{K_2}{\min \rho_t}\frac{\|e_t^{*^2}\|_\infty}{(1-\bar{\alpha}^2)}.$$

Proof: $\mathcal{L}_2$-stability of the map $(\bar{e}_t^*)^\alpha \to \bar{\psi}_t^\alpha$ (see Fig. 2) is ensured from Lemma 3.1 and the sector stability theorem. That is, $\exists\, K_2 < \infty$ such that

$$\|\bar{\psi}_t^\alpha\|_N^2 \leq K_2 \|(\bar{e}_t^*)^\alpha\|_N^2, \qquad \forall\, N \geq 0. \tag{4.4}$$

Notice that

$$\|\bar{\psi}_t^\alpha\|_N^2 \geq (\alpha^N \bar{\psi}_N)^2 \tag{4.5}$$

and

$$\|(\bar{e}_t^*)^\alpha\|_N^2 \leq \|\bar{e}_t^{*2}\|_\infty \sum_{t=0}^{N} \alpha^{2t} \leq \|\bar{e}_t^{*2}\|_\infty \frac{\alpha^{2N}}{1-\alpha^{-2}} \tag{4.6}$$

since $\alpha > 1$. Combining (4.4)–(4.6) we can conclude that uniformly in N

$$\bar{\psi}_N^2 \leq \frac{K_2}{\boldsymbol{\rho}(1-\alpha^{-2})} \|e_t^{*2}\|_\infty \tag{4.7}$$

where

$$\boldsymbol{\rho} \doteq \min_t \rho_t > 0. \qquad \Box \tag{4.8}$$

Remark 4.1: The same types of arguments were used in [23] to prove the boundedness of e_t assuming *a priori* constraints in the regressor vector.

VI. Main Results

In this section we will determine the conditions under which stability is preserved for the plant (2.1) in closed loop with the time varying regulator (2.3) and adaptive law (3.3), (3.4). For this purpose we will introduce the following normalization factor:

$$\rho_t = \mu\rho_{t-1} + \max\,(|\phi_{t-d}|^2,\ \boldsymbol{\rho}), \qquad \boldsymbol{\rho} > 0,\ \mu \in (0,\ 1) \tag{5.1}$$

which together with (3.0) completes the description of the PAA.

Remark 5.1: This type of multiplier was introduced in [25], and its importance for robustness established in [24], [30]. $\boldsymbol{\rho}$ is a small positive constant that defines a lower bound to ρ_t. The choice of the time constant μ will prove to be a compromise between PAA alertness and robustness.

The problem is solved by analyzing the error models depicted in Figs. 1 and 2. It should be recalled (see Remark 2.3) that under the stabilizability Assumption A.1 the key point is proving stability of ψ_t [see (2.8), (2.10)]. The proof proceeds as follows. First we prove using the Bellman–Gronwall lemma that $\mathcal{L}_2$-stability of $\bar{\psi}_t$ (given by Lemma 4.1) implies $\psi_t \in \mathcal{L}_\infty$. This in its turn assures that the regressor vector is bounded. As a consequence, the normalizing factor ρ_t is bounded and proceeding from the multiplier theory $\mathcal{L}_2$-stability of the normalized error model implies $\mathcal{L}_2$-stability of the adaptive system. For the $\mathcal{L}_\infty$-stability proof, boundedness of $\bar{\psi}_t$, as shown in Lemma 4.2, is used to establish boundedness of ψ_t.

The stability conditions derived in Lemma 4.1 and 4.2 are translated in terms of the designer chosen parameters (n_S, n_R, C_R, μ) and the MPM (H_2, ξ_t).

A. $\mathcal{L}_2$-Stability

Theorem 5.1: Consider $\bar{\psi}_t$ given in (3.0), (5.1) and ϕ_t as in (2.10), (2.11). Under these conditions if Assumption A.1 of Section II-B is verified, then

$$\bar{\psi}_t \in \mathcal{L}_2 \Rightarrow \psi_t \in \mathcal{L}_\infty.$$

Proof: Define the exponentially weighted signals [9, p. 251]

$$X_t^\mu \triangleq \mu^{-t} X_t. \tag{5.2}$$

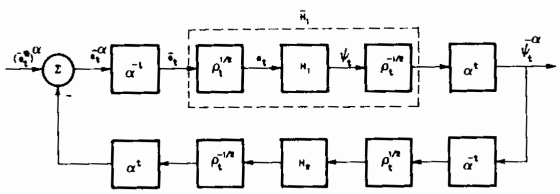

Fig. 2.

From (5.1)

$$\mu^{-N}\rho_N \leq \rho_0 + \|\phi_{t-d}^\mu\|_N^2 + \mu^{-N}\boldsymbol{\rho}/(1-\mu). \tag{5.3}$$

Applying the truncated $\mathcal{L}_2$ norm to the exponentially weighted version of (2.10) and taking into account A.1

$$\|\phi_{t-d}^\mu\|_N \leq \gamma_2'[\|\omega_t^\mu\|_N + \|\psi_t^\mu\|_N] + \gamma_2''\|\xi_t^\mu\|_N \tag{5.4a}$$

where γ_2', γ_2'' are $\mathcal{L}_2$-gains defined as

$$\gamma_2' \triangleq \gamma_2\{W_1[(\mu^{1/2}q)^{-1}]\},\ \gamma_2'' \triangleq \gamma_2\{W_2[(\mu^{1/2}q)^{-1}]\}. \tag{5.4b}$$

From the definition of $\bar{\psi}_t$, (3.0a) and (5.3), (5.4) we get

$$|\psi_N|^2 \geq \frac{\mu^{-N}\psi_N^2}{\rho_0 + \mu^{-N}\boldsymbol{\rho} + 2\{[\gamma_2']^2(\|\omega_t^\mu\|_N^2 + \|\psi_t^\mu\|_N^2) + [\gamma_2'']^2\|\xi_t^\mu\|_N^2}.$$

Since $\bar{\psi}_t \in \mathcal{L}_2$ by assumption, $\bar{\psi}_t \to 0$, so that for all $\delta > 0$, $\exists\, N_0$ such that for all $N \geq N_0$,

$$\bar{\psi}_N^2 \leq \delta. \tag{5.5}$$

Therefore,

$$\mu^{-N}\psi_N^2 \leq \delta\{\rho_0 + \mu^{-N}\boldsymbol{\rho} + [\gamma_2']^2\|\omega_t^\mu\|_N^2 + 2[\gamma_2'']^2\|\xi_t^\mu\|_N^2 + 2[\gamma_2']^2(\mu^{-N}\psi_N^2 + \|\psi_t^\mu\|_{N-1}^2)\}.$$

If we choose δ such that $1 - 2\delta[\gamma_2']^2 > \mu$, we get

$$\mu^{-N}\psi_N^2 \leq \delta^2 K_1 \mu^{-N} + \frac{2\delta[\gamma_2']^2}{1-2\delta[\gamma_2']^2} \sum_{t=N_0}^{N-1} \mu^{-t}\psi_t^2 \tag{5.6}$$

where we have used the fact that ρ_0, $\boldsymbol{\rho}$, ω_t $\{\psi_t\}_0^{N_0}$, $\xi_t \in \mathcal{L}_\infty$ to bound them by $\delta K_1 \mu^{-N}$.

Applying the Bellman–Gronwall lemma to (5.6)

$$\mu^{-N}\psi_N^2 \leq \delta^2 K_1 \mu^{-N} + \frac{2\delta[\gamma_2']^2}{1-2\delta[\gamma_2']^2} \sum_{t=N_0}^{N-1} \cdot \left[\frac{1}{1-2\delta[\gamma_2']^2}\right]^{N-t-1} \delta^2 K_1 \mu^{-t}$$

which may also be written as

$$\psi_N^2 \leq \delta^2 K_1 \left\{1 + 2\delta(\gamma_2')^2 \sum_{t=0}^{N-1} \left[\frac{\mu}{1-2\delta(\gamma_2')^2}\right]^{N-t}\right\}. \tag{5.7}$$

The term inside the brackets is smaller than 1 and the series is convergent, therefore, we can conclude that $\psi_t \in \mathcal{L}_\infty$. $\Box$

Corollary 5.1: If $\bar{\psi}_t \in \mathcal{L}_2$, ω_t, $\xi_t \in \mathcal{L}_\infty$ and A.1 holds, then $\phi_t \in \mathcal{L}_\infty$ and consequently $\rho_t \in \mathcal{L}_\infty$.

Proof: Follows immediately from Theorem 5.1, (2.10), and (5.1). $\Box$

The following lemma will help us to find the *conicity conditions over* H_2 ensuring the ones required in Lemma 4.1.

Lemma 5.1: Let us consider the operator H: $\gamma_t \to \eta_t$. If $H[(\mu^{1/2}q)^{-1}]$ is inside the CONE (C, R), then $H \doteq \rho_t^{-1/2} H \rho_t^{1/2}$

(i.e., $H:\bar{\gamma}_t \rightarrow \bar{\eta}_t$) with ρ_t as in (5.1) is inside the same CONE (C, R).

Proof: See also [14]. Define

$$Z_t \triangleq (\gamma_t - C\eta_t)^2 - (R\eta_t)^2$$

$$\bar{Z}_t \triangleq (\bar{\gamma}_t - C\bar{\eta}_t)^2 - (R\bar{\eta}_t)^2 = \rho_t^{-1} Z_t.$$

Taking the sum

$$\sum_{t=0}^{N} \bar{Z}_t = \sum_{t=0}^{N} \mu^t \rho_t^{-1} \mu^{-t} Z_t = \rho^{N+1} \rho_{N+1}^{-1} \sum_{t=0}^{N} \mu^{-t} Z_t$$

$$+ \sum_{j=0}^{N} \left[\left(\sum_{t=0}^{j} \mu^{-t} Z_t \right) (\mu^j \rho_j^{-1} - \mu^{j+1} \rho_{j+1}^{-1}) \right].$$

The proof is completed noting that $\mu^t \rho_t^{-1}$ is decreasing since

$$\mu^{-(t+1)} \rho_{t+1} = \mu^{-t} \rho_t + \mu^{-(t+1)} \max\ [\boldsymbol{\rho}, |\phi_{t-d+1}|^2]$$

and the implications

$$H[(\mu^{1/2} q)^{-1}] \in \text{CONE } (C,\ R) \Rightarrow \sum_{t=0}^{N} [(\mu^{-t/2} \eta_t - C\mu^{-t/2} \gamma_t)^2$$

$$- (R\mu^{-t/2} \gamma_t)^2] < 0 \Rightarrow \sum_{t=0}^{N} \mu^{-t} Z_t < 0.$$

We establish that $\Sigma_{t=0}^{N} \bar{Z}_t < 0$, and consequently $\bar{H} \in$ CONE (C, R). □

We are now in position to present our main $\mathcal{L}_2$-result.

Theorem 5.2: Consider the process (2.1) in closed loop with the adaptive regulator (2.3), (2.4), whose parameters are updated according to (2.2), (3.3), (3.4) with the normalization (3.0), (5.1). If for given n_S, n_R and μ, Assumption A.1 holds and

i) $H_2[(\mu^{1/2} q)^{-1}]$ is strictly inside A (as defined in Lemma 4.1)
ii) ω_t, $\xi_t \in \mathcal{L}_\infty$ are such that $e_t^* \in \mathcal{L}_2$ then

$$\psi_t,\ e_t \in \mathcal{L}_2 \text{ and } \phi_t \in \mathcal{L}_\infty.$$

Proof: Condition i) and Lemma 5.1 ensure the stability of the normalized error model (Lemma 4.1). Stability of the adaptive system (Fig. 1) may be concluded using multiplier theory [9] if ρ_t qualifies as a multiplier, e.g., $\rho_t \in L_\infty$ (Fig. 2 with $\alpha = 1$). This is ensured by condition ii) and Corollary 5.1 since $e_t^* \in L_2 \Rightarrow \bar{e}_t^* \in L_2$, and consequently $\bar{\psi}_t \in L_2$. □

Discussion:

1) Theorem 5.2 may be stated in the following way. Given an LTI process of known delay, choosen n_S, n_R, μ and desired closed-loop poles, the adaptive system will exactly cancel the tracking error if there exists a value for the regulator parameters (an element of Θ_{LS}) such that for this linear scheme. a) The Nyquist locus of the closed-loop transfer function (Y_t^*/ω_{t+d}) is "sufficiently close" to the desired one ($1/C_R$). b) Robust servobehavior is possible. The notion of "sufficiently close" is precisely defined in terms of disks in the complex plane for the locus of the transfer function evaluated at $|q| = \mu^{1/2}$.

2) *The key modification to the PAA* used in this paper is the normalization. One of the main stumbling blocks to establish robust stability results for the RLS/PAA was the impossibility of proving that σ_{RLS}, in Lemma 3.1, is strictly smaller than 1 (see, e.g., [25], [14], [8], [23], [15]). This is necessary to disallow a vanishing radius for the cone. Normalization removes this defect, but then the error model is only in terms of normalized signals.

3) Notice that the cone $\mathcal{C}$ depends only on designer chosen parameters [σ_{CG} and σ_{RLS} in (4.2)]. In the limit the *conicity condition i) coincides with a positivity condition.* Thus robustness enhancement occurs at the expense of reducing the speed of convergence of the PAA

4) The coefficient μ establishes an *alertness-robustness tradeoff.* Its robustness effects appear in the conicity conditions. PAA alertness is directly affected since μ is the normalization filter time constant (5.1). See [24] for further discussion.

5) The restriction on the tuned tracking error: $e_t^* \in \mathcal{L}_2$ imposes requirements on $H_2 - 1$, ω_t, and ξ_t. If the nature of the reference and disturbance signals is known, incorporating an internal model in the design [16] allows one to ensure that this condition is met. In particular, it is verified for constant reference input and BOD if the open-loop system is type-1. In the following section we carry the analysis for the more interesting and practical case of $e_t^* \in \mathcal{L}_\infty$.

B. $\mathcal{L}_\infty$-Stability

The $\mathcal{L}_\infty$ result is given for the RLS/PAA (3.4b), (3.4c).

Theorem 5.3: Consider the adaptive system analyzed in Theorem 5.2 with a RLS/PAA.

If for n_S, n_R, λ, λ_0, λ_1, and μ.

i) Condition i) of Theorem 5.2 holds
ii) $(\lambda_{\max} F_t^{-1} F_t')^2 \leq \mu^d$

then there always exists a $\boldsymbol{\rho}$ (5.1) such that

$$\psi_t,\ e_t,\ \phi_t \in \mathcal{L}_\infty \qquad \text{for all } \omega_t,\ \xi_t \in \mathcal{L}_\infty.$$

Proof: Consider the normalized exponentially weighted feedback interconnection of Fig. 2. Notice that for $\alpha^2 = \mu^{-1}$ i) and ii) above imply the conditions of Lemma 4.2. Hence,

$$\bar{\psi}_N^2 \leq \frac{K_2}{\boldsymbol{\rho}(1-\mu)} \|e_t^{*2}\|_\infty. \tag{5.8}$$

The Bellman–Gronwall lemma may be now applied as in Theorem 5.1 proceeding from (5.5) with δ substituted by the right-hand side of (5.8). It becomes clear that the condition ensuring the boundedness of ψ_t becomes

$$1 - 2\frac{K_2}{\boldsymbol{\rho}(1-\mu)} (\gamma_2')^2 \|e_t^{*2}\|_\infty \geq \mu$$

which may be rewritten as

$$(1-\mu)^2 > 2K_2 \frac{1}{\boldsymbol{\rho}} \|e_t^{*2}\|_\infty (\gamma_2')^2. \tag{5.9}$$

Since all the terms in the numerator of the right-hand side are bounded and μ ranges in (0, 1), there exists a $\boldsymbol{\rho}$ which will make (5.9) true. This completes the proof. □

Discussion:

1) Condition ii) has been discussed in Remark 3.3. We know that it is met if a persistence of excitation condition is satisfied.

2) Inequality (5.9) defines the class of (non-$\mathcal{L}_2$) disturbances under which $\mathcal{L}_\infty$-stability is preserved. Notice that K_2 quantifies the stability margin of the H_1, H_2 feedback interconnection (4.7). γ_2 is the gain of the map $\xi_t \rightarrow \phi_{t-d}^*$ (2.11), (5.4b); that is, it measures the effect of the BOD on the regressor in the linear scheme. The conicity condition and (5.9) impose contradictory requirements in the choice of μ. The scalar $\boldsymbol{\rho}$ defines a lower bound for the normalization factor, hence directly affects the gain of the PAA. From (5.9) it appears to be interesting to have slow adaptation. A contradictory requirement would be given in case of a time-varying plant.

3) In a recent paper [29] $\mathcal{L}_\infty$-stability of the error model has been established incorporating into the PAA a parameter projection operation analogous to the one in [25]. This requires additional prior knowledge but allows one to extend the stability analysis without condition ii) and without the restriction (5.9) on the $\mathcal{L}_\infty$-norm of e_t^*.

VI. Concluding Discussion and Further Research

To conclude let us summarize the results reported in the paper. A proof of robust stability for a discrete-time adaptive controller with a normalized estimator has been presented. Systems with arbitrary relative degree may be considered (in contrast to the continuous-time robustness studies [10], [21]) however we require the latter to be known. The stability conditions reduce to the existence of a linear regulator (of the chosen structure) such that: 1) the closed-loop tracking transfer function "approaches" the desired closed-loop behavior; 2) "good" disturbance rejection properties are attainable. Increasing the speed of adaptation renders these requirements more stringent.

Although the two previous conditions preserve the essence of the usual performance (in the sense of pole-placement) and disturbance rejection design objectives, they unfortunately do not offer any engineering design guidelines. The primary culprit here is the notion of transfer function vicinity (as stated in 1) above) which requires that the phase-shift between the attainable and the desired transfer functions should not exceed 90°, at all frequencies. This has been referred to in the literature as the positive real condition (of H_2).

One fundamental difference arises at this point between continuous and discrete-time robustness results. In the latter the assumption of known delay permits us to obtain a parametrization where H_2 has the relative degree zero. In terms of the Nyquist locus this implies that for all stably invertible processes the overall phase shift contribution is zero, i.e., the locus starts and ends in the same side of the complex plane. Therefore, since phase modification (usually phase lead) is only required over a limited frequency range, it will always be possible by proper filtering to satisfy the positivity condition. Two important questions remain however to be solved. How should we incorporate the available prior knowledge to convert the conicity conditions into tests for robustness? The second question is more disturbing. How should we deal with nonstably invertible process, very likely to appear in a discrete-time context?

Appendix

From (3.4c), (3.8), (3.9), $d = 1$, we have the following property.

Lemma: If there exist $\epsilon > 0$ and N_0 such that

$$\sum_{i=0}^{N} \beta^{N-i}\bar{\phi}_i\bar{\phi}_i^T \geq \epsilon I \qquad \forall\, N \geq N_0$$

with

$$\beta = \frac{\lambda(\lambda_1-\lambda_0)}{\lambda(\lambda_1-\lambda_0)+\lambda_1(\lambda+\lambda_0)}$$

then we have

$$\max_x \frac{x^T F_t^{-1} x}{x^T F_t'^{-1} x} \leq 1 - \frac{\epsilon\lambda_0\lambda_1}{\lambda(\lambda_1-\lambda_0)+\lambda_1(\lambda+\lambda_0)}.$$

Proof: Let us remark some facts.

i) F_t', F_t are invertible for any finite t and

$$F_{t+1}'^{-1} = F_t^{-1} + \frac{\bar{\phi}_t\bar{\phi}_t^T}{\lambda}, \qquad \lambda > 0 \tag{A.1}$$

$$F_t = \left(1-\frac{\lambda_0}{\lambda_1}\right)F_t' + \lambda_0 I, \qquad 0 < \lambda_0 < \lambda_1 \tag{A.2}$$

$$\|\bar{\phi}_t\| \leq 1. \tag{A.3}$$

Hence, by induction, if we choose F_0 such that

$$\lambda \max F_0 < \lambda_1$$

then we have for any finite t

$$\lambda \max F_t < \lambda_1.$$

Therefore $\lambda_1 F_t^{-1} - I$ is positive definite for any finite t.

ii) F_t' has a symmetric positive definite square root $F_t'^{1/2}$ and we have

$$F_t^{-1}F_t' = F_t'^{1/2}F_t^{-1}F_t'^{1/2} = F_t'F_t^{-1}.$$

Hence, if we let:

$$y = F_t'^{1/2}x$$

we have

$$\frac{x^T F_t^{-1} x}{x^T F_t'^{-1} x} = \frac{y^T F_t'^{1/2} F_t^{-1} F_t'^{1/2} y}{y^T y}.$$

This proves that:

$$\max_x \frac{x^T F_t^{-1} x}{x^T F_t'^{-1} x} = \lambda \max F_t^{-1} F_t'.$$

iii) If A is a symmetric positive definite matrix, then

$$x^T A x \leq (1+\lambda \max A)\, x^T A (I+A)^{-1} x, \qquad \forall\, x.$$

This is proved by noticing that we can choose a symmetric positive definite square root $A^{1/2}$ which commutes with $(I + A)^{-1}$. Then with

$$y = A^{1/2}x.$$

The inequality becomes simply

$$y^T y \leq y^T (I + A^{-1}) y. \ \ (1 + \lambda \max A), \qquad \forall\, y.$$

Let us now study the matrix G_t defined as

$$G_t = I - F_t^{-1} F_t'.$$

From fact ii), G_t is symmetric, with eigenvalues smaller than 1 [see (A.2)]. With (A.2), we have

$$F_t^{-1} = \frac{1}{\lambda_1} I + \frac{1}{\lambda_0}\left(1-\frac{\lambda_0}{\lambda_1}\right) G_t.$$

Hence, from fact i), G_t is positive definite. We have also

$$F_{t+1}'^{-1} = \frac{1}{\lambda_1} I + \frac{1}{\lambda_0}\left(1-\frac{\lambda_0}{\lambda_1}\right) G_t + \frac{\bar{\phi}_t\bar{\phi}_t^T}{d}.$$

Therefore, since

$$F_{t+1}'^{-1} F_{t+1} = \left(1-\frac{\lambda_0}{\lambda_1}\right) I + \lambda_0 F_{t+1}'^{-1}$$

we have

$$F_{t+1}'^{-1} F_{t+1} = I + \left(1-\frac{\lambda_0}{\lambda_1}\right) G_t + \frac{\lambda_0}{\lambda_1}\bar{\phi}_t\bar{\phi}_t^T - (I - G_{t+1}).$$

This proves that

$$G_{t+1} = \left[\left(1-\frac{\lambda_0}{\lambda_1}\right) G_t + \frac{\lambda_0}{\lambda}\bar{\phi}_t\bar{\phi}_t^T\right]\left[I + \left(1-\frac{\lambda_0}{\lambda_1}\right) G_t + \frac{\lambda_0}{\lambda}\bar{\phi}_t\bar{\phi}_t^T\right]^{-1}$$

We remark that, with the properties of G_t and (A.3), we have

$$\lambda \max \left[\left(1-\frac{\lambda_0}{\lambda_1}\right) G_t + \frac{\lambda_0}{\lambda}\bar{\phi}_t\bar{\phi}_t^T\right] \leq 1 - \frac{\lambda_0}{\lambda_1} + \frac{\lambda_0}{\lambda}.$$

Then with fact iii), it follows that (in the sense of quadratic form)

$$G_{t+1} \geq \frac{\lambda_1 \lambda}{\lambda_1(\lambda+\lambda_0)+\lambda(\lambda_1-\lambda_0)} \left[\left(1-\frac{\lambda_0}{\lambda_1}\right) G_t + \frac{\lambda_0}{\lambda} \bar{\phi}_t \bar{\phi}_t^T \right]$$

This implies

$$G_{t+1} \geq \sum_{i=0}^{t} \left(\frac{\lambda(\lambda_1-\lambda_0)}{\lambda_1(\lambda+\lambda_0)+\lambda(\lambda_1-\lambda_0)} \right)^{t-i} \cdot \frac{\lambda_0 \lambda_1}{\lambda_1(\lambda+\lambda_0)+\lambda(\lambda_1-\lambda_0)} \bar{\phi}_i \bar{\phi}_i^T.$$

The conclusion follows from the assumption and the properties of G_t. □

Acknowledgment

The authors are grateful to C. E. Rohrs and the anonymous reviewers for many valuable suggestions.

References

[1] J. C. Doyle and G. Stein, "Multivariable feedback design: Concepts for a modern/classical synthesis," *IEEE Trans. Automat. Contr.*, vol. AC-26, pp. 4-17, Feb. 1981.

[2] M. C. Safonov, *Stability Robustness of Multivariable Feedback Systems.* Cambridge, MA: M.I.T. Press, 1980.

[3] R. L. Kosut, "Analysis of performance robustness for uncertain multivariable systems," in *Proc. 21st Conf. Decision Contr.*, Orlando, FL, Dec. 8-10, 1982.

[4] C. E. Rohrs, "Adaptive control in the presence of unmodeled dynamics," Mass. Inst. Technol., Cambridge, MA, Rep. LIDS-TH-1254, Nov. 1982.

[5] R. Ortega and I. Landau, "On the design of robustly performing adaptive controllers for partially modeled system," in *Proc. 22nd IEEE Conf. Decision Contr.*, San Antonio, TX, Dec. 14-16, 1983.

[6] I. D. Landau and H. M. Silveira, "A stability theorem with applications to adaptive control," *IEEE Trans. Automat. Contr.*, vol. AC-24, pp. 305-311, 1979.

[7] P. J. Gawthrop, "On the stability and convergence of a self-tuning controller," *Int. J. Contr.*, vol. 31, pp. 973-998, 1980.

[8] P. J. Gawthrop and K. W. Lim, "Robustness of self-tuning controllers," *IEEE Proc.*, vol. 129, pp. 21-29, Jan. 1982.

[9] C. A. Desoer and M. Vidyasagar, *Feedback Systems: Input-Output Properties* New York: Academic, 1975.

[10] R. L. Kosut and B. Friedlander, "Performance robustness properties of adaptive control systems," in *Proc. 21st Conf. Decision Contr.*, Orlando, FL, Dec. 8-10, 1982; also in "Robust adaptive control conditions for global stability," in *IEEE Trans. Automat. Contr.*, vol. AC-30, no. 7, pp. 610-624, July 1985.

[11] I. D. Landau, "MRAC and stochastic STR-a unified approach," *Trans. ASME J. Dynam. Syst. Meas. Contr.*, Dec. 1981.

[12] R. Ortega, "Assessment of stability robustness for adaptive controllers," *IEEE Trans. Automat. Contr.*, vol. AC-28, p. 1106, 1983.

[13] K. S. Narendra, "Stable adaptive controller design: proof of stability," *IEEE Trans. Automat. Contr.*, vol. AC-25, June 1980.

[14] P. J. Gawthrop, "Some properties of discrete adaptive controllers," in *Self-Tuning & Adaptive Control,* Harris and Billings. Eds. New York: Peregrinus, 1981.

[15] R. Ortega and I. D. Landau, "On the MPM tolerance of various PAA: A sectoricity approach," *IFAC Workshop Adapt. Syst.*, San Francisco, CA, June 20-22, 1983.

[16] S. Shah, "Internal model adaptive control," *Stanford Univ.*, Stanford, CA, Rep. 63-81-2, Aug. 1981.

[17] G. Zames, "On the I/O stability of time varying nonlinear feed-back systems Part I & II," *IEEE Trans. Automat. Contr.*, vol. AC-11, 1966.

[18] B. Peterson and K. S. Narendra, "Bounded Error adaptive control," *IEEE Trans. Automat. Contr.*, vol. AC-27, Dec. 1982.

[19] G. Kreisselmeier and K. S. Narendra, "Stable MRAC in the presence of bounded disturbances," *IEEE Trans. Automat. Contr.*, vol. AC-27, Dec. 1982.

[20] M. J. Balas and C. R. Johnson, "Adaptive identification and control using reduced-order models," *Yale Adapt. Contr. Conf.*, 1981.

[21] P. Ioannou and P. W. Kokotovic, *Adaptive Systems with Reduced Models.* New York: Springer-Verlag, 1983.

[22] R. Kosut and C. Johnson, "An input-output view of robustness in adaptive control," *Automatica,* (Special Issue on Adaptive Control), 1984.

[23] K. W. Lim, "Robustness of self-tuning controllers," Ph.D. dissertation, Hertford Coll., Oxford, England, 1982.

[24] L. Praly, "Robustness of model reference adaptive control," in *Proc. 3rd Yale Workshop,* New Haven, CT, June 15-17, 1983.

[25] B. Egardt, *Stability of Adaptive Controllers.* New York: Springer-Verlag, 1979.

[26] G. Goodwin, P. Ramadge and P. Caines, "Discrete time multivariable adaptive control," *IEEE Trans. Automat. Contr.*, vol. AC-25, June 1980.

[27] T. Hagglund, *New Estimation Techniques for Adaptive Control.* Coden: LUTFD2/(TFRT-1025)/1-20/1983. Lund University.

[28] L. Praly, "Commande adaptive indirecte multivariable," *Coll. Nat. du CNRS.,* Belle Ile, Sept. 1982.

[29] ——, "Robust MRAC: Stability analysis," in *Proc. 23rd IEEE Conf. Decision Contr.*, Dec. 1984.

[30] ——, "Robustness of indirect adaptive control based on pole placement design," in *Proc. IFAC Workshop on Adaptive Syst. in Contr. and Signal Processing.*, June 1983.

[31] R. Ortega, "Robustness enhancement of adaptive controllers by incorporation of process *a priori* knowledge," *Syst. Contr. Lett.*, vol. 4, pp. 135-141, May 1984; see also "Correction," ibid. vol. 4, Oct. 1984.

Romeo Ortega was born in Mexico, on March 12, 1954. He received the B.S. degree in mechanical and electrical engineering from the National University of Mexico in 1975, the M.on E. degree (with honors) in control theory from the Leningrad Polytechnical Institute, USSR, and the "Doctorat d'Etat-es-Sciences" degree from the Polytechnical Institute of Grenoble, Grenoble, France.

He has held teaching and research positions at the National University and Polytechnical Institute of Mexico. He is currently a Professor in the Faculty of Engineering, National University of Mexico. His main research interests are in the development of analysis and design techniques for reliable control systems.

Laurent Praly was born in 1954. He graduated from Ecole Nationale Supérieure des Mines de Paris, Paris, France, in 1976.

After working as Engineer in a private laboratory for three years, in 1980 he joined the Centre d'Automatique et Informatique, Ecole Nationale Supérieure des Mines de Paris, Fontainebleau, France. From July 1984 to June 1985, he spent a sabbatical year as Visiting Assistant Professor in the Department of Electrical and Computer Engineering, University of Illinois, Urbana-Champaign. His main interest is in automatic control with contribution to adaptive systems.

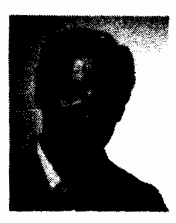

Ioan D. Landau received the Docteur-es-Sciences Physiques degree from the University of Grenoble, Grenoble, France.

He was an Associate Professor at the Institut National Poytechnique de Grenoble from 1973 to 1976 and a Senior Post-Doctoral Research Associate at NASA-Ames Research Center from 1971 to 1972. At present he is Research Director at the Centre National de la Recherche Scientifique (C.N.R.S.). He is also Director of a national coordinated research group at the Laboratoire de'Automatique, Institut National Polytechnique de Grenoble. He is the author of the book. *Adaptive Control—The Model Reference Approach* (New York: Marcel Dekker, 1979) and coauthor (with M. Tomizuka) of the book *Adaptive Control—Theory and Practice* in Japanese (Ohm, 1981).

Dr. Landau is the Chairman of the I.F.A.C. Working Group on Adaptive Systems in Control and Signal Processing. He received the Great Gold Medal at the Invention Exhibition, Vienna in 1968, the C.N.R.S. Silver Medal in 1982 and the "Best Review Paper Award (1981-1984) for his paper "Model reference adaptive controllers and stochastic self-tuning regulators—A unified approach" published in the *ASME Journal of Dynamical Systems Measurement and Control.*

Zeevaert, Leonardo

SEISMIC RESPONSE OF PILES IN FINE SAND

Proceedings of the Eighth World Conference on

Earthquake Engineering

San Francisco, California

Volume III

Prentice-Hall, Inc., Englewood Cliffs, New Jersey

SEISMIC RESPONSE OF PILES IN FINE SAND

Leonardo Zeevaert (1)

SUMMARY

The piers of the Navy Yard in the State of Veracruz, Mexico, located at the Coatzacoalcos River Bank suffered large permanent displacements during an earthquake 6.5 magnitud with epicenter at about 35 Km from the site. The author describes in the paper a tentative quantitative correlation of the phenomenon using the geometry of one of the pier units and based on the subsoil conditions available.

The problem is analysed theoretically from a practical engineering point of view establishing the pile-soil interaction, and considering that during the strong ground motion high pore water pressures developed in the sand deposit, thus reducing the lateral rigidity of the sand supporting the piles of the pier. The results of the theoretical calculations obtained by the method proposed by the author are confronted with the damage observations at the site.

INTRODUCTION

In August 26, 1959 a mayor earthquake was recorded with epicenter in the Gulf of Mexico with latitude 18°27'N, longitud 94°16'W and approximately at 35 Km from the mouth of the Coatzacoalcos River in the State of Veracruz, Mexico. The earthquake was rated 6.5 Richter Magnitud and its intensity estimated on the order of VII M.M. with maximum ground surface acceleration of 200 gal (Ref. 1). The installations at the Navy Yard located at the river banks close to the mouth of the river, suffered severe damage. Observations by the author just after the earthquake reported permanent relative displacements on the order of 25 cm between pier units supported on steel pipe piles, Fig 1 and 2. The pipes used are 20 cm diamter standard steel pipes driven through the loose sand to point bearing on a soft sand stone. The geometry of the pier analysed, the mechanical properties of the pipe piles and the subsoil characteristics are shown reported in Fig 3.

The phenomenon was analysed considering that during the seismic motion the maximum ground surface acceleration reached 200 gal at the dredge line. The following actions are assumed to have taken place:

1) High pore water pressures in the sand deposit reducing the soil rigidity during the seismic motion.

2) Amplification of the ground surface acceleration at the pier deck elevation.

---

(1) Professor DIVISION ESTUDIOS DE POSGRADO, FACULTAD DE INGENIERIA, UNAM. Mexico 04510, D. F. - Consulting Engineer.

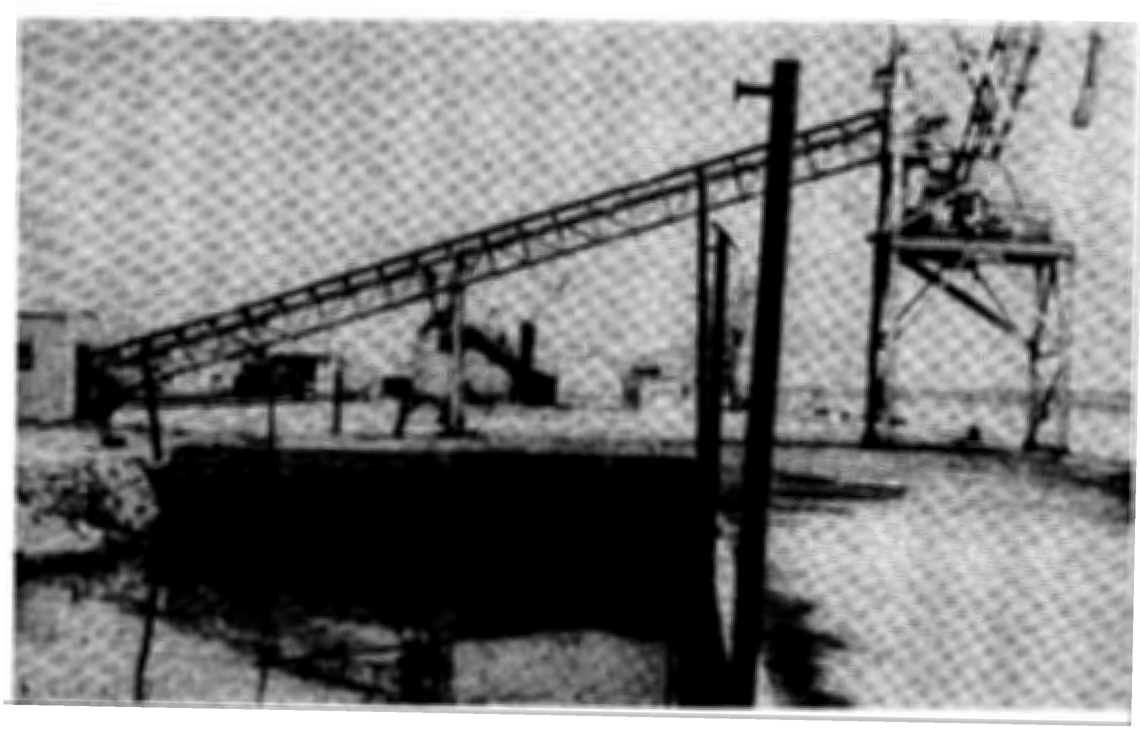

FIG 1. PIER AT THE COATZACOALCOS RIVER

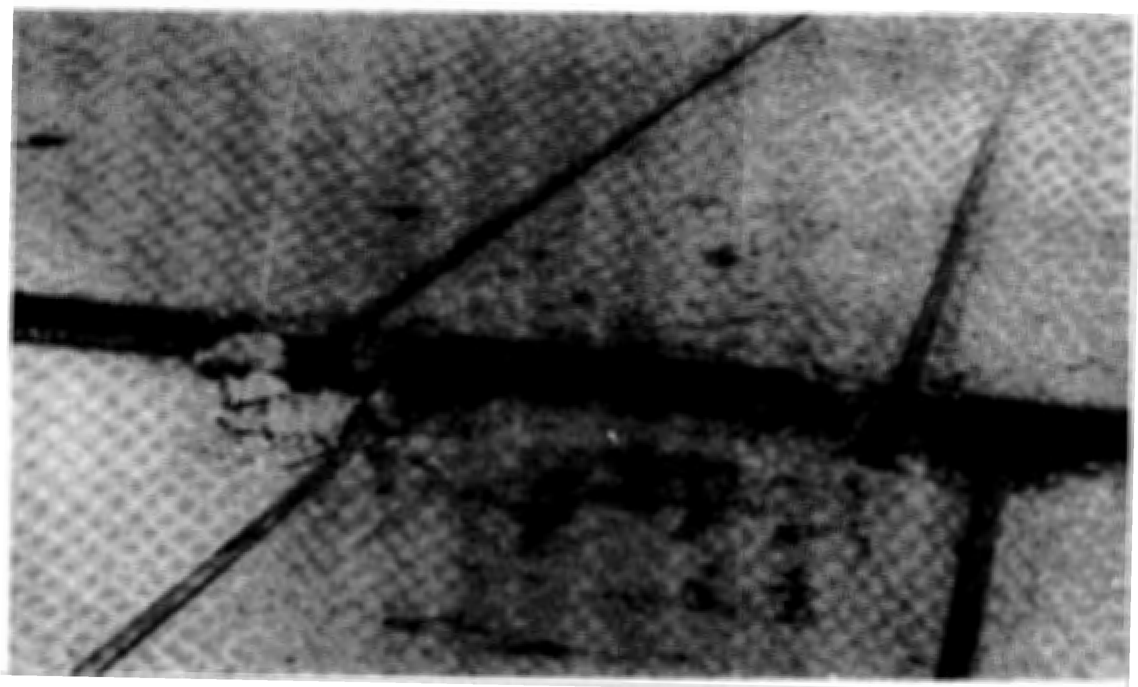

FIG 2. DISPLACEMENT BETWEEN PIER UNITS

The evaluation of points (1) and (2) permitted the computation of the approximate behavior of the pier to be compared with the observed damage.

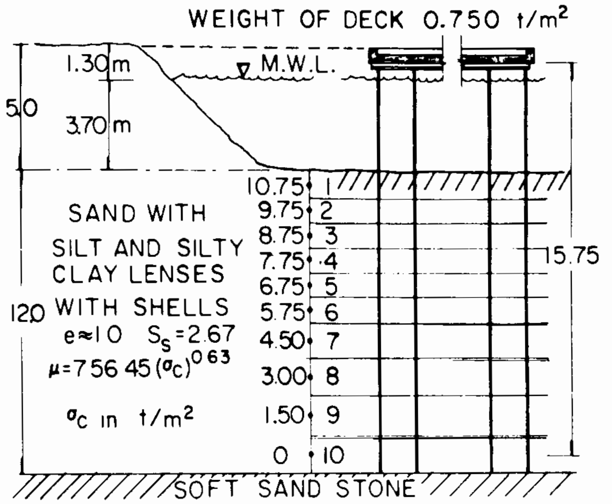

1)- DECK ON 8"ϕ STANDARD STEEL PIPES 1.5m CENTERS PROPERTIES: $I = 1118.83$ cm^4, $A = 3.48$ cm^2, $I/c = 110.72$ cm^3 $EI = 240.55$ t·m^2, CHELLIS, D.R, PILE FOUNDATIONS (SECOND EDITION) p.585, Mc. GRAW-HILL. (1000 KILOGRAMS = 1 ton)

2)- WEIGHT OF DECK PER PILE: 1.69 ton.

FIG 3. CROSS SECTION OF PIER

SUBSOIL BEHAVIOR

To estimate the subsoil behavior it was necessary to learn on the soil rigidity. The author performed in the past dynamic soil investigations for a similar fine sand at the mouth of the Grijalva River in the Gulf of Mexico, located in the State of Tabasco, (Ref. 3). The results of this investigation yielded the following value for the loose fine sand dynamic soil rigidity

$$\mu = 756.45(\sigma_c)^{0.63}\text{ton/m}^2 \qquad (1)$$

in which σ_c given in ton/m^2 is the confining effective stress at the depth where μ is required. Hence, knowing the maximum seismic pore water pressure U_{sis}, the seismic sand rigidity during the earthquake may be estimated by

$$\mu_{sis} = 756.45(\sigma_c - U_{sis})^{0.63} \qquad (2)$$

The next problem was to determine the approximate maximum seismic pore water pressure. The calculation was performed with the method explained in

Ref. 2, Chapter XII, Section 3.5, it was justified by means of a confrontation made with field seismic pore water pressure measurements in fine sand reported by Ishihara et.al, in Owi Island, Japan, Ref. 4 and 5.

The theoretical dominant period T_s of the sand deposit at the site, the maximum seismic relative horizontal soil displacements δ_{si}, and the apparent angle of internal friction during the seismic action are reported in Table I

TABLE I

SEC	DEPTH	HEIGHT	d	$\bar{\gamma}$	σ_{oi}	σ_{oc}	U_{sis}	δ_{sis}	μ_{sis}	ϕ_{sis}
1	0.5	10.75	1.0	0.85	0.430	0.275	0.187	1.589	163.61	10°.3
2	1.5	9.75	1.0	"	1.28	0.819	0.544	1.451	335.40	10°.8
3	2.5	8.75	1.0	"	2.13	1.363	0.869	1.305	485.10	11°.7
4	3.5	7.75	1.0	"	2.98	1.907	1.157	1.144	631.06	12°.7
5	4.5	6.75	1.0	"	3.83	2.451	1.406	0.978	777.72	13°.8
6	5.5	5.75	1.0	"	4.68	2.995	1.615	0.814	926.63	14°.9
7	6.75	4.50	1.25	"	5.74	3.674	1.821	0.576	1115.69	16°.4
8	8.25	3.00	1.50	"	7.01	4.486	1.996	0.357	1343.96	18°.1
9	9.75	1.50	1.50	"	8.29	5.306	2.097	0.158	1576.86	19°.8
10	11.25	0	1.50	"	9.56	6.118	2.130	0	1808.24	21°.4
	m	m	m	t/m³	t/m²	t/m²	t/m²	cm	t/m²	

$\phi_d = 34°$, $\mu_{sis} = 756.45(\sigma_c - U_{sis})^{0.63}$ $T_s = 0.56$ sec

1 ton = 1000 Kg

PILE-SOIL INTERACTION

The second problem was to analyse the pile-soil interaction to determine the ratio of the free period of vibration of the pier T_p to the dominant period of vibration T_s of the sand deposit. With the value of T_p/T_s we determine the probable acceleration amplification at the deck of the pier, (Ref. 6 and 7). The value of T_p may be determined knowing the static horizontal deflection at the deck, therefore

$$T_p = 2\pi\sqrt{\frac{\delta_{st}}{g}} \tag{4}$$

To estimate the value of T_p it was necessary to calculate the unit soil flexibility matrix and the unit pile flexibility matrix. These may be obtained assuming unit pile-soil horizontal reactions in so many horizontal sections as necessary for accuracy, Fig 3.

From conditions $X_i = +1$, Fig 4, we obtain $[\bar{S}_{ji}]$ the pile flexibility matrix and $[\bar{\delta}_{ji}]$ the soil flexibility matrix. Hence, the total horizontal displacements are

$$\{[\bar{S}_{ji}] + [\bar{\delta}_{ji}]\} \cdot |X_{ji}| \tag{5}$$

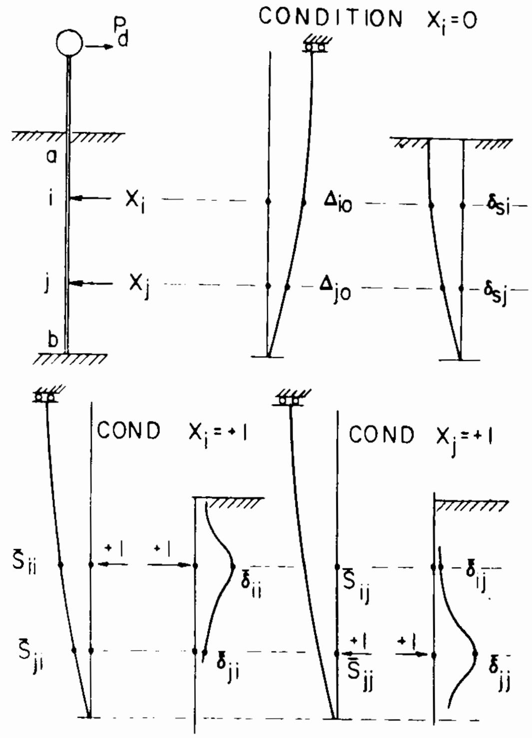

FIG 4. PILE-SOIL INTERACTION CONDITIONS

In which $|X_i|$ is the vector of the unknown horizontal reactions. Assuming $X_i = 0$, and the load per pile at the deck of 1.688 tons applied horizontally, we calculate the static deflections of the pile Δ_{io}, Fig 4. Therefore, we establish the matrix interaction equation for the static condition

$$\left[\bar{S}_{ji} + \bar{\delta}_{ji} \right] \cdot |X_i| = \Delta_{io} \qquad (6)$$

Solving this equation we determine the values of X_i, and thereafter the pile configuration by

$$\left[\bar{S}_{ij} \right] \cdot |X_i| - |\Delta_{io}| = |S_i| \qquad (7)$$

The maximum static deflection at the deck level is found to be 0.128 m. Therefore, the free period of vibration of the pier is approximately $T_p = 0.72$ sec, and $T_p/T_s = 1.29$. Using this value and assuming a fraction of critical damping of 5% we obtain an amplification factor on the order of three (Ref. 7). Therefore, the estimated dynamic maximum force at the deck elevation is $P_d = (3)\cdot(2)\cdot 1.69/9.81 = 1.034$ ton.

The dynamic behavior of the pier in its maximum amplitud is now calculated with $P_d = 1.034$ ton at the pier deck elevation and with the maximum horizontal soil displacements δ_{si} due to the seismic action given in Table I.

The following matrix equation may be established to investigate the seismic maximum response of the pier (*)

$$[\bar{S}_{ji} + \bar{\delta}_{ji}] \cdot |X_i| = |\Delta_{io} + \delta_{si}| \qquad (8)$$

The method in the application of equation (8) is iterative, because during seismic deformation the soil assumes a plastic condition at the upper sections. The pile and soil was divided in 10 sections as shown in Fig 3. The analysis indicated that the upper three sections enter into plastic condition with the following values:

Section 1	0.20 ton
Section 2	0.70 "
Section 3	1.10 "

The results of the final cycle of the pile-soil interaction calculations are shown in Fig 5, where the bending moments and deflection of the steel pipe are reported. The method used is called "HEMISES" it may be found in Ref. 2, Chapter XII, pp 567-588 or Ref. 7, Chapter IV.

From the results of the analysis reported it may be observed that the stresses of the steel pipe pile at the support of the deck increased on the order of 3450 kg/c^2 and at a depth of 8 mts into the sand deposit 2250 kg/c^2.

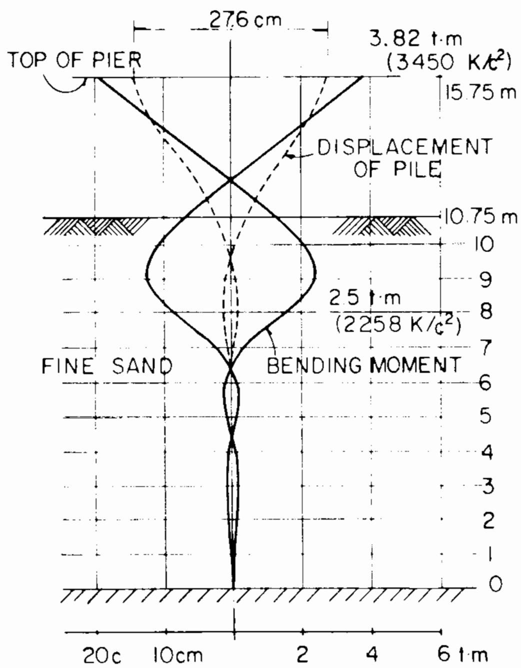

Fig 5. MAXIMUM AMPLITUDE SEISMIC BEHAVIOR OF STEEL PIPE PILES OF THE PIER

(*) The inertia of the mass of the pile is not considered

The elastic limit of the steel pipe material is on the order of 1900 kg/c^2 (27,000 lbs/in^2). Therefore, as the pipe pile reached these high stresses it was forced to yield, not recovering its original position. On the other hand, at this moment the free period of vibration of the pier T_p increased, and consequently the acceleration amplification at the deck elevation decreased, (Ref 2). The calculated double displacement amplitud of the pile head reached as a minimum 28 cm. Fig 5, showing a reasonable good agreement with the relative displacements and permanent distortions observed in the pier, Fig. 2.

CONCLUSIONS

A tentative interpretation of the seismic damage observed in this particular pier has been given based on the following working assumptions.

1) The maximum seismic pore water pressure in the soil is attained at the maximum ground surface acceleration of 200 gal.

2) The sand rigidity μ expressed by equation (2) based on the fine sand at the mouth of the Grijalva River is assumed to be valid at the site close to the mouth of the Coatzacoalcos River, for the same index properties.

3) The plastic forces in sections 1, 2 and 3 were estimated by the conventional plastic theory under instantaneous loading conditions. Deep sections show an elastic response.

It is recognized, however, that an "exact solution" cannot be obtained due to the approximate values of the parameters. Nevertheless, the analysis may be considered within the accuracy of engineering practice.

One may conclude, that following the method of analysis herein explained a designer could find that the size of the piles used were not suitable for the expected seismic ground surface acceleration. This method of analysis, however, was not known at the time these piers were designed and constructed.

In the present, the behavior of similar piers may be forcasted, and with a nominal factor of safety a safe design achieved.

REFERENCES

1 Marsal R.J. (1961) Behavior of a Sandy Uniform Soil During the Jaltipan Earthquake, Mexico. Proceedings of the Fifth International Conference on Soil Mechanics and Foundation Engineering. Vol I pp 229-233, Paris, France.

2 Zeevaert L. (1982) Foundation Engineering for Difficult Subsoil Conditions, Second Edition, Van Nostrand-Reinhold Co. Chapter XII

3 Ref 2 Chapter XII pp 553

4 Zeevaert L. (1983) Computation of Seismic Pore Water Pressure against Field Measurements in Fine Sand.- Division Estudios de Pos-

grado, Facultad de Ingenieria, U.N.A.M. Mexico 04510, D. F.

Seismic Pore Water Pressure Analysis Confronted With Field Measurements in Fine Sand. To be published in Soil and Foundations J.S.F.E.

5 Ishihara K. Shimizu, K. Yamada, Y. (1981) Pore Water Pressures Measured in Sand Deposits During an Earthquake. Japanese Society of Foundation Engineering. Vol 21, No. 4

6 Ref 2 Chapter XII, pp 510

7 Zeevaert L. (1980) Interacción Suelo-Estructura de Cimentaciones Superficiales y Profundas Sujetas a Cargas Estáticas y Sísmicas, Editorial Limusa, México 1, D. F.

GRADUADOS

Durante el año de 1985, obtuvieron el diploma de Especialista en Ingeniería diez alumnos; el grado de Maestro en Ingeniería 55, de los cuales 35 realizaron tesis; y seis alumnos optaron por el grado de Doctor en Ingeniería.
A continuación se presentan los resúmenes de las tesis doctorales y los títulos de las tesis y de los trabajos de maestría.

GRADUATE STUDENTS

During the year of 1985, 10 students obteined the Specialization Diploma in Engineering; 55 the Master Degree, 35 of them made a thesis; and 6 students got a Doctoral Degree.
The abstracts of doctoral dissertations and the masters' degree thesis and research titles are presented in the next pages.

RESUMENES DE LAS TESIS DOCTORALES EN 1985

ABSTRACTS OF DOCTORAL DISSERTATIONS IN 1985.

HACIA UNA METODOLOGIA PARA LA PLANEACION INTEGRAL DE LOS SISTEMAS DE DISTRIBUCION DE ENERGIA

TOWARD TO A METODOLOGY FOR INTEGRAL PLANNING OF THE ENERGY DISTRIBUTION SYSTEMS

Alejandro Afuso Higa Doctor en Ingeniería (Investigación de Operaciones)

Asesor: M. Cobián S.

RESUMEN

La planeación de sistemas de distribución de energía eléctrica constituye un problema muy complejo por la cantidad de variables e interrelaciones a considerar. En la última década se han desarrollado diversas aplicaciones de la programación matemática a este campo. Sin embargo, se presentan fuertes problemas de dimensionalidad y, por lo tanto, de requerimientos de cómputo. Esto resulta dispar con la creciente tendencia al uso de equipos de cómputo pequeños, además de que en la mayoría de los trabajos sólo se resuelve el problema a corto plazo y se omiten sus implicaciones a largo plazo. En este trabajo se utiliza una estructura multiestrato que permite elaborar programas de corto, mediano y largo plazo, integrándose un conjunto de algoritmos que permiten reducir notablemente los requerimientos de cómputo; se desarrollan los programas requeridos y se hace una aplicación a la Ciudad de Managua, Nicaragua.

ABSTRACT

Planning systems of electric energy distribution is a very complex problem due to the large quantity of variables and interrelations that have to be considered. In the last decade, various applications of mathematical programming in this field have been observed. However, strong problems of dimensionality and computational requirements exist. This results in contradiction with the rising tendency to use small computational equipments. Moreover, in most papers the solution is given only for a short term, that is, long term implications are omitted. In this paper a multistrata structure is used, which permits to design programs for short, medium, and long term, a set of algorithms is integrated so computational requirements are remarkably reduced, the required programs are developed and an application to the city of Managua, Nicaragua is made.

SIMULACION NUMERICA DE FLUJO SUPERCRITICO TRANSITORIO

NUMERICAL SIMULATION OF TRANSIENT SUPERCRITICAL FLOW

Francisco Javier Aparicio Mijares   Doctor en Ingeniería (Hidráulica)

Asesor: C. Cruickshank V.

RESUMEN

Algunos esquemas de diferencias finitas usuales en la simulación numérica de flujos transitorios a superficie libre presentan comportamientos anómalos no siempre atribuibles a defectos esencialmente computacionales de los mismos; se observa que tales anomalías se presentan en esquemas basados en ecuaciones de energía y no en aquellos que usan el principio de conservación de la cantidad de movimiento. Además, las anomalías aparecen cuando el número de Froude es mayor de tres. Se demuestra que el programa radica en cambios bruscos de energía a través de ondas de choque, presentes en prácticamente todo flujo supercrítico, cuyo valor es proporcional al cubo del número de Froude, lo cual invalida el uso de formulaciones que impliquen la conservación de la energía y explica las razones de las anomalías.

ABSTRACT

Some finite-difference schemes frequently used in numerical simulation of transient, free surface flows show abnormal behaviours which are not always attributable to essentially computational defects of such schemes; it is observed that these anomalies appear in energy conservation-based schemes and not in those using the momentum conservation principle. Morever, the anomalies appear when the Froude number is greater than three. It is shown that the problem is due to sudden changes in energy across shock waves present in practically every supercritical flow, whose magnitude is proportional to the cube of the Froude number. This invalidates the use of formulation which imply energy conservation and explains the reasons for the observed anomalies.

AIREACION Y SUPERFICIES POLIEDRICAS

AERATION AND POLIEDRIC SURFACES

Felipe I. Arreguín Cortés   Doctor en Ingeniería (Hidráulica)

Asesor: G. Echávez A.

RESUMEN

Se presentaron los resultados obtenidos de un estudio teórico-experimental con flujos con velocidades de 22.5 m/s.
El modelo teórico está basado en las ecuaciones de transporte de sedimentos y de la longitud de mezcla de Prandtl, los resultados obtenidos son similares a los presentados por Straub y Anderson.
Las mediciones se hicieron en una instalación de alta velocidad en la cual pueden alcanzar velocidades de hasta 42 m/s. Para hacer las mediciones se empleó una versión modificada del equipo de Viparelli, que después de calibrado demostró ser útil para mediciones de concentración de aire de hasta 0.64.
Se analizó la difusión turbulenta en una dirección y se obtuvieron los coeficientes respectivos.
Se estudiaron las superficies poliédricas cóncavas y convexas.

ABSTRACT

Results obtained from an experimental and theoretical study with water velocities of 22.5 m/s are presented.
The theoretical model is based in the equations of sediment transport and in the Prandtl's mixing length, the equations obtained are similar to those presented by Straub and Anderson.
Measurements in the high velocity water flume of the National University of Mexico, in wich velocities up to 42 m/s can be reached, were done. A modified version of the technique used by Viparelli was applied to measure the air concentration. After several calibrations it was found that the method is usefull for air concentrations no greater than 0.64.
The turbulent diffusion of the entrained air in one-dimensional chute flow was analyzed and the equation of diffusion was solved.
The use of plane surfaces instead of the traditional curved once in spillway was probed.
Results of both, convex and concave changes in direction are presented.

AISLAMIENTO DE CIMENTACIONES MEDIANTE BARRERAS DE PILOTES

ISOLATION OF FOUNDATIONS BY THE USE OF PILE BARRIERS

Javier Avilés López   Doctor en Ingeniería   (Estructuras)

Asesor: F.J. Sánchez S.

RESUMEN

Se presenta un método para resolver el problema de aislamiento de cimentaciones, de vibraciones generadas en su cercanía, mediante barreras de pilotes. El problema se formula bidimensional y tridimensionalmente como uno de difracción múltiple de ondas elásticas y se resuelve al satisfacer las condiciones de continuidad y equilibrio en las interfases suelo-pilote con la ayuda del teorema de adición de Graf.
Para el modelo bidimensional se obtiene la solución exacta, construyendo el campo difractado por cada pilote mediante expansiones de funciones de ondas cilíndricas que forman un conjunto completo de soluciones de la ecuación reducida en onda.
Para el modelo tridimensional se obtiene una solución aproximada, en el sentido de mínimos cuadrados, pues se supone que el campo difractado por cada pilote está dado solamente por ondas de Rayleigh.
Se realiza un análisis paramétrico para estudiar la influencia del diámetro de los pilotes, la separación entre ellos y su longitud en la efectividad de la barrera. Se define un índice de transmisibilidad como medida de la efectividad de este sistema de aislamiento. Finalmente, se discuten las posibles extensiones de este trabajo.

ABSTRACT

A method for solving the isolation of foundations, from sources generated in their neighborhood, is presented by the use of barriers of piles. The problem is solved in two and three dimmensions by multiple diffraction of elastic waves, taking into consideration continuity and equilibrium in the interphases of soil and piles, with the help of Graf's addition theorem.
For the bidimentional model an exact solution is obteined, generating a diffracted field for each pile by expansions of functions representing cylindrical waves that form a complete set of solutions for the wave reduced equation.

For the three dimmentional model an approximated solution was obtained in the sense of minimum squares, because the diffracted field for each pile is given by Rayleigh's waves only.
A parametric analysis was developed to define the influence of the diameter of the piles, their separation and the effectivity of the barrier depending on their length. A transmissibility index is defined as a mesure of the effectivity of this isolation system. Possible extensions of this work are also discussed.

SIMULACION NUMERICA DEL FLUJO EN ACUIFEROS SEMICONFINADOS CON CARGA Y DESCARGA

NUMERICAL SIMULATION OF WATER FLOWS IN SEMICONFINED AQUIFERS TO LOADING AND UNLOADING

Carlos Cruickshank Villanueva Doctor en Ingeniería (Hidráulica)

Asesor: J.L. Sánchez B

RESUMEN

Se desarrolló un método aproximado para el cálculo de intercambio de agua entre un acuitardo y los acuíferos que tenga en contacto, que toma en cuenta el comportamiento histerético del material sedimentario saturado cuando se descarga su estructura después de un período de carga. El método propuesto se recomienda para la evaluación del flujo y del hundimiento del terreno debido al bombeo en acuíferos en contactos con formaciones compresibles con variaciones cíclicas de carga.

ABSTRACT

An approximated method for the computation of the interchange of water between an aquitard and its aquifer was developed. The method takes into consideration the hysteretical behavior of the saturated sedimentary clay when its structure is unloaded after a sustained loading period. The method is recommended for the evaluation of water flows and of the land subsidance caused by pumping in aquifers in contact with compressible formations and with cyclical variations of load.

APLICACION DE LA TEORIA DE LA CATASTROFE AL ESTUDIO DE FENOMENOS CON HISTERESIS EN HIDRAULICA

APPLICATION OF THE CATASTROPHE THEORY TO THE STUDY OF PHENOMENAE WITH HYSTERESIS IN HYDRAULICS

Polioptro F. Martínez Austria   Doctor en Ingeniería (Hidráulica)

Asesor: G. Echávez A.

RESUMEN

Se presentan los conceptos fundamentales de la teoría de la catástrofe. Se aplica al estudio de estabilidad de flujos potenciales, como el flujo alrededor de un cilindro con circulación y de flujos permanentes e incompresibles, como el flujo de Covette. Se analizan sus posibilidades de aplicación como técnica de modelación descriptiva, a condiciones como la transición flujo laminar-turbulento en tuberías, o el comportamiento del coeficiente de arrastre de cuerpos inmersos, entre otros. Se analiza el problema del salto hidráulico forzado, proponiendo un modelo de catástrofe que se corrobora experimentalmente. Se analiza el problema de estabilidad de cauces, y se propone un modelo cualitativo de catástrofes, basado en la teoría de mínima potencia de corriente. Se presentan conclusiones y se propone una primera clasificación de procesos de catástrofe en hidráulica.

ABSTRACT

A summary of fundamental concepts of the elementary catastrophe theory is presented. The theory is applied to the structural stability study of some potential flows, such as the flow around a cilynder, and of some permanent and incompressible flows, such as the Covette flow. The possibilities of the theory use as a descriptive modeling tool are discuted, and applied to flow conditions as the laminar-turbulent transition in pipes, problem of the hydraulic jump formation is studied and proposed a catastrophe model which is experimentally verified. The problem of river regimen is studied too, and a qualitative catastrophe model is proposed, based upon the minimum stream power theory. Conclusions, and a first catastrophe clasification are presented.

ALUMNOS QUE OBTUVIERON EL GRADO DE MAESTRIA EN 1985.

NOMBRE DEL ALUMNO	Especialidad
Título de la tesis o trabajo	
Nombre del Director de tesis	Fecha

MASTERS DEGREE IN ENGINEERING IN 1985.

STUDENT'S NAME	Field
Thesis or Research Title	
Director's Name	Date

JAIME RAMIREZ ORTIZ Selección automática de contingencias E. Arreola V.	Eléctrica 10-I
JESUS EFREN PEREZ PEREGRINA Necesidad de metodología para desarrollar e implantar sistemas de información basados en computadora J. J. Acosta	Investigación de Operaciones 11-I
JUAN MANUEL PADILLA MIRANDA Métodos de votación en índices de poder S. Fuentes M.	Investigación de Operaciones 22-I
MARCO ANTONIO GUERRERO ALVARADO Estudios de tratabilidad de efluentes líquidos provenientes de la industria procesadora de maíz. S. González M.	Ambiental 11-I
LEONARDO ALZATE LOPEZ Fricción negativa en pilotes Sin tesis	Mecánica de Suelos 25-I
RUTH ROSALES ROJAS Análisis del tránsito de mercancías en los puertos: Un enfoque sistémico Sin tesis	Investigación de Operaciones 12-II
ERNESTO HOLGUIN GOMEZ LAMADRID Inclinómetro para suelos blandos R. J. Marsal C.	Mecánica de Suelos 1o-III
ALEJANDRO DURAN OSORNO Análisis crítico de estabilidad de cámaras de oscilación, con base en el artículo. Sin tesis.	Aprovechamientos Hidráulicos 15-III

MA. JOSELINA CLEMENCIA ESPINOZA AYALA Turbulencia en la hidráulica G. Echávez A.	Hidráulica 22-III
JUAN PADILLA CABALLERO Análisis del funcionamiento en régimen transitorio de una red de canales para riego. Sin tesis	Hidráulica 22-III
ENRIQUE BARRERA CALVA Filtración de aguas residuales con medios granulares (comparación de la práctica americana y europea). Sin tesis	Ambiental 28-III
SALVADOR DURON HUERTA Desarrollo con el MC 68000 Sin tesis	Electrónica 24-IV
JUAN CARLOS ROA BEIZA Prácticas con el MC 68000 Sin tesis	Electrónica 24-IV
NOEL ERNESTO SANTAMARIA GUEVARA Soluciones al problema de flujo en bache. F. Sánchez A.	Petrolera 30-IV
SONIA CRISTINA POSADA BOLIVAR Factores que afectan la prueba de consolidación. L. Zeevaert W.	Mecánica de Suelos 26-IV
LUIS FEDERICO SAINZ LOPEZ Diseño de columnas de marcos rígidos de acero de varios pisos Sin tesis	Estructuras 13-V

FRANCISCO J. ZURITA ERAÑA Efectos del agrietamiento en las propiedades dinámicas de un edificio de 7 niveles Sin tesis	Estructuras	16-V
LI XIAN GUE Influencia de los incrementos de esfuerzo para realizar la prueba del odómetro L. Zeevaert W.	Mecánica de Suelos	22-V
CARLOS FLORES IBARRA Desarrollo de un modelo para definir políticas de operación óptima de una presa R. Domínguez M.	Hidráulica	30-V
JOAQUIN COLLADO MOCTEZUMA Modelos de orden reducido G. Medrano C.	Control	7-VI
MA ALEJANDRA LARA FLORES Modelo matemático para simular algunos aspectos morfológicos de ríos M. Berezowsky V.	Hidráulica	10-VI
ENRIQUE VARGAS DE LEON Evaluación de la metodología usada en PEMEX para la planeación, desarrollo e implantación de sistemas de información J. J. Acosta F.	Investigación de Operaciones	10-VI
FEDERICO ERICK ROMO HEREDIA Propuesta de normas de estados límite para el diseño de uniones clavadas en estructuras de madera Sin tesis	Estructuras	11-VI
GIOVANNI ESPINAL FERRUFINO Una evaluación de la práctica de filtración americana y europea. Sin tesis	Ambiental	26-VI
MIGUEL CAMILO BACHA PEÑA Consideraciones generales para el diseño de descargas submarinas de aguas residuales municipales Sin tesis	Ambiental	26-VI

JORGE GUZMAN DE LA LLAVE Ampliación del método de los elementos finitos de la simulación del proceso constructivo de túneles en suelo blando. Sin tesis	Estructuras 17-VII
ALFREDO PIERO MATEOS PAPIS Códigos permutacionales F. Kuhlmann R.	Eléctrica 22-VII
LESTER ANIBAL GALVEZ ROBAYO Análisis comparativo en la clarificación de aguas residuales mediante carbonato de magnesio y sulfato de aluminio. Sin tesis.	Ambiental 19-VIII
OMAR JOSE MARIN ALVAREZ Dinámica de sistemas rotor flexible chumacera hidrodinámica. V.Muciño Q.	Mecánica Teórica y Aplicada. 16-VIII
JESUS MARIA MORENO LOPEZ Análisis y sistematización de métodos para determinar avenidas de diseño para vertedores presas grandes. R. Domínguez M.	Hidráulica 16-VIII
JORGE SANCHEZ SESMA Vientos máximos debidos a ciclones tropicales. M. Sen.	Mecánica Teórica y Aplicada. 12-VIII
ERIC MORENO VILLALOBOS Red automática micrometereológica. A. Velasco L.	Electrónica 9-VIII

AGUSTIN HUESCA LAGUNES Aplicaciones del método del elemento finito a la hidráulica G. Echávez A.	Hidráulica 3-IX
JAIME PALACINO AFANADOR Determinación experimental de índices de cavitación Sin tesis .	Hidráulica 6-IX
TANG YU Estudio comparativo de controladores para servoválvulas G. Medrano C.	Control 10-IX
GERMAN JAVIER HERNANDEZ BECERRA Análisis inspeccional y su aplicación en la hidráulica. Sin tesis.	Hidráulica 26-IX
VICTOR MANUEL FLORES ZAVALA TORRES TORRIJA Aplicaciones de la computadora manual a la enseñanza de la inv.de operaciones y el análisis numérico. S. Fuentes M.	Investigación de Operaciones 26-IX
FRANCISCO JAVIER GARFIAS CAMPOS Círculos de calidad R. Téllez S.	Investigación de Operaciones 27-IX
JOSE LUIS GASTELUM RAMOS La inflación en México: un enfoque econométrico R. Téllez S.	Planeación 21-X

JOSE ABEL HERRERA CAMACHO — Electrónica
Códigos permutacionales
Sin tesis. — 10-X

VICTOR ELIAS ROSALES INZUNZA — Planeación
Planeación del aeropuerto de Culiacán,Sin.
J. Díaz-Padilla G. — 25-X

AMALIA ADRIANA CAFAGGI FELIX — Hidráulica
Fenómenos oscilatorios en sistemas a presión, resonadores y excitadores
R. Guarga F. — 31-X

FILEMON RIOS CHAVEZ — Petrolera
Simulador numérico de brotes de pozos de gas durante la perforación.
P. Caudillo M — 31-X

SALVADOR AGUILERA CONTRERAS — Eléctrica
Método generalizado para el cálculo Eléctrico de parámetros en líneas de transmisión.
G. Enríquez H. — 6-XI

CARLOS TEJEDA GONZALEZ — Sanitaria
Uso de las aguas residuales en riego agrícola, en zonas con escasa disponibilidad de agua'
P. Martínez P. — 8-XI

MA. TERESA ORTA LEDEZMA — Sanitaria
Criterios para el aprovechamiento de aguas residuales en riego agrícola en México.
P. Martínez P. — 12-XI

YOU JIANYU El problema del viajero y sus extensiones S. Fuentes M.	Investigación de Operaciones 6-XII
JORGE HUMBERTO SIERRA CARMONA Alternativas para el manejo de las aguas residuales en la industria de curtiduría un análisis de la bibliografía. Sin tesis	Ambiental 5-XII
ALAN LYNN ROSAS LEVIN Remoción de aceite de un efluente de fabricación de detergentes. S. Ayanegui J.	Ambiental 4-XII
FERNANDO OJEDA TORRES Vertedores de cresta controlada Sin tesis	Aprovechamientos Hidráulicos. 4-XII

CHAOMING ZENG Análisis de enlaces de comunicación con conmutación híbrida . F. Kuhlmann R.	Control 13-XI
MIGUEL GILBERTO GUEVARA RODRIGUEZ Paquete de programas para computadora para identificación de sistemas dinámicos G.Medrano C.	Control 13-XI
CARLOS ALBERTO HERRERA CACERES Transmisión de calor en cavidades anulares aisladas O. San Román G.	Mecánica 15-XI
WELLINGTON LEONIDAS TEJADA GERMAN Capacidad de incineración de lodos de tratamiento biológico por incineradores de basura existentes. Sin tesis.	Ambiental 19-XI
JOSE ALBERTO ESCOBAR SANCHEZ Efecto de incertidumbre en las características de sistemas estructurales sobre su respuesta nodal espectral. G. Ayala M.	Estructuras 29-XI
RICARDO CAMPOS CAMPOS Pruebas de compresión triaxial no drenadas, en arcilla del Valle de México. E. Juárez B.	Mecánica de Suelos 11-XII
HE NING Codificación de voz basada en cuantización vectorial de la transformación discreta de Fourier de duración corta. A. Buzo P.	Control 6-XII